ESTIMATION OF
ISOMETRIC RECRUITMENT CURVES OF ELECTRICALLY STIMULATED MUSCLE

by

KARON E. MACLEAN

B.S. Mechanical Engineering and Biological Sciences, Stanford University (1986)

SUBMITTED TO THE DEPARTMENT OF
MECHANICAL ENGINEERING
IN PARTIAL FULFILLMENT OF THE REQUIREMENTS
FOR THE DEGREE OF

MASTER OF SCIENCE IN MECHANICAL ENGINEERING

at the

MASSACHUSETTS INSTITUTE OF TEHCNOLOGY
DECEMBER 1988

Signature of Author_____
Department of Mechanical Engineering
December 29, 1988

Certified by_____
Professor William K. Durfee
Thesis Supervisor

Accepted by_____
Professor Ain A. Sonin
Chairman, Departmental Committee on Graduate Studies

ESTIMATION OF ISOMETRIC RECRUITMENT CURVES OF ELECTRICALLY STIMULATED MUSCLE

by

KARON E. MACLEAN

Submitted to the Department of Mechanical Engineering
on December 29, 1988 in partial fulfillment of the
requirements of the Degree of Master of Science in
Mechanical Engineering

ABSTRACT

The use of electrical stimulation to restore function to spinal-cord injured individuals is presently hampered by inadequate muscle characterization, in particular its time varying qualities. This work's purpose was to rapidly and accurately identify parameters of stimulated muscle systems. The parameters may be used to calibrate feedforward controllers to combat system time variation.

The isometric, stimulated muscle was modeled as a Hammerstein system with a static nonlinear subsystem (the isometric recruitment curve or IRC) in series with a dynamic linear one. Long-term system time variation was found to occur primarily as IRC shape change. Muscle dynamics appear to be represented adequately here by a second-order, critically damped model.

Four methods for estimating the IRC were developed. Three of the methods, employing step, impulse and deconvolved ramp responses, were tested experimentally in isolated feline tibialis anterior and medial gastrocnemius. The fourth method, a stochastic iteration technique, was partially developed but not tested. IRCs were compared for shape differences and for effectiveness in open loop control. The results demonstrate that IRC estimation depends on the method used and that all methods are sensitive to short- and long-term time variations in muscle properties. Although the step response technique is the traditional method for estimating recruitment curves, the other methods are less fatiguing and offer improvement in accuracy with shorter testing times. Of these, the ramp deconvolution method appears to have the greatest potential.

Thesis Supervisor : William K. Durfee, Ph. D.
Title : Assistant Professor
Department of Mechanical Engineering

Acknowledgements

I chose to explore the field of biomechanics because I thought the problems were interesting and because I would still like myself if I happened to solve any of them.

Finishing my thesis, I want to make paralyzed people walk. I want to give hands back to amputees, hearing back to the deaf, hearts to those whose own have failed them. It is a worthy calling which fixes people instead of breaking them, and the generosity of its aims gets much of the credit for my continued enthusiasm for it. I hope that more of this country's intellectual as well as financial resources come its way in the future,

The thesis itself was a people project, enriched by the participation and unselfish support of other members of the Biomechanics Lab. I first thank Will Durfee for being a trusted friend as well as an able counselor, and for his unfailing stamina and wit when mine was fading.

Will, Mike Murphy, Pete Mansfield, Dov Adelstein, Jugy Raju, Bill Murray, Crispin Miller, Cary Abdul-Haj, John Mansfield, Greg Brown and Keita Ito have given to me from their immense collective body of knowledge, with patience far beyond the call of duty. They kept the computers alive for those of us too immersed in our own projects to do our share, and initiated me in the MIT rites of wire-wrapping, signal processing and late-night peer review sessions. Far more importantly, they have been friends.

Jeff Hausdorff was an ally who learned with me some of the differences between books and the real thing. Undergraduates Deishin Lee, Robyn Jaloszynski, Catherine Anderson and Helen Greiner were bright and enthusiastic participants in my projects; Nate Osgood has created a legend in his own time. Karen Palmer helped with some important final touches. Lisa Freed, co-habitant of the Whitaker labspace, exchanged a sense of humor and a sound friendship for instruction in the use of a screwdriver.

My house/labmates (the distinction was often unclear) during these two years, first Lou Jandura and presently Mike and Pete, have supported me at home as well as at work. Shared moments away from the lab have been all too rare, and I look forward to more of them in the future.

My (biological) family is three thousand miles away but that has never stopped them from letting me know they are there for me. I will always be somewhere for them.

This work was funded by the Whitaker Foundation and by the W.M. Keck Founda-

tion, and was conducted in the Eric P. and Evelyn E. Newman Laboratory for Biomechanics and Human Rehabilitation.

Karon Elisabeth MacLean

This thesis is dedicated to my grandmother and to my mother and father,
who first showed me that the best kind of world to live in
is one where people care about other people.

Contents

List of Figures

List of Tables

Nomenclature

OLC	=	open loop control
SCI	=	spinal-cord injured
CNS	=	central nervous system
SNLS	=	static nonlinear subsystem
$\widehat{\text{SNLS}}$	=	estimated static nonlinear subsystem
IRC	=	isometric recruitment curve
dls	=	dynamic linear subsystem, time domain
$\widehat{\text{dls}}$	=	estimated dynamic linear subsystem, time domain
DLS	=	dynamic linear subsystem, frequency domain
$\widehat{\text{DLS}}$	=	estimated dynamic linear subsystem, frequency domain
σ	=	second-order dynamic system pole
$\hat{\sigma}$	=	estimated second-order dynamic system pole
$\hat{\omega}$	=	estimated second-order dynamic system damped frequency
ς	=	second-order dynamic system damping ratio
F	=	muscle force
$\bar{\text{F}}$	=	normalized muscle force
F_{peak}	=	peak muscle force
f_{co}	=	filtering cutoff frequency
f_{ny}	=	Nyquist frequency
f_s	=	force sampling frequency
f_{stm}	=	stimulation frequency
T_{hr}	=	half-ramp period
T_{on}	=	stimulus on-time
T_{off}	=	stimulus off-time
τ_{del}	=	observed time delay between stimulus and force onset
τ_{peak}	=	time-to-peak of muscle impulse response

SS	=	stimulus strength
$\overline{\text{SS}}$	=	normalized stimulus strength
THR	=	threshold stimulus strength
THR_{TB}	=	THR, as estimated by boundary algorithm
THR_{meth}	=	THR, as estimated by specified ID method via an IRC
ϵ(THR)	=	difference between THR_{TB} and THR_{meth}
SAT	=	saturation stimulus strength
SAT_{meth}	=	SAT, as estimated by specified ID method via an IRC
AZ	=	active zone or region between threshold and saturation
AZW	=	active zone width, or difference between SAT and THR
ΔAZW	=	norm. change in active zone width
ZZ	=	zoom zone, or stimulus region chosen for data acquisition
SHAPE	=	summated IRC shape characterization parameter
ΔSHAPE	=	normalized IRC shape change
ϵ(SOLC)	=	summated error in static OLC test
ϵ(DOLC)	=	summated error in dynamic OLC test

Chapter 1

Introduction and Background

In the U.S. today, 150,000 people [1] can't walk, ride a bicycle or pick up a glass of water. They have suffered neurological damage to their spinal cord which has resulted in a loss of motor control.

Spinal cord injured (SCI) individuals pose a unique rehabilitation opportunity. The link has been broken between the motor command's origin in the central nervous system (CNS) and the muscles carrying out the command, but the muscles themselves are intact and viable, as is most of the peripheral nervous system. The obvious solution is to replace the physiological command generator with an artificial one, or — more ambitiously — to reinstate direct motor control by bridging the gap between CNS and muscle. This is the eventual goal of Functional Electrical Stimulation (FES), and in some limited cases it has already been achieved. To proceed beyond the execution of simple, repetitive tasks, however, the properties of stimulated muscle must be better understood at a fundamental level, and mechanisms of activating it developed which mimic physiological ones more closely. In this thesis, the stimulated muscle is modeled mathematically, and an animal model is employed to develop and verify an essential control tool: a means of rapidly and accurately characterizing a muscle's isometric recruitment curve.

1.1 Functional Electrical Stimulation

1.1.1 Spinal Cord Injury

Partial or complete loss of motor control results when a lesion in the spinal cord interrupts the conduction path form the CNS to the peripheral nervous system. In an able-bodied person, voluntary movement is the result (Figure 1.1) of an electrical action potential which originates in the motor cortex of the brain, passes through the upper motor neuron in the spinal cord, enters the anterior horn cell of the lower motor neuron and continues through the extremities. At the lower endplate of the neuromuscular junction, the action potential is translated to chemical and electrical events which excite the muscle and cause it to contract. The degree to which an SCI individual's

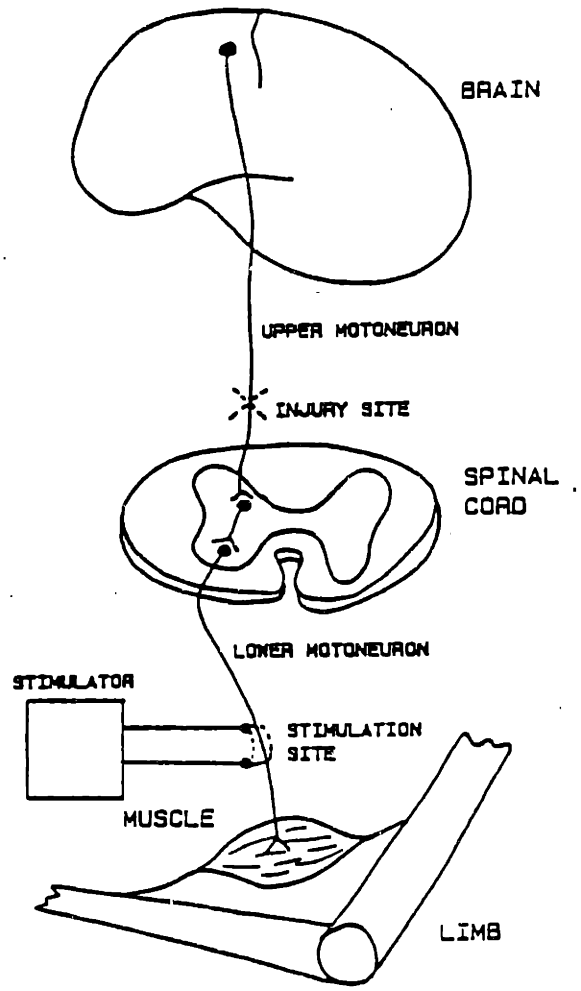

Figure 1.1: The motor command conduction path [18].

control is impaired depends on the location of the lesion, since only muscles whose lower motor neurons originate below the lesion will be affected.

Because upper motor neurons do not regenerate naturally and as yet there is no indication that they may be induced to do so in the near future, normal function cannot be restored after injury of this sort. SCI rehabilitation programs are therefore limited to holding a status quo; they maintain any remaining function and prevent muscle disuse atrophy, but can do little to improve an affected person's ability to use his or her limbs.

1.1.2 Artificial Stimulation

An action potential can be induced in a nerve or muscle through electrical stimulation from an external source. The sequence of events following the action potential's initiation is the same as if the depolarization began at the CNS. The fundamental challenge with FES is not in exciting muscle tissue but in doing so in a selective and controlled manner, as the intact nervous system does. This is firstly because of the complexity of the neuromuscular junction, composed of many motor units which would have to be activated independently for perfect control, and secondly because in the absence of either a precise knowledge of muscle response to stimulation and adequate feedback channels, a controller cannot deliver the input signal that will produce a desired contraction.

1.1.3 Applications of FES

At this time, FES techniques are used with the greatest success in tasks which are simple, cyclic and require little or no voluntary monitoring. Examples are the cardiac pacemaker, which stimulates the phrenic nerve continuously in an ungraded, on-off manner; correction of hemiplegic stroke victims with foot drop (a paralysis of the dorsiflexor muscles causing the foot to drag during walking) by means of a pressure-sensitive trigger in the the shoe's heel wich excites the dorsiflexors at the appropriate point in the gait cycle; and in occupational and physical therapy to prevent muscular

atrophy, increase muscle strength, maintain range of motion and to re-educate nerve pathways when the nature of the injury permits it.

Current FES techniques are unable to provide active control that is adequate for functional, nonrepetitive and usually complex tasks relating, for example, to hand grasp, posture and walking. These applications are the focus of current FES research in many places.

1.1.4 Stimulation Techniques and Their Problems

The problem of how to reconstruct physiological stimulation using either surface or neural methods is far from solved. The current state of the art is unsatisfactory both in sensitivity of nerve or muscle to stimulus strength and in recruitment specificity.

Electrodes

The quality of the electrode/neuromuscular interface is a function of the stimulation technique used. In surface stimulation, an electrical signal passing through an impedance of skin and subcutaneous tissue is attenuated, distorted and noise-ridden by the time it reaches the nerve axon or muscle. A cleaner contact may be made by implanting an electrode in direct contact with the nerve, but at the price of an invasive procedure and a risk of nerve damage.

Motor Unit Recruitment Order

The central nervous system (CNS) has two ways of modulating muscle force. The first is spatial summation, or control of the activated muscle fiber population. Muscle fibers are activated asynchronously according to fiber type and location, through a neural network that constructs and transmits a different signal to each motor unit. Physiological recruitment proceeds from slow twitch (slowly fatiguing) to fast twitch (rapidly fatiguing) muscle fibers, corresponding to a small-to-large diameter nerve fiber activation order, known as the "size principle". When a bundle of nerve fibers is

externally and nonselectively stimulated, however, fiber recruitment depends on each axon's stimulus threshold and on the stimulus strength. Large diameter fibers are excited earlier because of their lower stimulus threshold, as are the fibers closest to the signal's source. The resulting sequence of muscle fiber recruitment, opposite to the physiological one, is much more fatiguing.

Temporal Summation

The second means of force modulation is temporal summation. Each naturally activated muscle motor unit is subjected to a random excitation history independent of those around it, the stochastic frequency content of which is related to the unit's muscle fiber content and the strength of the stimulus coming from the CNS [15]; as the stimulus level increases, so does the frequency of action potentials exciting motor units in the activated pool. The staggered motor activity of adjacent units permits modulation of smooth tetanic contractions with comparable contributions from all units. One complication of nonspecific external stimulation is that a small subpopulation of activated muscle fibers are forced to contract in synchrony, and high stimulation frequencies are required to produce a fused tetanus.

Forms of Stimulus Modulation

Stimulus strength may be regulated by varying the electrical input signal's amplitude, width or interpulse interval (inverse frequency) in techniques known respectively as PAM, PWM and FM. However, none of these methods correct the problem of nonselectivity, since that is a function of the electrical input channel rather than the mode of stimulation and consequently are unable to deal with the issues of either aphysiological recruitment order or synchronous excitation. PAM has the additional disadvantage of applying large current levels to the neuron at high stimulus strengths, creating a danger of tissue damage. PWM is able to deliver the same amount of charge at safer current levels.

...

Any means of artificial stimulation currently in use lays a disproportionate burden of force generation on a few highly fatiguable muscle fibers. The artificially stimulated muscle as a whole is able to produce less force and tires more quickly than it would if intact and under the control of the CNS.

1.2 Controlling Electrically Stimulated Muscle

1.2.1 Importance of the Muscle Model

The success of any type of control strategy in either open loop (OLC) or closed loop (CLC) control depends on how well the controlled system is characterized. In FES, this situation is especially true since feedback channels are generally nonexistent or limited and unreliable. An accurate model of the stimulated muscle is therefore imperative for controller robustness.

Contraction of electrically stimulated mammalian muscle has been modeled by others, as will be discussed in Chapter 2. In general the isometric contraction of different muscles and of different individuals and species has been found to be similar in form, *i.e.* describable by the same generalized, parametric model, but with substantial variation in the values of the model's parameters. The job of muscle modeling thus has two steps: the determination of a general model, and the assignment of its parameters for a specific muscle.

1.2.2 System Time Variation

FES control is further complicated by the presence of a system time variation independent of and slower than the muscle's dynamic response. Because of short- and long-term fatigue [21] and possibly other chemical changes in the muscle as well, stimulation/response relations have been seen to drift with time [18]. No techniques of modeling a time-varying system are in existence today, and in any event the underlying causes of the time variation are not understood precisely enough to permit their

prediction. For this reason, a one-time characterization is inadequate if the muscle is to be controlled over an extended period ot time. Inherent in a robust control strategy must be a means of rapidly and accurately assessing the nature and extent of system changes. The importance of this characterization element depends on the precision of control required for the execution of a particular task and on the degree of variation observed in a particalar system.

1.3 The Isometric Recruitment Curve

The isometric recruitment curve (IRC) is the nonlinear gain relation between stimulus activation level and steady-state output force when the muscle is held at a fixed length (Figure 1.2). It is an electrically stimulated muscle's fingerprint, its most fundamental

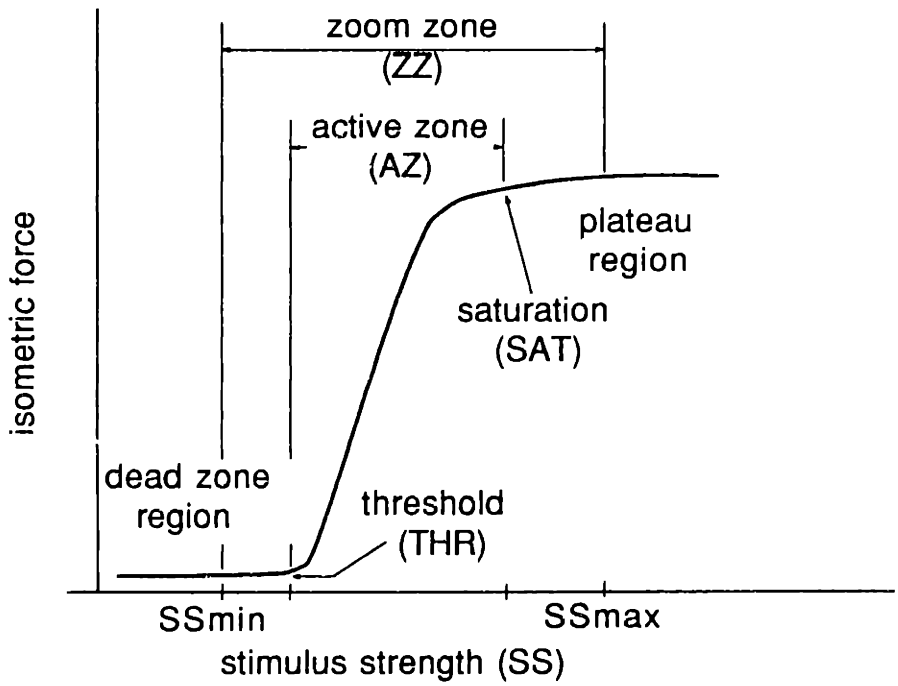

Figure 1.2: The isometric recruitment curve.

and distinguishing characteristic, but one which can change over time and is affected by the method of stimulation, values of stimulus parameters and even the exact configuration and position of the electrodes. The feasiblity of accurate regulation of muscle force is dependent on the presence of an accurate estimate of the IRC in a controller's feedforward block. However, because it is difficult to measure it is generally known only approximately, and any estimate is likely to contain some degree of identification method dependency and contamination from system time variation.

1.3.1 Physiological Basis

The IRC's sigmoid shape is due to the fact that different motor unit populations are brought into the activated pool ("recruited") at different stimulus strengths. Every motor unit has a threshold excitement level which must be exceeded for propagation of an action potential. Threshold can be met through an increase in either the stimulus pulse's amplitude or its duration according to the motor unit's characteristic strength-duration relation, an example of which is shown in Figure 1.3. This phenomenon explains why muscle contraction can be modulated by both pulse amplitude and duration.

Since a motor unit's strength-duration curve depends on fiber type and diameter, threshold levels vary in a roughly Gaussian manner with a sub-threshold or "deadzone" region where no or few motor units are activated, a high-slope area where the activated population increases rapidly, and a plateau where a large increase in stimulus strength is required to activate more fibers. Typically the plateau does not become completely flat within the operational stimulus range.

It is important to note that this sigmoid shape is characteristic of *artificially* stimulated muscle. A "natural" recruitment curve, if such a thing exists, would represent a different activation scheme regulated simultaneously by both temporal and physiological spatial modulation, and its shape will not necessarily be the same.

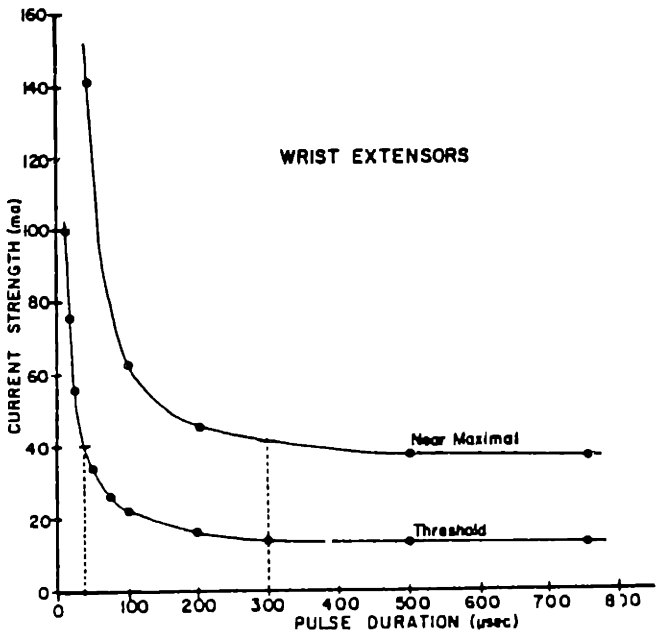

Figure 1.3: A typical strength-duration curve [8].

1.3.2 Definitions

It is convenient at this point to formally define some IRC parameters which will be referred to frequently throughout this text.

Stimulus strength (SS) is a general term for muscle activation level. In this study muscle activation was achieved by pulsewidth modulation (PWM) at a constant frequency (f_{stm}= 40 Hz) and pulse amplitude (PA), where pulse width input was in the range 0.0 to 100.0 μsec with a resolution of 0.1 μsec.

Stimulus threshold and saturation, occasionally referred to as THR and SAT, respectively, are characteristics of the real system IRC. The threshold stimulus strength is the lowest to elicit a force output, while saturation is that at which force response reaches a plateau. Both real and estimated THR and SAT values are often nebulous because of the IRC's indeterminate shape. THR and SAT can be estimated in a variety of ways which will be described later.

Stimulus Active Zone (AZ) is the high-slope region of the recruitment curve between THR and SAT.

Zoom Zone (ZZ) is the operator-chosen stimulus region (between SS_{max} and SS_{min} in Figure 1.2) within which identification data is taken, named for its functional analogy to the capability of a camera zoom lens to focus on a small region within a large picture. In the interests of optimizing map resolution, ZZ is usually chosen to include the active zone and enough more to provide a safety factor in IRC estimation. Cases where it is selected differently will be noted and justified.

1.3.3 Existing Estimation Methods and their Shortcomings

The means of IRC estimation in most common use today is that of assembling a set of points relating the muscle's "steady state" response to a number of step stimuli (Figure 1.4). Since a muscle's steady state response, if it actually existed, would be the same as its static response, this approach satisfies the letter of the IRC's definition and in addition it is straighforward to execute. Precisely speaking, however, steady

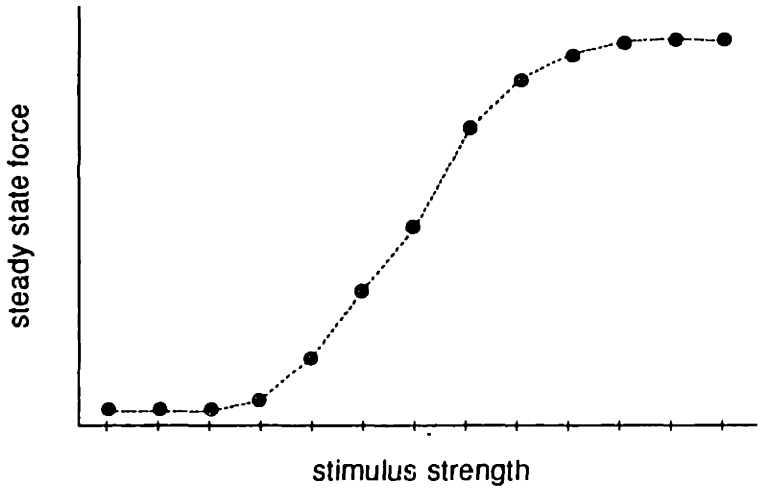

Figure 1.4: A steady-state step response isometric recruitment curve.

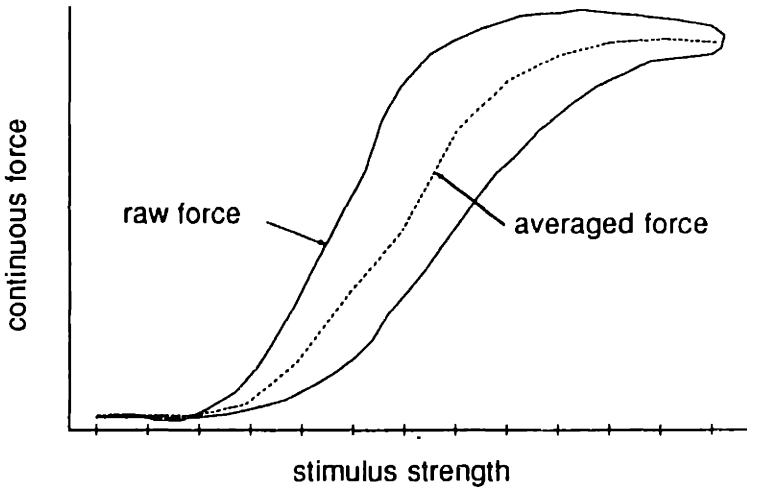

Figure 1.5: An isometric recruitment curve constructed from a ramp response.

state does *not* exist for a time-varying system. The step-response IRC estimate may be corrupted by fatigue and influenced by muscle activation history as well. Furthermore, this method is time and stimulation intensive, tiring the muscle and altering the IRC even as it measures it. Finally, the result is generally of a low resolution since all of those problems are exacerbated as more points are added to the curve.

Another simple approach to muscle static response characterization is to approximate it from the muscle's response to a dynamic input such as a sawtooth ramp (Figure 1.5). There is hysteresis in the force-stimulus strength crossplot of the ramp response due to muscle dynamics, but when the ascending and descending sides are averaged the familiar sigmoid curve reappears. The ramp response approach is certainly quicker, less fatiguing and affords a higher resolution than that using the step response, but its theoretical basis and therefore its accuracy is questionable.

...

It is impossible to look at two estimates of a muscle's IRC and say one is right and one is wrong according to solely morphological traits, since there is no correct standard to which they may be compared. The only relevant criterion is an IRC estimate's functionality: how well it improves control when used as a feedforward control element.

1.4 Thesis Aims

In order for functional control of electrically stimulated muscle to advance far beyond its existing state, the muscle itself must be better understood. Reliable feedback channels are unguaranteed in clinical and even in many experimental situations, laying an even greater importance on robust feedforward compensation. Although much attention in the literature has been given to muscle modeling, it is difficult to verify or parameterize a model in typical *in vivo* situations, because a single muscle cannot be studied independently of other muscles in its group, free of skeletal and neurological interference.

There is therefore a need for a controlled and precise study of the properties of isolated muscles. This need motivated the development here at MIT of Durfee's experimental animal model [18] and its use in the investigation of simple FES control strategies. It became clear through that work that even in such a well defined and monitored situation, the nonlinear and time-varying properties of the stimulated muscle complicate efforts at control. Specifically, the muscle's IRC, already difficult enough to characterize, was observed to shift dramatically and unpredictably over the course of time.

At this date, there has been no careful study of the relative effectiveness and other virtues of different methods of IRC estimation, nor has there been an effort to develop new and more effective methods. The purpose of this thesis is to develop and to comprehensively test in static and dynamic open loop control situations a set of IRC estimate methods which address the problems besetting those in use now, with recognition of the improbability of solving all complications with a single answer. Our emphasis is rather to present some options to scientists and therapists employing FES control which may be more or less appropriate in different situations, and to provide a deeper level of understanding of how much or little effort is necessary or possible to maintain an accurate system characterization in the face of unpredictable time variation.

1.5 Thesis Contents

This thesis begins with a description of the experimental animal model used for the isometric muscle studies (Chapter 3), and a definition of the mathematical isometric muscle model itself with a discussion of its applicability and limitations with respect to FES muscle control (Chapter 2).

The format of the document's remainder echoes the sequence in which the thesis work was undertaken. Chapter 4 describes the various IRC identification strategies that were investigated, including a section discussing their development and final implementation for this project. Chapters 5 and 6 detail respectively the methods and

present the results of comparing the estimation methods with respect to a number of morphological IRC parameters and to the IRC estimates' performance in open loop control. Chapter 7 discusses these results, and in Chapter 8 conclusions are drawn and recommendations made.

Chapter 2

The Isometric Muscle Model

Some of the identification methods described in this thesis are based on fundamental system characteristics, such as the existence of a step response or a peaked impulse response. These methods may be employed in static control tasks without further knowledge of other muscle properties.

The dynamic identification methods utilizing the muscle's continuous ramp and stochastic responses, however, require a model of the muscle dynamics. By defining the stimulated muscle system more completely than the simpler methods do, they are potentially more powerful as control tools but their success is linked to the muscle model's viability.

2.1 Description and Justification

The stimulated muscle is modelled here by a Hammerstein system (Figure 2.1), composed of a static nonlinear subsystem (SNLS) followed by a dynamic linear subsystem (DLS). The DLS is symbolized by its impulse response. The isometric recruitment

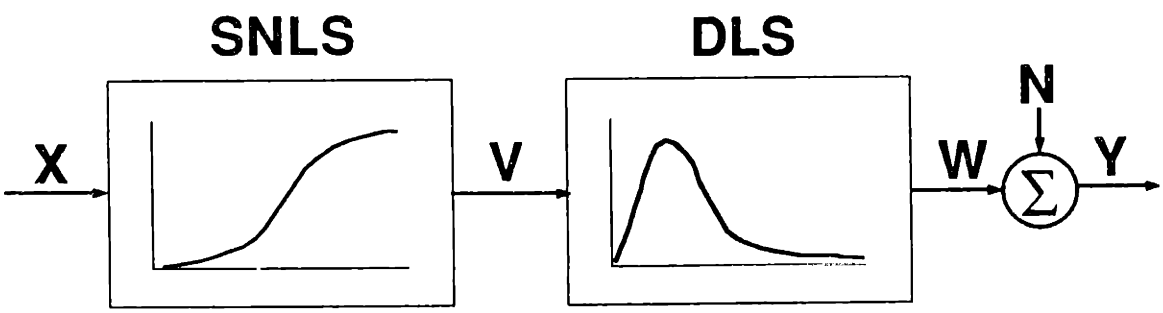

Figure 2.1: A Hammerstein system.

curve (IRC) was defined earlier as the static relation between a stimulated muscle's activation level and its force output. For the Hammerstein system model, the SNLS is the IRC.

The Hammerstein model was chosen as the best way to take advantage of the finer control afforded by recognition of the system's complexity, while avoiding cumbersome and unwarranted detail. It has been used by others also, *e.g.* [26]. Some investigators chose to neglect the dynamic part of the system, a reasonable route when only steady state control is desired. Certain other models were rejected as being too detailed for the purposes of this study. Some, for instance, subsect the dynamic system by representing musculotendon units or individual muscle fibers with contractile, elastic and damping elements [20]. Until nonlinearities in the system are identified, such complexity will not improve control.

An anatomical grounding for the Hammerstein model can be found if it is assumed that the bulk of the system's nonlinearity lies in the static electrode-nerve interface[1]. This interface is nonlinear because a cuff electrode does not stimulate all the nerve axons in a cylindrical bundle with equal strength, and because the smaller diameter neurons corresponding to fast twitch muscle fibers have a lower threshold of excitation than do the large diameter neurons associated with slow twitch muscle. The activated fiber population thus changes as activation level increases.

The musculotendon unit has been found to contract with critically or slightly overdamped second order dynamics [4,5,9,24]. A second-order model can be justified on the grounds that it captures the basic features of muscle dynamics, including the twitch (impulse) response and step response characteristics. The locations of the two poles, and consequently the shape of the twitch response, vary with fiber composition [10,28,29] and muscle geometry. A predominance of fast twitch fibers quicken the muscle's response and draw its poles away from the s-plane origin, while a mixed fiber population separates the poles and produces an impulse response which still rises quickly but falls

[1] Refer to the hardware descriurption in Section 3.2.2

more slowly.

It is not known how much variation in pole separation and absolute location exists among different muscles, individuals and species, or across time in a single muscle. One goal of this thesis is to establish how detailed this part of the muscle model need be for effective control.

2.2 Limitations

Real muscles are complicated machines subject to outside influences, some poorly understood and few well characterized. They are likely to diverge from the Hammerstein model in several important aspects. The magnitude of these divergences depend on the muscle and on the way it is restrained, stimulated and monitored. When differences become significant, the model's limitations become inadequacies for that situation.

Time Variation

Muscle time variation is not accounted for by the Hammerstein model, nor do any techniques of nonlinear system identification in use today offer a solution to it. Some muscle parameters, in particular the IRC's active zone and amplitude, drift over a period of minutes and hours because of fatigue and other unidentified physiological changes.

Fatigue, a reduction in the muscle force elicited by a maximal stimulus strength because of metabolic depletion, may be loosely characterized for the purposes of this study as short term (previous force levels attainable after a few minutes of rest) or long term (a downward trend in maximal force over hours of muscle activity). It occurs in all muscles, but those composed primarily of fast twitch fibers are more susceptible because of their higher metabolic demands[21].

This shortcoming is a serious one for a system that is to be controlled in open loop, using a curve like the one in Figure 1.2. It is easy to imagine the chaos that a shifting RC would cause. Since time variation is not modelled, a controller must have access

to an up-to-date estimate of the recruitment curve, and the time invariant model must be supplemented with a convenient means of characterizing the nonlinearity.

Number and Ordering of Static and Dynamic Blocks

Some experimental models might be appropriately described by a more complex combination of model blocks than the Hammerstein SNLS-DLS pair. When surface stimulation is used, capacitance of superficial tissue may result in electrode/nerve or electrode/muscle interfaces. On the other hand, surface stimulation of muscle rather than nerve may bypass the "size principle" of the neuromuscular junction and reduce that particular source of nonlinearity. Dynamics in nerve conduction, apart from a pure time delay, would serve only to increase the order of the dynamic block describing muscle contraction, unless there is an additional nonlinearity in the neuromuscular interface. Nonlinearity in the measuring apparatus, whether it monitors position, velocity or force, could necessitate an additional nonlinear static or dynamic block following the Hammerstein model's dynamic one.

Two variations on the Hammerstein system which might be used to describe stimulated muscle are the Weiner model (Figure 2.2), which reverses the sequence of the SNLS and the DLS, or the more general LDL model (linear–dynamic–linear; Figure 2.3) which assumes an SNLS on both sides of the DLS.

Dynamic System Nonlinearity

In an ideal Hammerstein system, all nonlinearity is static and straightforward to identify. A real muscle's division into static nonlinear and dynamic linear parts loses physical reality to the extent that nonlinearity spills over into the dynamic subsystem. Muscle force is generated by individual mucle fibers with a distribution of contractile speeds [25]. The shape of a muscle's twitch response will depend on the level of stimulus activation and its stimulus-twitch response amplitude relation may be nonlinear as well, since different populations of fibers will be recruited [10,28,29]. In addition, if

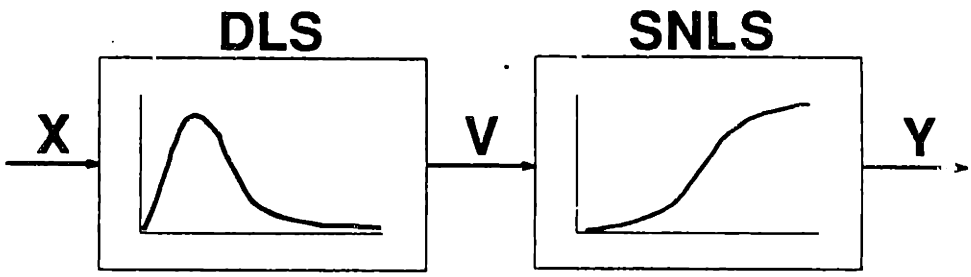

Figure 2.2: The Weiner model.

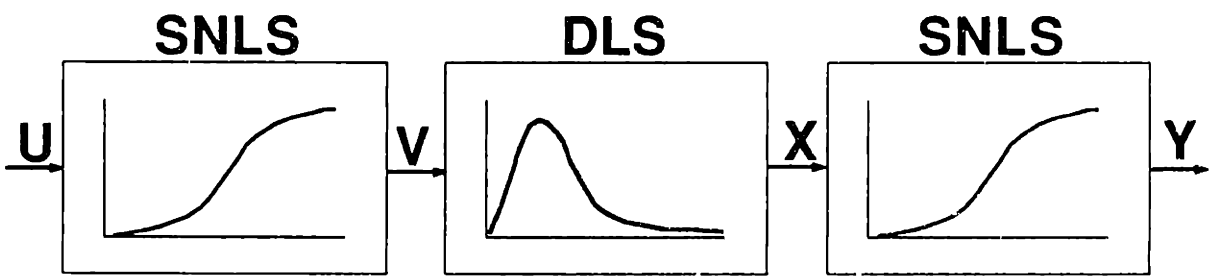

Figure 2.3: The LDL model.

the tendon is included in the system being studied it may act as a nonlinear spring, especially for highly pinnated muscles with long attachment sites.

This raises a twofold issue. First, exactly which quantity is most desirable to know for muscle control? Should separate estimates of static and dynamic nonlinearity be made, should the two be lumped together or should the dynamic nonlinearity be neglected altogether? The answers depend both on the nonlinearities' location and magnitude and on the nature of the control task. Secondly, there is the more pragmatic question of what *can* be known, and moreover what can be known accurately, quickly and without fatiguing the muscle.

Sensitivity of Input and Output Channels

Dependency of control quality on input and sensor quality is less a fault in the model than the ineviteable consequence of any attempt to force order onto a biological system. Poor selectivity of stimulation means that the muscle isn't receiving the same input that the controller is sending it, while output corrupted by noise and measurement error makes it difficult to either characterize the muscle response (*e.g.* estimate its IRC) or to control it in closed loop.

Nonisometric Contraction

Although the model may adequately describe the basic behavior of isometric muscle, it is not accurate when the muscle is allowed to move. This limitation is encountered to some extent even in this so-called isometric study, since what is being modeled as a muscle is actually the musculotendon unit. The elastic tendon permits some change in muscle length in proportion to its tension, the magnitude being related to the tendon's length and thickness.

Chapter 3

The Animal Model

3.1 Requirements and Rationale for the Animal Model

This thesis investigates the behavior of artifically stimulated muscle under controlled and monitored conditions. Whenever feasible, simulations were used to develop and test the muscle model and identification methods. If FES technique is to evolve from an idea to an aid for disabled humans, however, it must be applied in physiological situations to identify both potential pitfalls and successful strategies.

Several considerations dictated the use and development of the animal model described in this chapter:

1. An *in vivo* preparation. Because the neuromuscular system is incompletely known, some aspects of muscle response could not be modelled mathematically. The methods and the simulation models had to be verified with real mammalian muscles under physiological conditions, *i.e.* in a living animal.

2. Accurate measurement of isometric, isolated muscle force. Neither the accuracy nor the specificity achievable through external immobilization and measurement were sufficient to answer the questions being posed. A more invasive procedure implemented in an acute animal protocol was required.

3.2 Experimental Apparatus

The animal model used in this study was similar to that designed by Durfee [18]. Its central elements are subject animal and supporting hardware and software. Improvements made to Durfee's experimental apparatus are noted.

3.2.1 Animal Preparation

A cat was chosen for the role of experimental subject because it is the smallest available animal with muscle size, geometry and fiber composition similar or analogous to human ones. A rat's skeleton and muscles would be too small to immobilize, and its nerves inaccessible. A rabbit's hindlimbs were too powerful for the torque motor to restrain.

Two antagonist hindlimb ankle dorsi and ankle plantar flexors could be restrained and monitored simultaneously. For this and Durfee's work, the dorsi flexor tibialis anterior (TA) and plantar flexor medial gastrocnemius (MG) were always used. Containing a mix of fast and slow muscle fibers [14,17,25], their dynamic properties are similar although the MG has a larger peak force. The two peak muscle forces were equalized with hardware and calibration procedures described below.

In addition, the TA and the MG are more straightforward to surgically isolate and secure than some other muscles in the two groups. The TA has a long tendon, easily found and cut, that crosses the front of the ankle joint and wraps around the inside of the foot. The MG terminates in the calcaneous tendon along with the lateral gastrocnemius, soleus, and biceps femoris. The plantaris runs with the calcaneous tendon but passes beyond the heel on its way to the toes. One can easily separate all parts of the tendon except for the MG-LG pair which fuse at the muscles. Since separating these two might damage the tendon, both gastrocnemius halves were clamped to the cable. MG isolation was achieved by cutting all the ti ner nerve branches except for the one that ennervated the MG.

Muscle Isolation and Restraint

Figure 3.1 shows how the anaesthetized animal was positioned on the experiment table and immobilized with clamps at hip, knee and ankle. Some slippage between skeleton and layers of soft tissue and skin was observed with the original system of hip, knee and ankle clamps. The clamps were redesigned with pointed centers to penetrate the superficial tissue overlaying the joints of the anaesthetized animal and to hold the skeleton more securely. After amputating the foot, the distal tendon of each muscle was detached from the skeleton and extended with lightweight airline cable, clamped to the tendon through a 10 or 12 gauge uninsulated crimp butt connector. The failure of the larger, stronger MG's connection became a recurrent problem for larger animals in particular, both because of the greater forces generated and a thicker tendon which

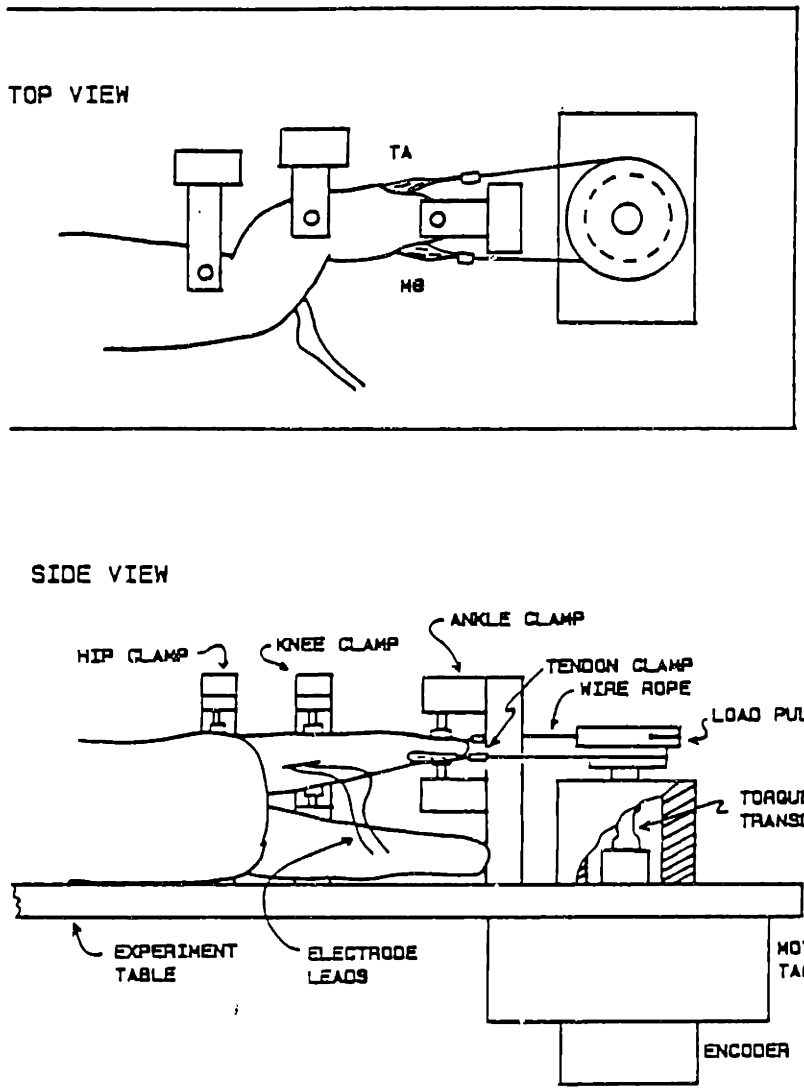

Figure 3.1: Animal immobilization. Top and side views of anaesthetized cat's hind limb fixed to the experiment apparatus [18].

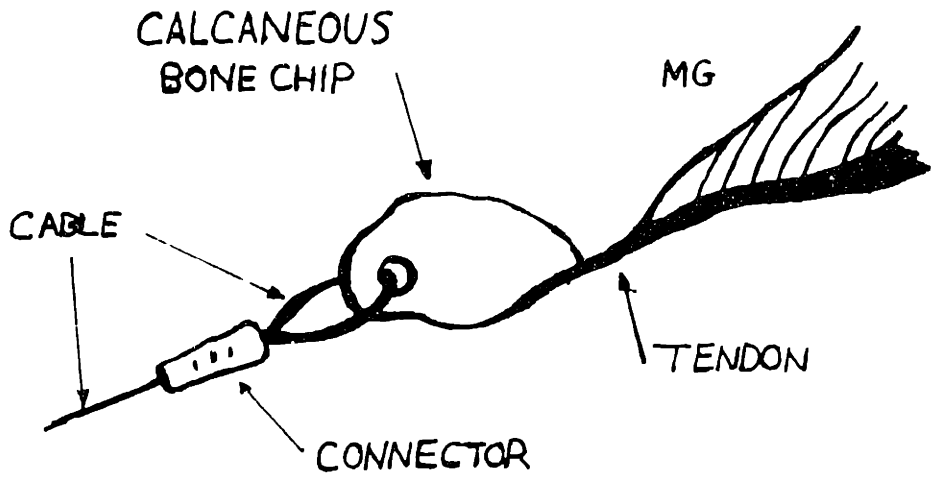

Figure 3.2: MG cable attachment.

the crimp could not grip well. This problem was eliminated for the MG by leaving the tendon attached to a portion of the calcaneous during surgical preparation (Figure 3.2). A hole was drilled in the bone fragment, through which the cable was threaded and then clamped to itself, producing a secure and inelastic connection.

The two cables wrapped around a pulley which was coupled through an in-line torque transducer to the shaft of a DC torque motor, described in the following section. The muscles pulled on the pulley and the motor exerted a torque back on the muscles. For isometric studies, the pulley could be locked into one position with a clamp. The horizontal layout eliminated gravity as a factor.

There are three advantages to using a pulley as a pseudo joint in place of the cat's own ankle:

1. The linear geometry is easier to analyze than the real ankle where muscle moment arms change with joint angle;

2. Unlike the complex joint of the ankle, the pulley has a fixed center of rotation;

3. The surgical isolation of the two muscles is simpler since amputating the foot ensures that no other muscles or connective tissue acts across the joint.

The stepped pulley had two rings, a small one of diameter 25.0 mm for the TA and a larger one of diameter 33.6 mm for the MG, approximate values for the TA and MG physiological moment arms. The unequal moment arms helped counteract the wide strength range in muscles from the two groups. The tendon cables were attached so that the dorsi flexor pulled the load shaft clockwise, the plantar flexor counterclockwise.

Electrodes and Implantation

The two muscles were stimulated via bipolar cuff electrodes (Figure 3.3). The electrodes were constructed of silastic tubing, of external diameter 5 mm for the tibial and 3 mm for the peroneal nerve. The leads were seven stranded 36g stainless steel teflon insulated wire, stripped at contact points and fastened to the silastic base with silicon cement.

The electrodes were implanted by wrapping them around the tibial (ennervating the TA) and peroneal (ennervating the MG) nerves and suturing them in place. To preserve the simplicity of the animal model, all neural signals originating from the CNS, including reflexes, were blocked by transecting the sciatic nerve proximal to the implantation point (Figure 3.4).

3.2.2 Hardware

The layout of the central computer control components is shown schematically in Figure 3.5.

PC Controller

The original hardware setup was controlled by a DEC LSI-11/23 [18] which was shared with other members of the Biomechanics Laboratory. This computer was replaced for increased autonomy as well as for performance and compactness.

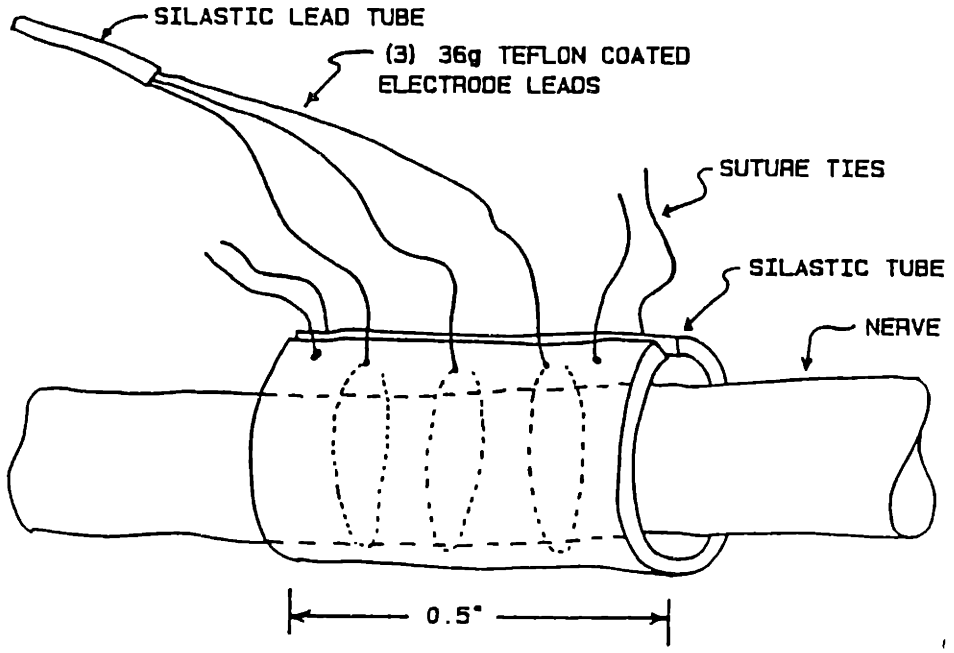

Figure 3.3: Bipolar cuff electrode [18].

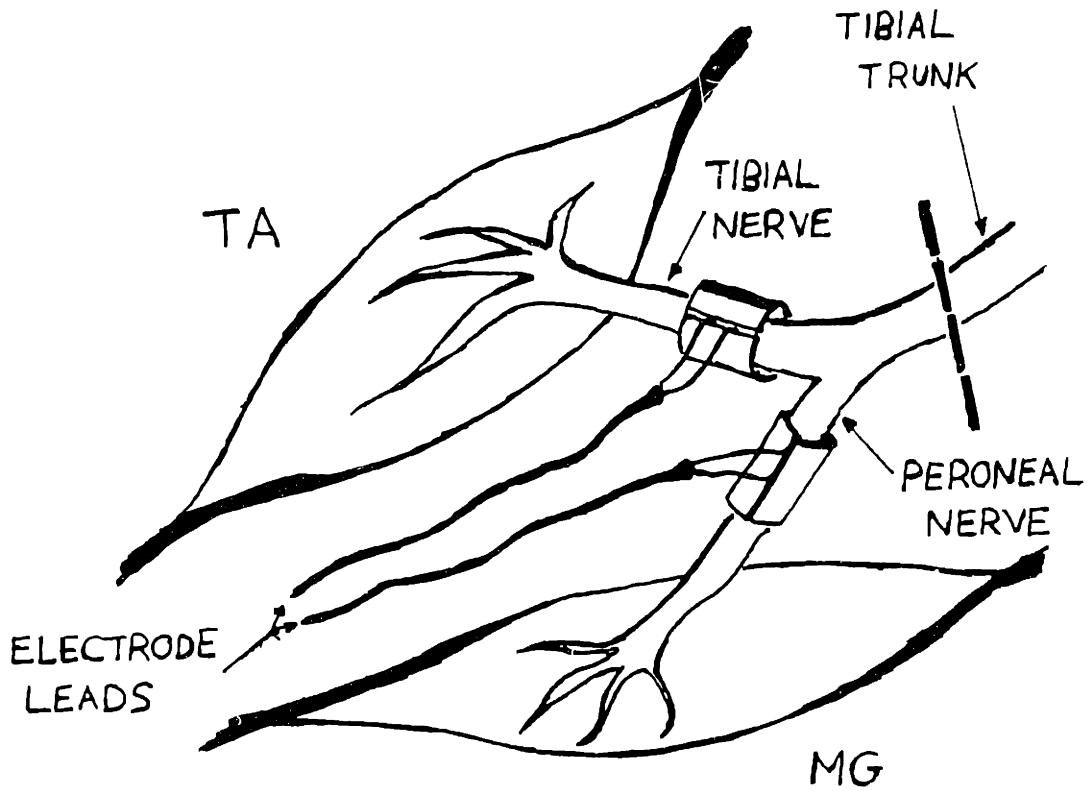

Figure 3.4: Electrode implantation [18].

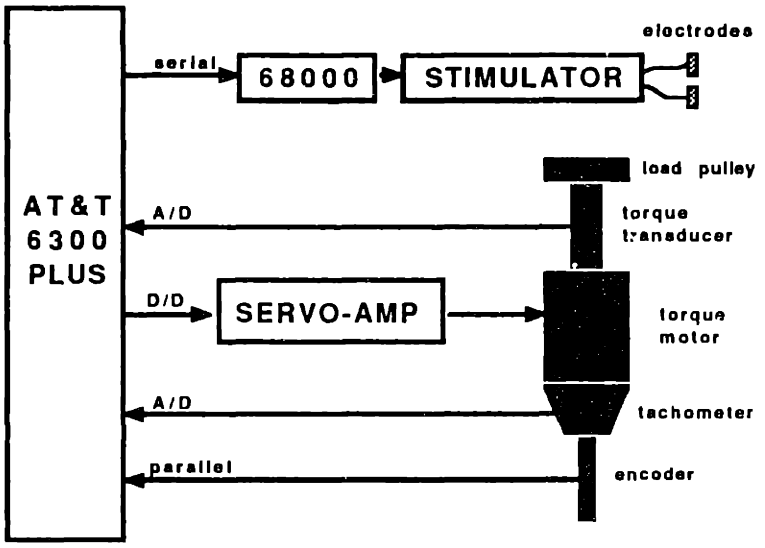

Figure 3.5: Hardware schematic.

The new host CPU was an AT&T 6300 Plus personal computer (an 80286 microprocessor-based IBM PC/AT clone), with 1.2 Mb RAM, an 80287 math coprocessor, a 40 Mb SEAGATE hard disk drive with a Western Digital controller and an MS-DOS operating system. It was expanded with a Metrabyte P1012 24-bit parallel digital I/O interface, an Analog Devices RTI-815-A 8- to 16-channel A/D and 2-channel digital interface, and an ARNET COMH 100 4-port RS-232 serial interface.

Nerve Stimulator

Serial stimulation sequences were delivered to the muscle through a two-channel stimulator unit (Figure 3.6) designed and built by Durfee [18] for this project. It was directly controlled by a satellite single board microcomputer, based on the Motorola 68000 processor, programmed in 68000 assembly language and connected to the AT&T 6300 Plus over a 38.4 baud RS-232 serial line.

The stimulator produced charge-balanced, biphasic square current pulses with 50 μsec spacing between pulse phases (Figure 3.7), a waveform chosen to minimize damage to delicate nerve tissue [12]. It provided a continuous range of pulse amplitude (PA) from 0 to 1.5 milliamps, pulse width (PW) range from 0 to 100.0 μsec in steps of 100 ηsec, and inter-pulse-interval (IPI) range from 0 to 13 seconds in steps of 0.2 msec. For these experiments IPI was held constant at 25 msec (40 Hz), the shortest interval producing an acceptably tetanized contraction while avoiding rapid fatigue. The computer actively controlled the muscles by pulse width modulation (PWM). Since the full dynamic range of TA and MG force was generally recruited over a relatively narrow band of PW, the 100 nsec stimulus resolution was necessary, allowing 200 control values for a dynamic muscle control range of only 20 μsec. PA was manually adjusted for each electrode during the muscle calibration procedure to a value (generally around 1 milliamp) which approximately minimized the slope of the IRC, in order to give the widest range of useful PWM.

The satellite processor computed stimulus PW commands every 5 msec and sent

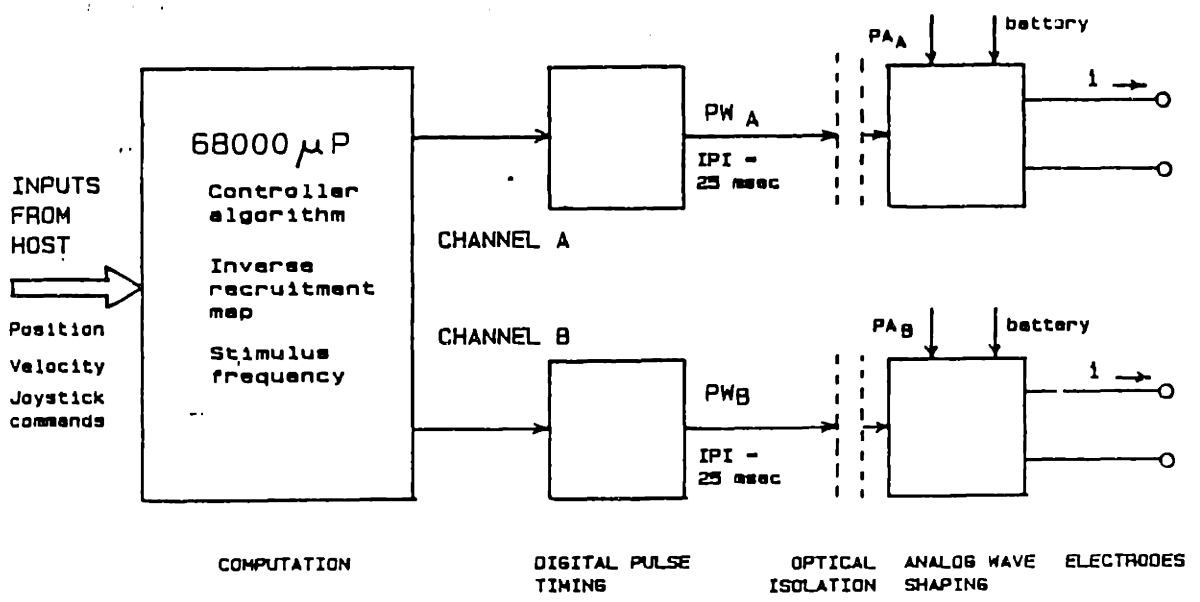

Figure 3.6: Stimulator block diagram [18].

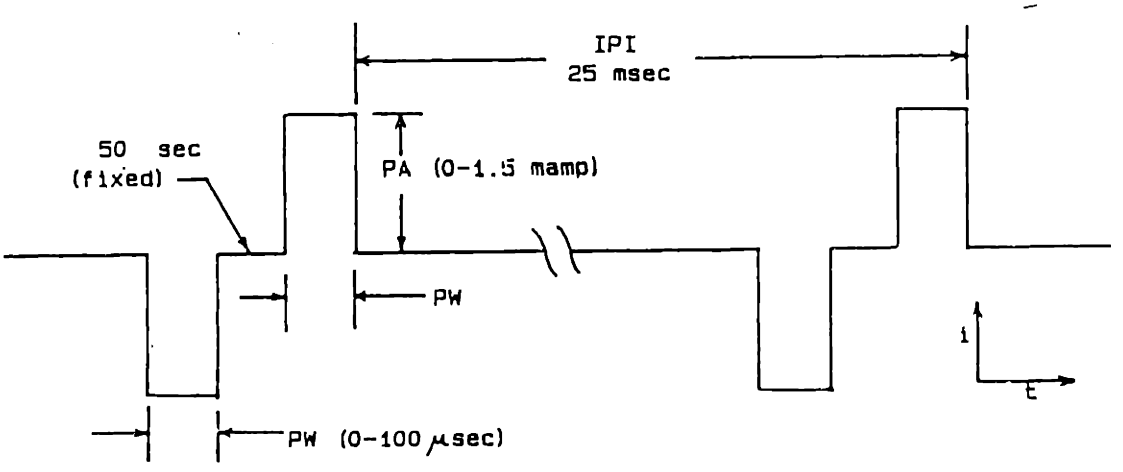

Figure 3.7: Stimulator current waveform [18]. Center electrode contact is (+). Action potential initiation under center contact.

them to two sets of digital and analog circuitry every 25 msec (the IPI) to be converted into the stimulus waveform shown in Figure 3.7.

Primary Torque Motor

A DC torque motor and matching servo-amplifier were coupled directly to the torque load shaft that restrained the muscle tendons. When controlled through a PC analog output channel, it could impose arbitrary lengths, velocites and torques on the torque shaft and the muscles connected to it. The motor's specifications are listed in Table 3.1.

Feedback Channels

The torque motor described above contained an integral tachometer for measuring velocity and an incremental optical encoder for measuring position. Their specifications are listed in Table 3.1. Electronic circuits [18] conditioned these signals for computer input. Although velocity can be derived by sending the output pulses of an incremental encoder to a frequency-to-voltage convertor, tachometers have a better frequency response, producing less ripple at low velocites.

Muscle force was measured by a single in-line torque transducer, based on a full bridge, strain-gauge instrumented aluminum tube, and mounted on the torque load shaft [18]. (Figure 3.8) The sensitivity of the transducer at the strain-gauges was 30.6 micro-strain/lb-in, close to the 30.3 micro-strain/lb-in sensitivity predicted from the solid mechanics of a tube in torsion.

Because of the large differences in the maximum forces generated by the muscles employed (ratios as great as 10/1 were observed), the use in Durfee's setup of a single, fixed operational amplifier circuit to provide bridge gain for both muscles compromised the resolution achievable for either. In order to monitor torques of each muscle over the PC's entire A/D input range, it was replaced with a dual op-amp circuit. Channel gains were independently adjusted with dial potentiometers and sent to the PC through

PRIMARY MOTOR SPECIFICATIONS		
Model Number	JR16M4CH	
Peak Torque	5307.2	oz-in
Continuous Stall Torque	498.4	oz-in
Peak Current	100.8	amps
Continuous Stall Current	9.65	amps
Cogging Torque	0.0	oz-in
Torque Constant (Kt)	53.77	oz-in/amp
Back EMF Constant (Ke)	39.0	volts/krpm
Armature Resistance	0.94	ohms
Average Friction Torque	11.0	oz-in
Viscous Damping Constant	9.12	oz-in/kprm
Moment of Inertia	0.084	oz-in sec-sec
Armature Inductance	<100.0	micro henry
Mechanical Time Constant	3.15	milli sec
Electrical Time Constant	<0.14	milli sec
Diameter	7.38	in
Length (with encoder & tach)	9.5	in
Weight (with encoder & tach)	21.0	lbs

TACHOMETER SPECIFICATIONS		
Open Circuit Output (Ke)	3.0	volts/krpm
Tolerance	1.5	% Ke
Ripple (w/2 KHz single-pole LPF)	4.0	%
Moment of Inertia	0.005	oz-in sec-sec

ENCODER SPECIFICATIONS		
Dual Channel Outputs		
Track Density	1024.0	
Maximum Data Rate	15.0	Khz

Table 3.1: Selected motor, tach and encoder specifications. Reprinted from manufacturer's data sheets (PMI Motors, Syosset, New York).

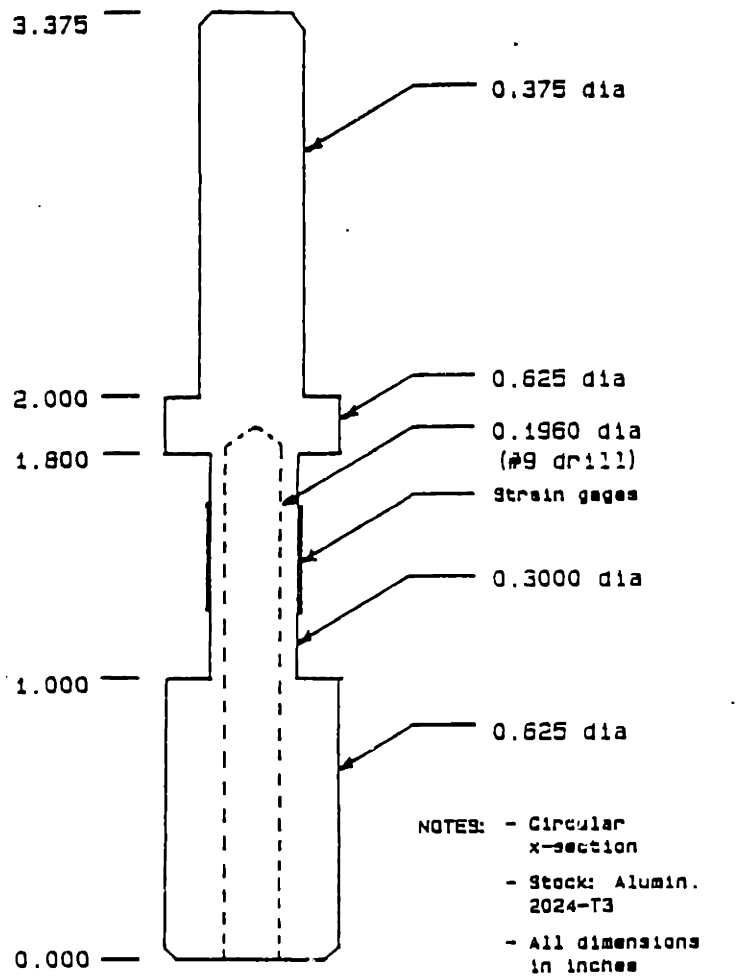

Figure 3.8: Torque transducer [18].

separate A/D channels.

For this study, torque was always sampled at 200 Hz to avoid aliasing by at the 40 Hz stimulus frequency.

Control and Monitoring of Rest Tension

Formerly, isometric tests were conducted with the torque load shaft locked in a single position and the primary torque motor inactive. Because both muscles were attached to the same load shaft so that they pulled in opposite directions, it was not possible to measure either absolute or net torques due to a single muscle. Rest tensions could be measured approximately only once at the beginning of an experimental day. It was observed that the musculotendon unit lengthened and slackened over a period of hours or even minutes. The creep was presumably due to repeated loading and to property changes in the partially exposed tendon, and it was the cause of accumulated error in the initial estimate of rest tension.

It became crucial both to be able to identify independent, absolute muscle rest tensions at any time and to hold them at a constant value throughout the day. A small, geared PM DC servomotor with worm shaft was mounted on the experiment table adjacent to to the torque load shaft, and a matching worm gear (120 teeth, 2.5 in pitch diameter) installed on the main load shaft (Figure 3.9). This secondary motor was controlled independently of the main torque motor by the PC through an analog output channel and matching servo-amplifier. The same servo-amp could be used for both torque motors, since only one motor was ever used at a time.

To best exploit this resource, the two tendon cables were attached to the load pulley and maintained in a slack state when not in use. The load shaft was servoed to the proper rest tension for that muscle prior to every single-muscle test and locked by the nonbackdrivable motor, leaving the other muscle unloaded. Note that this strategy must be modified for the two-muscle, co-contraction tests that are planned for future experiments on this apparatus. No experiments involving simultaneous activation of

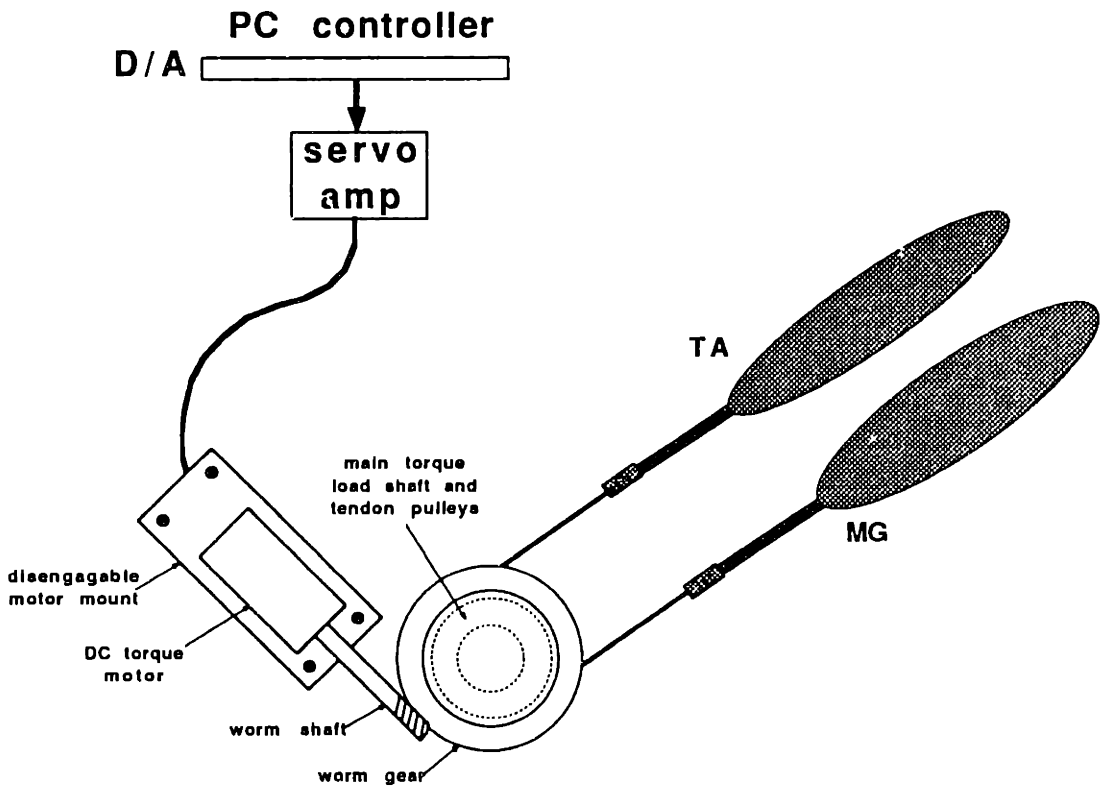

Figure 3.9: Top view of secondary torque motor providing an isometric lock on muscle length.

both muscles were performed in this study.

3.2.3 Software

The replacement of the LSI-11/23 with the AT&T 6300 Plus PC necessitated revision of the low-level libraries supporting the altered hardware interfaces. In addition, new high- and intermediate-level software modules were designed and constructed to execute new tasks of automated data collection for different input types and combinations, of data processing and of model simulations. Software design and library contents are outlined in Appendix B.

In general, low-level hardware-interface subroutines were implemented in Version 4.0 Microsoft Macro Assembler for speed and convenience, while all higher level modules were written in Version 5.0 Microsoft C. The commercial mathematical software libraries utilized (Numerical Recipes [30] and LINPACK [16], generally consisted of Fortran object code which required interfacing.

3.3 Disposition of Subject Animals

Eleven adult cats, referred to as subject animals C1 through C11, were used for this project. One (C1) died prematurely during induction of anaesthesia. Eight (C2–C9) were used to test equipment and procedures and to develop the identification methods; they are the source of most of the data used in Chapter 4.

The last two animals, C10 and C11, were devoted largely to testing of the ID methods in open loop control. They provided the bulk of the results, presented in Chapter 6 and discussed in Chapter 7, on which the conclusions of this thesis rest.

Chapter 4

IRC Identification Methods

The recruitment curve identification methods described in this chapter differ in their complexity, generality, requirements and assumptions, and in the amount and quality of information they supply.

The most fundamental categorization is the use of discrete or continuous input for estimation of a muscle's recruitment curve. The discrete algorithms, the Step Response and Impulse Response Methods, obtain each point of their recruitment curves individually. Were the muscle a time invariant system unaffected by activation history, each point would be independent of the others. In reality, recent activation history does play an important role in muscle response, and the shape of the discretely estimated IRC may exhibit a dependency on the order of command amplitudes. The discrete approach simplifies the process of removing dynamic effects from the sampled output so that the static nonlinearity may be reconstructed, but also associates a cost of time and fatigue with high IRC resolution.

The continuous methods, on the other hand, estimate their recruitment curves from continuous force responses to dynamic inputs. IRC resolution is not expensive in terms of activation and data acquisition time but algorithm development and data processing might be, depending on how well the muscle model describes the system under analysis and on available computational power. These methods are both complicated and enriched by their utilization of dynamic information. A greater effort is required to deduce static relations from continuous data, but estimates of the dynamic system may be made to supplement and correct the muscle model, enhancing dynamic control.

It is plain that the selection of an identification method from among these or others should be influenced by control task type, by the availability and sensitivity of input and output channels — a method's precision need only match that with which the system can be stimulated and measured — and by computational resources. In all cases there remains room for customization to a specific application's requirements.

Organization

The remainder of this chapter is divided into two sections. The first describes and comments on the general algorithms of each identification method. The second details the parameters and techniques used to execute each method in the animal model described in Chapter 2. It also delves into the problems that were encountered during identification method development, and summarizes the steps taken to resolve them.

4.1 Algorithms

4.1.1 Step Response Method

The discrete Step Response Method (**SRM**) estimates a muscle's recruitment curve by activating the muscle at a series of fixed stimulus strengths for periods T_{on}, separated by rest periods T_{off}. The steady state region (T_{ss}) following the initial transient region (T_{trans}) of the force response to each stimulus level is averaged (Figures 4.1 and 4.2). A recruitment curve is constructed from the crossplot of average force against stimulus strength and contains as many points as there are step inputs.

The SRM is the traditional means of estimating a muscle's static nonlinearity. By measuring static response, in the absence of procedural artifacts it conforms to the accepted definition of the recruitment curve. It is unaffected by dynamic nonlinearites and may give a truer estimate of the system static nonlinearity than other (continuous) methods which rely on less fail-safe means of separating the two. Simple to execute, steady state force responses may be found with unsophistocated instrumentation such as a strip chart recorder or a spring scale. If computerized, the method entails a low programming overhead.

Shortcomings of the SRM become obvious when it must be used repeatedly or when a high resolution map is desired. The method is time consuming and fatiguing, and becomes more so with each additional point generated. Even when each stimulus period is followed by a rest period, the muscle is left in a depleted state. For a fast twitch,

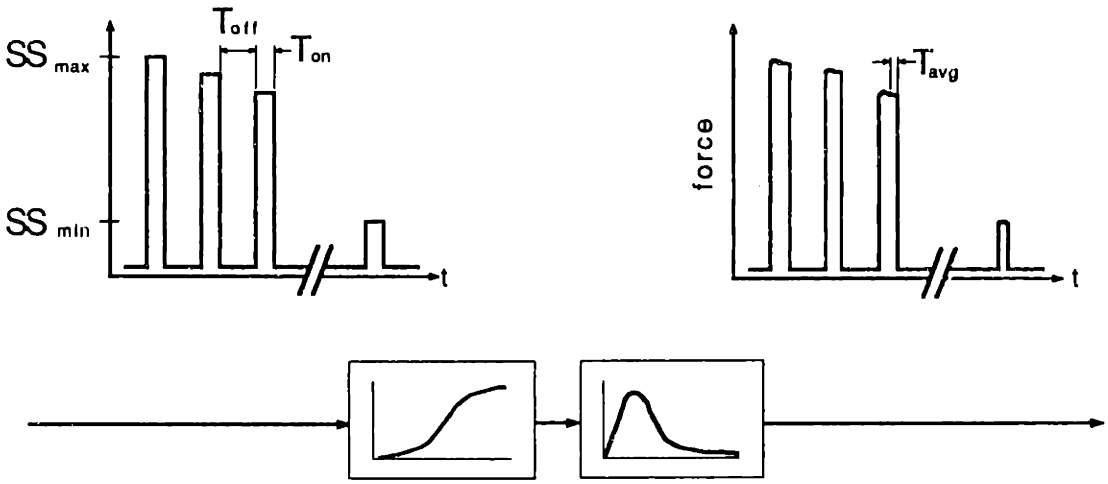

Figure 4.1: Step Response Method I/O time history.

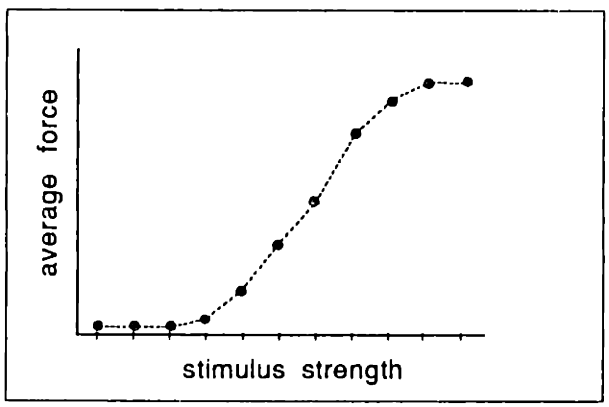

Figure 4.2: Step Response Method recruitment curve.

highly fatiguable muscle, the act of measuring the IRC may cause the actual active zone to shift so far that the estimate is obsolete before it can be used.

The very definition of "steady state" is open to interpretation when the object is muscle force. Short term fatigue sets in before the response has settled out, so that a constant stimulus level will not sustain a steady force level for any length of time. This effect is heightened for later points as the muscle becomes more fatigued. Even with long rest periods, the incidence of fatigue causes the stimulation time history to affect the magnitude of force response to each step input, so that the estimated curve's shape is dependent on the order in which the points are taken.

The method's entirely static nature is a handicap for continuous control of a system with dynamics slow compared to the input signal. The SRM is unable to provide an estimate of dynamic nonlinearity, nor does it offer any means of characterizing the muscle dynamics themselves.

Thus, while steady state response defines a system's *static* nonlinear part it does not necessarily identify all nonlinearity present in the system, and the SRM's usefulness depends on the magnitude and functional significance of system time variation, dynamic nonlinearities and procedural artifacts.

4.1.2 Impulse Response Method

The discrete Impulse Response Method (**IRM**) pairs the peak of the muscle's impulse resonse to a single stimulus pulse with the strength of that pulse (Figures 4.3 and 4.4). Scatter in the stimulus impulse/peak force response relation may be reduced by averaging either multiple responses to the same stimulus strength before measuring peak force, or the peak forces from a number of unaveraged responses. As in the Step Response Method, the resolution of the estimated recruitment curve is determined by the number of distinct impulse inputs applied.

Although the IRM is a discrete method, the fact that impulses are essentially non-fatiguing permits the elimination or reduction of intervening rest periods, shortening

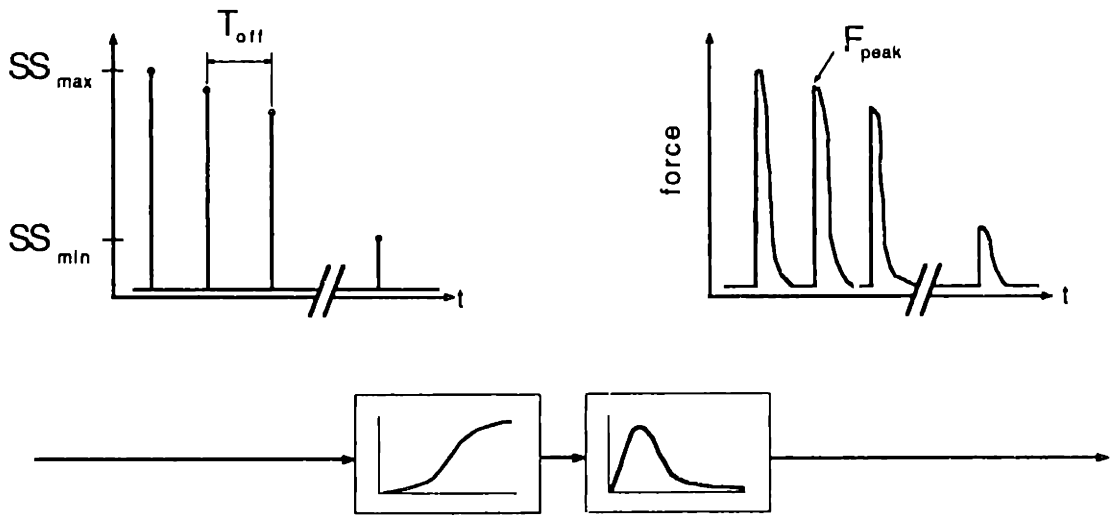

Figure 4.3: Impulse Response Method I/O time history.

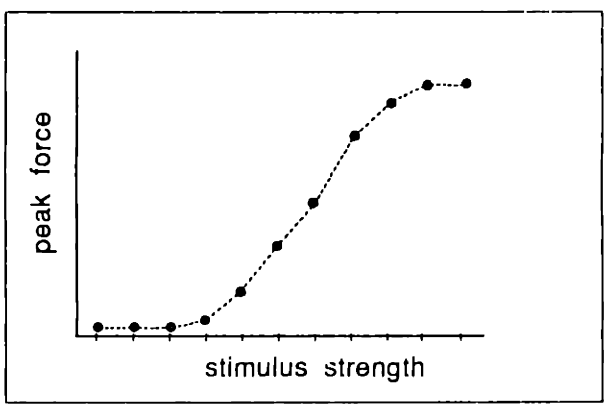

Figure 4.4: Impulse Response Method recruitment curve.

procedure time and minimizing muscle stress. It has the additional virtue of providing a means of estimating muscle dynamics from the recorded impulse response.

The IRM assumes only that the muscle has an impulse response with a peak. However, the degree to which the IRC it estimates reflects static or dynamic nonlinearity is ambiguous since the method utilizes the system's dynamic rather than its steady state response. If the muscle were actually an ideal Hammerstein system with linear dynamics, the step response would be a superposition of impulse responses and the SRM and IRM would give proportional IRC estimates.

In fact, one measure of actual muscle dynamic linearity is the linearity of the impulse/step (also known as twitch/tetanus) ratio to stimulus strength. Other studies have found an impulse/step ratio that varies with stimulus strength, with the magnitude of variation apparently a function of stimulus frequency [29]. However, a nonconstant impulse/step ratio to stimulus strength relation may also be a result of fatigue induced by the step stimuli and of the order sensitivity referred to in the description of the Step Response Method. A parallel means of assessing the linearity of the muscle's dynamics is to observe impulse response shape and pole location dependency on activation level; this will be discussed further in the implementation section of this chapter.

4.1.3 Deconvolved Ramp Response Method

The continuous Deconvolved Ramp Response Method (**DRRM**) deconvolves the force response to one or more triangular SS ramps through a linear approximation of the dynamic system transfer function, obtained from the measured impulse response. The system's static nonlinearity is estimated by crossplotting the deconvolved force sequence against stimulus input (Figure 4.5).

The DRRM is designed for an ideal Hammerstein system, the SNLS–DLS pair described in Chapter 2. In its most general form, the DRRM makes no assumption as to the order or parameters of the DLS other than its stability. In practice, however,

(i)

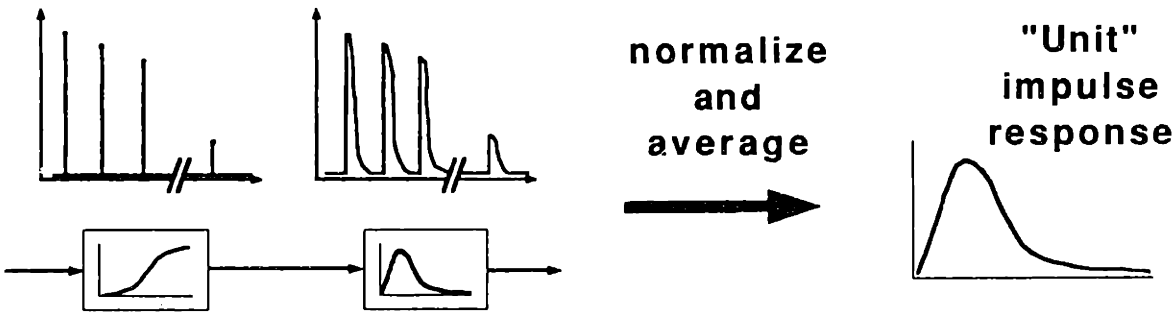
normalize
and
average
"Unit"
impulse
response

(ii)

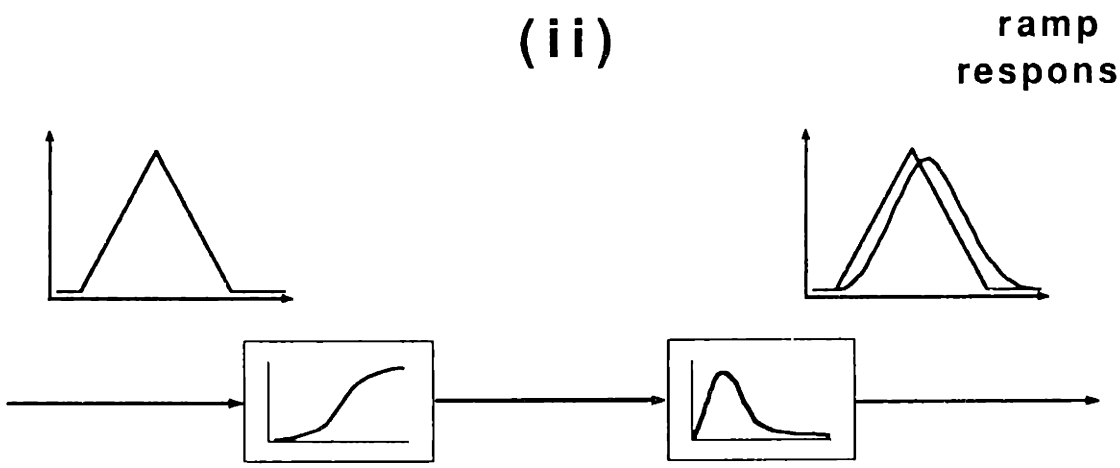
ramp
response

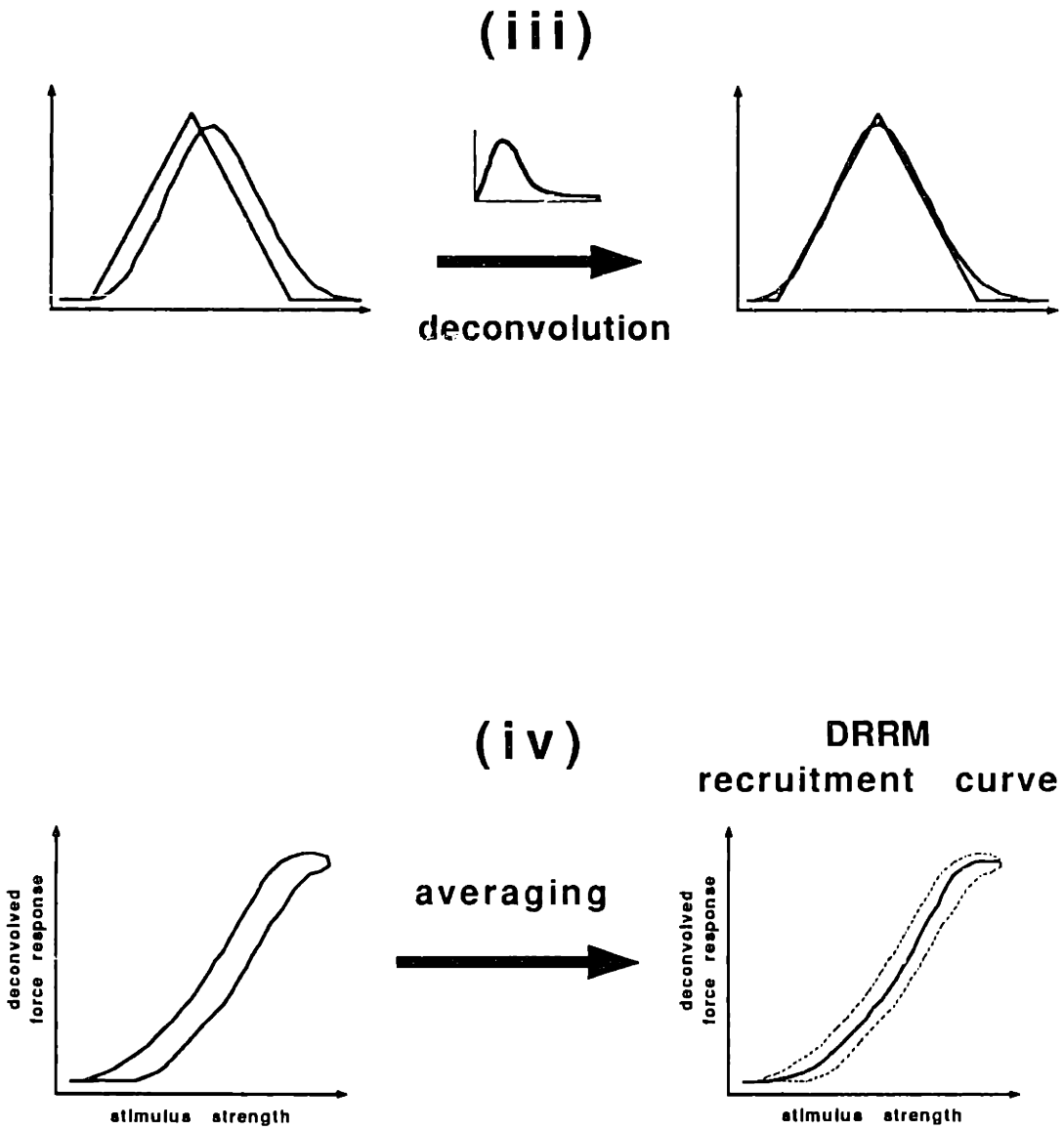

Figure 4.5: Algorithm for the DRRM. Its IRC is the averaged, deconvolved force response to multiple ramp SS inputs.

noise in the output may necessitate smoothing or other processing of the experimental impulse response prior to deconvolution. It is also convenient to constrain the dynamic system's order and/or damping ratio (ζ) so that a noiseless system may be synthesized and used in place of the actual one. As noted in Section 4.2.3, the stimulated muscle dynamics are approximated in this work as second order and critically damped ($\zeta = 1$) with real and equal poles. The method's power depends in part on such an assumption's validity for the system under consideration.

The DRRM offers an estimate of the muscle dynamics to go along with its estimate of the static nonlinearity, a boon for continuous signal processing. The ramp input signal is both physiologically realistic and clinically useful. It requires less total activation time than does the Step Response Method, and consequently causes less fatigue.

Although simple in concept, the DRRM's implementation may be plagued with stubborn complications such as deconvolution noise amplification and the need for parameter optimizations. The procedure must be a compromise between noise reduction and retention of important information, an optimization of a number of parameters and techniques.

Without the DRRM deconvolution, hysteresis caused by muscle dynamics may distort a dynamic identification method's IRC estimate beyond usability. To verify this the Ramp Response Method (**RRM**), a quick-and-dirty version of the deconvolved method using the ramp response to estimate the IRC directly without incurring the expense of dynamic system estimation and deconvolution, is tested here as well. Hysteresis is dealt with in the RRM by averaging force responses to the ascending and descending sides of the ramp stimulus (Figure 4.6).

The RRM is trivial to implement and requires negligible stimulus and processing time, but it mixes static and dynamic information. It would be technically correct only for a muscle with no dynamics, in which case there would be no hysteresis to reduce. The ability of response averaging to account for the presence of a dynamic system must be assessed empirically, since it depends on characteristics of the actual system's static

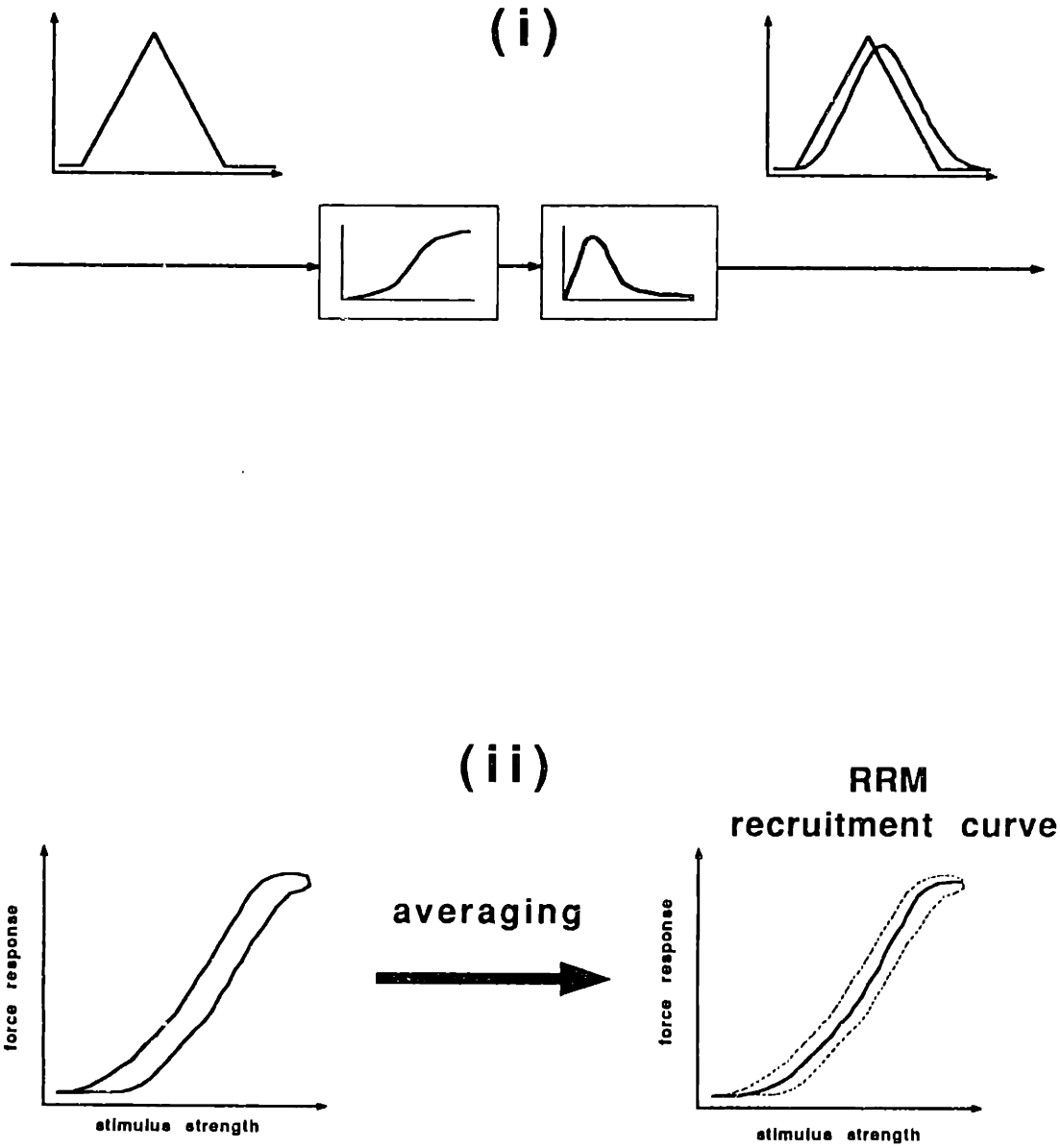

Figure 4.6: The RRM IRC is estimated by averaging force response to the ascending and descending sides of ramp SS input.

and dynamic parts. When slow ramp inputs are used (ramp period large compared to the muscle's impulse response time to peak), dynamic effects in the ramp response can be ignored but fatigue contamination may become a problem, and it is not clear whether the method becomes more reliable. Map points near input discontinuities (ramp base and peak) remain distorted, with the extent of contamination dependent on the ramp's slope.

4.1.4 Stochastic Response Method

The Stochastic Response Method (**StoRM**) is a technique of nonlinear system identification which iteratively determines the best-fit static and dynamic parts of the system described by a stochastic input-output pair. Based on the Hammerstein model, it is the same concept as a procedure described by Hunter and Korenberg [10,28,29], although characteristics of the stimulated muscle structure being studied here were better accommodated with a different implementation (Section 4.2.4).

Figure 4.7 illustrates StoRM's algorithm. The objective is to find the intermediate state

$$V = Q(X) = \frac{Y}{H}, \tag{4.1}$$

where Q is a static relation defined by the SNLS block of the Hammerstein muscle model and H is the transfer function corresponding to the DLS block. In this discussion, consider X, V, Y, Q and H as generalized, dimensionless states and functions referring to either time or frequency domains, subject to the algorithm's implementation.

(*i*) After obtaining an experimental Y in response to input X, an initial guess of V is made by approximating a linear Q so that $\hat{V}_x$ (V as estimated from X) is initialized as X.

(*ii*) The best-fit dynamic linear system $\hat{H}$ is found between $\hat{V}_x$ and Y.

(*iii*) A new estimate of V, $\hat{V}_y$, is formed by deconvolving Y through the estimated $\hat{H}$.

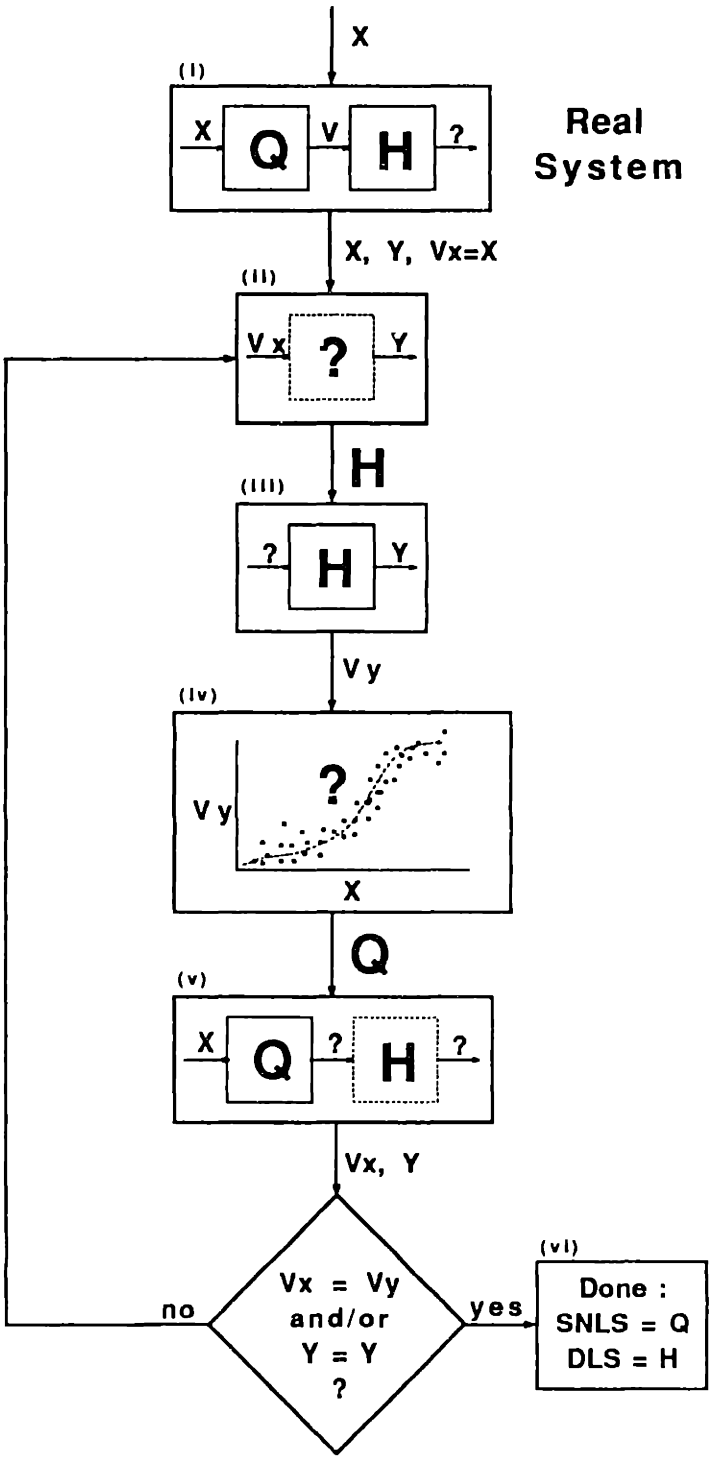

Figure 4.7: Algorithm for the StoRM.

(*iv*) $\hat{V}_y$ is then used with X to find the best-fit $\hat{Q}$ relating them.

(*v*) $\hat{V}_x$ is updated by evaluating $\hat{Q}(X)$.

(*vi*) If desired, the output may be predicted ($\hat{Y}$) by convolving $\hat{V}_x$ through $\hat{H}$ for comparison with the actual output Y. This step is not necessary for the iteration to proceed.

Steps ($ii - v$) of the procedure are iterated to satisfactory convergence, defined by either $\hat{V}_x \rightarrow \hat{V}_y$ or by $\hat{Y} \rightarrow Y$. Both criterion should converge at the same rate, since they are interdependent. Although there is no mathematic proof that the iteration will converge, it has been shown to do so for many reasonable cases of nonlinearities [2] and has always done so in simulations performed here. It is unclear what the method returns if the actual system is not adequately described as a Hammerstein system, although presumably it finds some best-fit combination of SNLS and DLS. In between the cases of a perfect Hammerstein system and a system which does not conform to the model at all is a gray area where the model's adequacy and this identification technique's viability are subjective questions.

Observe that the above procedure is readily modified for use by systems better described by cousins of the Hammerstein model, such as the Weiner or SDS models (Chapter 2).

The StoRM's chief usefulness, and the justification for the large investment of development, stimulation and processing time it requires,[1] is its generality. Since its only constraint is that the system fit a Hammerstein model, it may yield more immediate information about a system of which little is known (recall that in practice it is convenient to constrain the DRRM's DLS to be second order and critically damped). Further, excitation of the muscle with a stochastic input produces an output rich in frequency content, which theoretically should facilitate the estimation of the dynamic

[1] Because of the iterations, StoRM computations take longer than least-squares model parameter optimization [3,9].

system. This quality may be further exploited by band-limiting the frequency of the input signal to the range of interest for the system being studied.

The StoRM will fail if the Hammerstein model does not adequately describe the stimulated muscle. This is most likely to occur through the model's neglect of dynamic nonlinearity, of systemic and measurement noise and of system time variance (*i.e.* fatigue) during an input signal sequence. Where dynamic nonlinearity is significant, the first deficiency will be difficult to remedy without a more complex model. The second may be attacked with a variety of smoothing and filtering tools, while the third necessitates compromise between input duration and response information content.

4.2 Implementation and Development

This section describes how the identification methods were implemented in this study. Included for completeness, clarity and as an example, all implementation notes should be questioned and appropriately modified before transfer to other systems.

In addition, some questions and problems that were encountered during ID method development are discussed, and their resolution is supported by simulations and with experimental data obtained using the animal model of Chapter 3. For a complete disposition of experimental subjects please refer to Section 3.3.

Some of the algorithms were still under development at the time of this writing, and the listed processing times are greater than those achievable with more streamlined execution.

Modeling of Discontinuous Input

"Continuous input" is in some respects a misnomer when applied to pulsewidth modulation (PWM), the stimulation technique used in this experimental model. In reality, a continuous serial command is converted by the stimulator into biphasic spikes at an interval that just achieves tetanus, 25 milliseconds. A 40 Hz (f_{stm}) stimulus artifact is clearly visible in all of the continuous, 200 Hz (f_s) data and frequency response records in this study. A higher stimulation rate would give smoother contraction and greater forces, but because because of synchronous nerve and muscle fiber activation it would also time the muscle more quickly.

The continuous identification methods could not be successfully implemented without recognition of the discontinuous input. In fact, the stimulator input's discrete nature blurs the distinction between what have been labeled "discrete" and "continuous" identification methods. In fact, the latter also use discrete input, but spaced much more closely in time.

The input was modeled as a smooth command discretized by the stimulator to a sequence of 40 Hz impulses with amplitudes proportional to those of the continuous

command at that point, The output was modelled as a sampled sequence of superposed impulse responses.

4.2.1 Step Response Method

The generalized Step Response Method I/O time history was pictured in Figure 4.1. For this study, eleven step stimulus inputs of durations T_{on} of 1.0 seconds were applied in descending order, at 10.0 second (T_{off}) recovery intervals. They were preceded by a 2.0 second maximal strength conditioning burst and a 10.0 second rest.

The first input was the maximum available stimulus strength (100.0 μsec), while the remaining input amplitudes were distributed uniformly in the current zoomed stimulus range. For example, the input sequence for a muscle whose current stimulus range was 30.0 to 80.0 μsec would be [100.0, 75.0, 70.0, 65.0, ..., 35.0, 30.0] μsec.

The second 0.5 seconds of sampled force values were averaged to obtain the steady state response. The IRC estimate was constructed by plotting the eleven averaged steady state force responses against their corresponding input stimulus amplitudes.

Total data acquisition and processing time was 2.0 minutes, and had to be followed by a minimum of 10 minutes of rest.

Step Command Shape

Despite the SRM's reliance on its accuracy, "steady state" is at times a dubious description of the muscle step response. Figure 4.8 shows some particularly irregular force responses to step inputs of several different strengths, applied to the MG of subject C8. Force was averaged over the second 0.5 seconds of the response, and it is plain that for some records force did not settle in the entire 1.0 second, and sometimes began to drop off because of fatigue during the averaging period. In general, however, step responses resembled the highest of those displayed, where the muscle did reach a semblance of steady state.

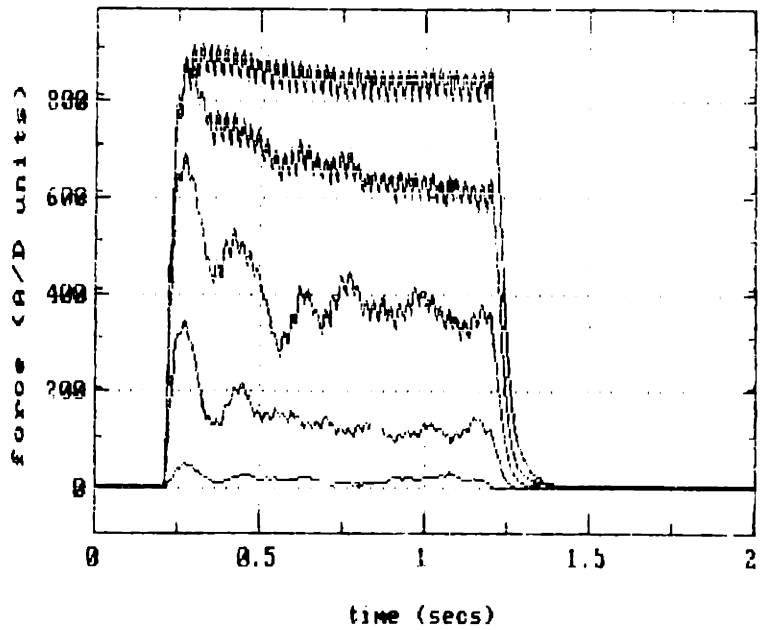

Figure 4.8: Step responses to stimuli of different amplitudes, exhibiting shape variation and "steady-state". MG, C8.

Step Command Order

Step responses are fatiguing, and it was expected that recent activation history would influence the shape of recruitment curves estimated by the Step Response Method. A muscle which has been subjected to a protracted, high-strength stimulus will have a diminished response to a later stimulus. The steady-state response to a particular step command becomes a function of the magnitude of not only that command but also of commands preceding it, so some discretion was required in the ordering of step input amplitudes.

Data sets were taken with SRM step input amplitudes arranged in descending, ascending and randomized sequences. The three command sequences were applied at 10 minute intervals in the order listed to the TA of subject animal C8. Their corresponding recruitment curve estimates are shown in Figure 4.9.

The three curves (shown unnormalized) are not identical; in fact, it will be seen later (Section 6) that they differ in shape even more than do some IRCs estimated by different

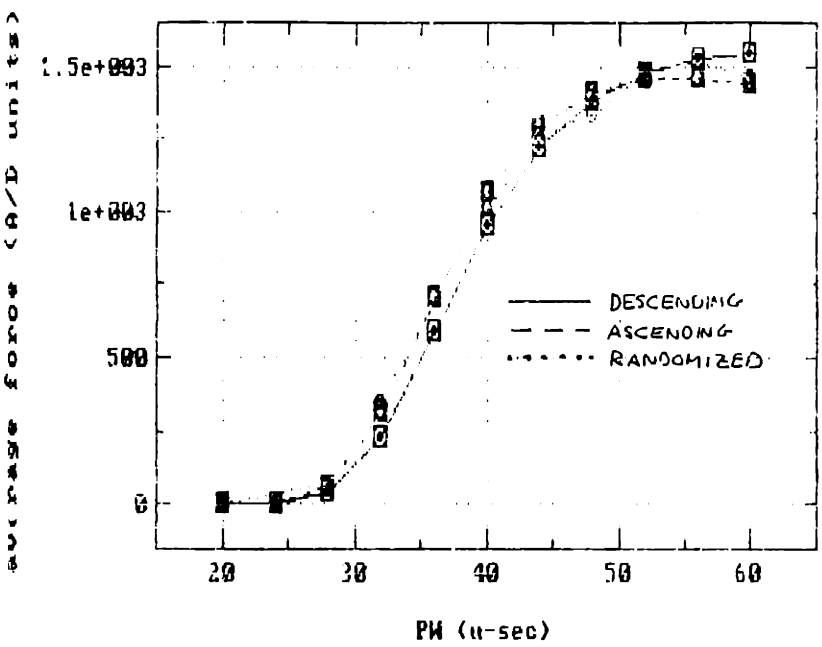

Figure 4.9: SRM recruitment curves for descending, ascending and random ordering of step amplitudes. TA, subject C8.

methods. For each given stimulus strength except the highest three, the descending curve predicts a smaller force than does the ascending curve, while the randomized curve wanders between the other two. This phenomenon is easily ascribed to fatigue. Note that when the curves are normalized to their own peaks[2], the discrepancy is exaggerated because the ascending curve peaks before the last stimulus, the final two points paying the toll of progressive fatigue.

The curves derived from normalized descending and ascending step commands will cause a controller to err in opposite directions because the descending IRC overestimates the stimulus required to produce a given force for all but the highest commands, so force from an unfatigued muscle will overshoot the command; likewise, the ascending curve will cause the muscle to undershoot the command. Further, in some OLC tests (Section 6.4) it was observed that the descending SRM curves had a tendency to overestimate threshold stimulus, with an accompanying degradation of control.

[2]Normalization is required preparatory to inversion for use in the feedforward block of an open loop controller, which recognizes commands between 0.0 and 1.0; Section 5.3

For this study, a descending curve was used for the SRM because it was considered the most accurate over the most points. However, for situations where control near threshold and the lower end of the active zone is more critical than over the rest of the curve, an ascending step ordering might be more appropriate.

4.2.2 Impulse Response Method

IRM input (Figure 4.3) was a train of four repetitions each of ten stimulus amplitudes distributed evenly over the current stimulus zoom zone, in the same manner as the step inputs of the SRM. The 40 impulses were randomized before application, preceded by a 2.0 second maximal conditioning burst and 10.0 seconds of rest, and applied at 1.7 second intervals dictated by the maximum of impulse response duration and (here) processing time.

Peak impulse response force as a function of stimulus strength was found after averaging the responses to the four repetitions of each stimulus strength. If desired, muscle dynamics could be estimated from the measured impulse responses as for the Deconvolved Ramp Response Method, with the procedure described in the next section.

Combined data acquisition and processing time as the IRM was used here was 1.4 minutes. If peak force was estimated from a single repetition of each impulse amplitude, the IRM took approximately 0.5 seconds.

Number of Impulse Responses to Average

Each point in the IRM recruitment curve was the peak force registered in response to an impulse of a particular stimulus strength. For this time-varying system, it was unreasonable to suppose that there would be no variation in peak force magnitude among different responses, even for a relatively nonfatiguing impulse input. Empirical evidence was needed to assess the extent of variation and to determine how many responses should be averaged to obtain a "typical" peak force.

Note that here we are concerned only with variation in magnitude, and to a lesser

degree the shape, of the response to constant impulse stimulus levels. The culprit is system time variation and fatigue sensitivity rather than the time-invariant relation of impulse response shape to stimulus strength.

Impulse trains were composed of four repetitions each of ten amplitudes distributed evenly over the current zoom zone. They were applied over several experiments with the same protocol as for the Impulse Response Method, with stimulus strengths randomly ordered and spaced by 1.7 seconds. The responses were sorted by input amplitude, and raw amplitudes and shapes were compared with averaged values for magnitude and shape differences. These results are shown in Figure 4.10 for the TA of subject C8, which contains four unaveraged impulse responses to a single stimulus pulse amplitude of 100 percent of the current zoom zone.

Recruitment curves are displayed in Figure 4.11. The three IRC estimates are peak force/stimulus strength crossplots, where each peak force is taken from four, two or one averaged impulse responses to that stimulus strength.

Impulse response amplitude is consistent enough at a given stimulus strength that four repetitions are probably unnecessary. Taking peak force from a single raw impulse response would cut the IRM's time requirement by nearly a fourth. However, the full allotment of repetitions (four) was used in this study since speed was not a critical factor.

4.2.3 Deconvolved Ramp Response Method

The DRRM's algorithm was shown graphically in Figure 4.5. In its implementation here, four triangular ramps over the current zoomed stimulus range were input. Half-ramp periods (T_{hr}) of 1.0 seconds were used for muscles that had impulse response time-to-peaks, τ_{peak}, of 20-60 msec and impulse response durations of 200-600 msec. Repeated ramps were separated in time by a minimum of the impulse response duration, here taken conservatively to be 0.5 seconds (T_{Roff}).

Ramp responses were filtered in the frequency domain to eliminate measurement

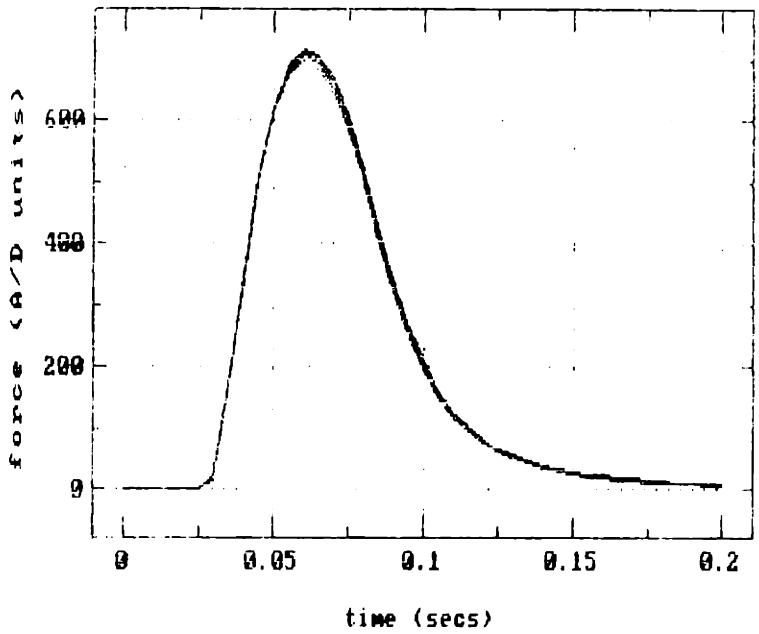

Figure 4.10: Four impulse responses showing magnitude and shape consistency for stimulus strength 100% of the current zoom zone. TA, C8.

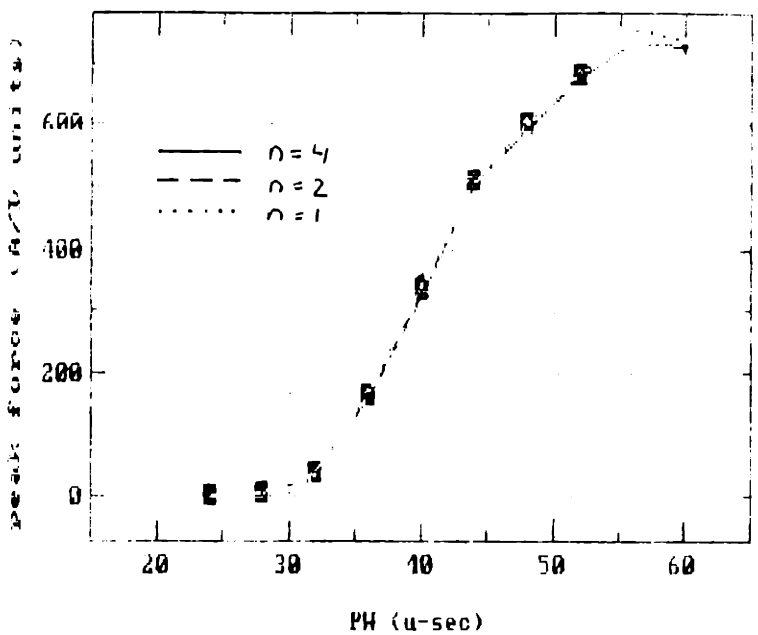

Figure 4.11: IRM IRCs with each peak force averaged from 4, 2 or 1 responses to maximal-strength impulses. TA, subject C8.

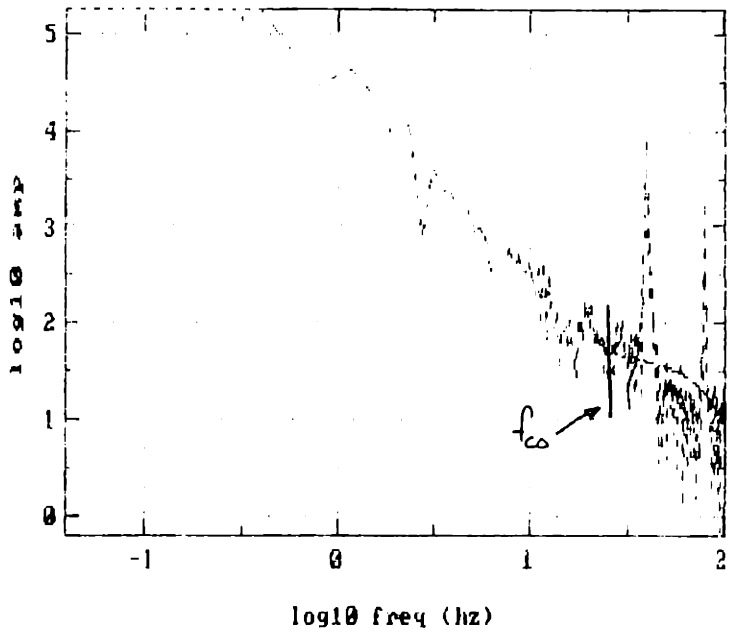

Figure 4.12: Ramp output dynamic response, illustrating choice of f_{co} for filtering.

noise and stimulus artifact. Each raw ramp response was individually Fourier transformed in a single segment, and a straight (linear scale) line drawn through the transform connecting the frequency response at cutoff (f_{co}) and Nyquist (f_{ny}) frequencies (Figure 4.12). The minimum f_{co} giving adequate noise reduction while retaining sufficient information to identify a hard nonlinearity varied with preparation; values from 12 to 25 Hz were used here.

Each ramp response was individually deconvolved in the frequency domain through a linearized approximation of the dynamic subsystem's transfer function. Transfer function poles were estimated by inverting τ_{peak} (as will be described shortly) of four averaged responses to maximal spike inputs which were applied immediately prior to the ramp ensemble. The spikes were preceded by a 2.0 second maximal conditioning burst and 10.0 seconds of rest (T_{Coff}), and spaced by 1.7 seconds (T_{Ioff}) as for the Impulse Response Method.

The DRRM IRC was estimated from the average of the ascending and descending sides of the four filtered, deconvolved ramp responses. Perfect deconvolution of an

output consisting of a train of impulse responses would give a deconvolved, intermediate sequence that was a series of 40 Hz spikes. The imperfect deconvolution here could not achieve this (which was why the output had to be filtered before deconvolution), but it was still advantageous to use only the spike points to form the map. Therefore, the estimated IRC's resolution was $T_{hr} \cdot f_{stm}$, rather than $T_{hr} \cdot f_s$. The averaging of multiple deconvolved ramp responses helped to reduce uncorrelated noise, permiting employment of a higher filtering f_{co}.

The RRM IRC was estimated from the average of the ascending and descending sides of the four raw ramp responses.

Total acquisition and processing time for a DRRM IRC estimate using four impulse responses and four repetitions of a ramp with a 1.0 second half-ramp period was approximately 1 minute.

Dynamic Subsystem Estimation from Impulse Response

The muscle's Dynamic Linear Subsystem (DLS) was estimated from the system impulse response in conjunction with its static nonlinear subsystem by the DRRM. In addition to serving in a descriptive capacity and as an integral part of the DRRM, the linearized dynamic subsystem estimate ($\widehat{\text{DLS}}$) was inverted as outlined in Section 5.3 to test IRC estimate effectiveness in open loop control tasks.

How good this approximation needed to be, the best way of getting it and the best way of using it were not clear to begin with. A single raw impulse response could not be used without any further processing because it was contaminated with noise and a time delay, and the linearity of its relation to activation level was uncertain.

Time Delay: A small pure time delay was consistently observed in recorded impulse responses and tentatively imputed to the time required for the signal to travel down the nerve axon from electrode to muscle. It was a matter of technical interest to ascertain the delay's source, although the knowledge would not affect the way it was treated. Whatever its cause, if ignored this delay would produce an erroneous time-to-peak

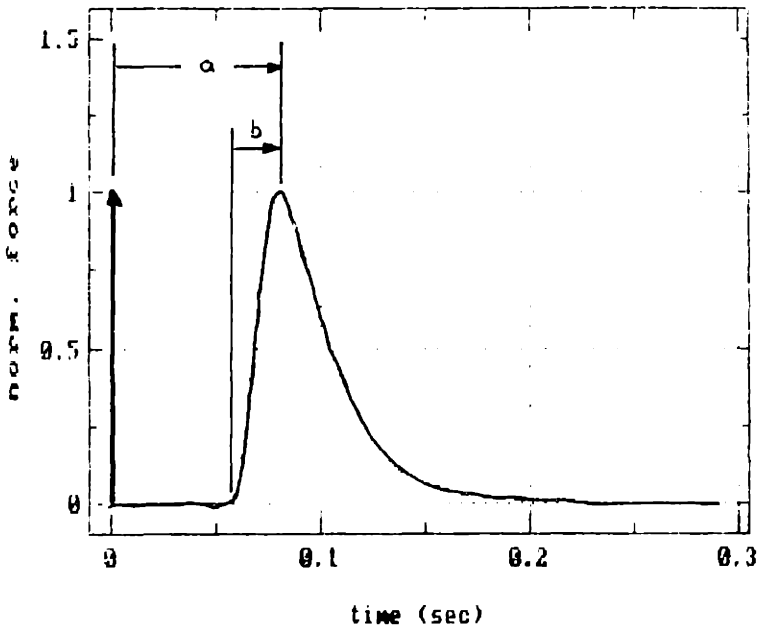

Figure 4.13: Typical impulse input and force response time history demonstrating the observed time delay. TA, C8.

(τ_{peak}) measurement and distortion of the dynamic system pole estimate.

The delay, τ_{del}, was measured from impulse application at t_0 to the first force response value greater than 10.0 percent of the impulse response maximum. It was found to vary with individual and muscle, less so within a muscle preparation. A typical experimental impulse and response time history, taken from the TA of subject C8, is shown Figure 4.13; note the incorrect (a) and correct (b) ways in which τ_{peak} might be measured. Values for τ_{del} ranged from 10 to 30 with a mean of 21 and standard deviation of 73 milliseconds over 8 muscles; specific values are listed in Table 4.1.

During surgical preparation, the nerve cuff electrodes were placed on the tibial and peroneal nerve axons approximately 5 cm proximal to their connection with the TA and MG muscles, respectively.

It was first conjectured that nerve conduction was responsible for the time delay. If so, the signal must have been traveling with a velocity of .05 meters/.02 sec, or about 2.5 m/sec. Conduction velocities of 100 to 120 m/s have been reported for Group Ia

Subject	TA τ_{del}(msec)	MA τ_{del}(msec)
C8	25	25
C9	30	30
C10	15	10
C11	15	15

Table 4.1: Measured time delay (τ_{del}) for several subjects.

nerve axons [19], of which these nerves are composed. Therefore, nerve conduction is not a plausible explanation for this time delay.

It is not clear what is causing the time delay, nor whether it is a hardware detail or an actual physiological phenomenon. The experimental impulse response was corrected before further processing by left-shifting it $\tau_{del} \cdot f_s$ points.

Modeling of the Dynamic Linear Subsystem: Both direct time deconvolution through the raw impulse response and Fourier transformation of the raw impulse response for frequency domain deconvolution produced an intermediate sequence estimate severely contaminated with amplified noise. Mere averaging of multiple n-point experimental impulse responses proved to be an inadequate means of noise reduction, and application of a variety of filtering techniques improved the result only marginally.

Another approach was to use poles estimated from the raw impulse response to synthesize a noiseless transfer function estimate, $\widehat{\mathrm{DLS}}(s)$. The only remaining source of noise was the more manageable level in the recorded output sequence itself. This "purification" process had the additional virtue of compacting the information contained in the experimental impulse response, generally 40 to 100 values, into one or two variables which were more conveniently manipulated and compared. By the same token, some potentially useful information was thrown away.

Muscle dynamics have been assumed (Chapter 2) to be representable by a second-

order linear system:

$$\widehat{\mathrm{DLS}}(s) = \frac{\hat{\sigma}_1\hat{\sigma}_2}{(s+\hat{\sigma}_1)(s+\hat{\sigma}_2)}, \tag{4.2}$$

where $\hat{\sigma}_1, \hat{\sigma}_2$ refer to the poles of the dynamic system. In estimating system roots from the impulse response, a decision had to be made whether to narrow the model's generality by constraining the damping ratio, ς, to unity (a critically damped system with repeated real poles) in order to simplify the estimation step. To see how well the $\varsigma = 1$ assumption described the muscle dynamics, four cases were considered and their closed-form impulse response solutions compared with an averaged experimental one:

1. $\varsigma = 1$ (critically damped):
   $\hat{\sigma}_1 (= \hat{\sigma}_2) = 1/\tau_{peak}$ where τ_{peak} is the time-to-peak measured directly from the averaged, shifted experimental impulse response function [27].

2. $\varsigma = 1$ (critically damped):
   $\hat{\sigma}_1 (= \hat{\sigma}_2)$ found by a parametric optimization of the impulse response unit closed-form solution to the averaged, shifted experimental impulse response function using the method of Marqhardt and Levinson [30].

3. $\varsigma > 1$ (overdamped):
   $\hat{\sigma}_{1,2}$ found by parametric optimization as in (2).

4. $\varsigma < 1$ (underdamped):
   $\hat{\sigma}$, $\hat{\omega}$ found by parametric optimization as in (2).

Note that the parametric optimization is costly in terms of both development and computational time, demanding a significant boost in performance to justify its routine use.

The case of $\varsigma < 1$ was included because some experimental twitch responses (particularly those of the MG) displayed oscillatory, albeit non-second order and perhaps nonlinear behaviour; one such record is used in the following examples. Although the

(a) TA

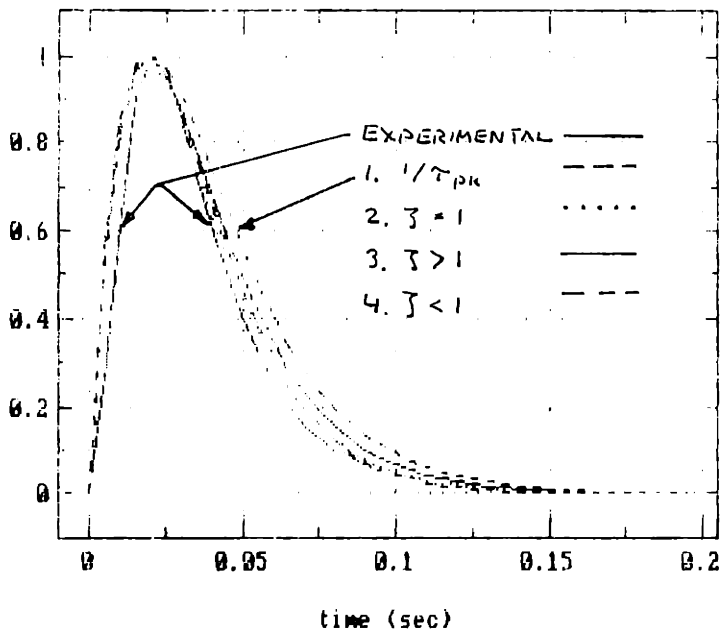

(b) MG

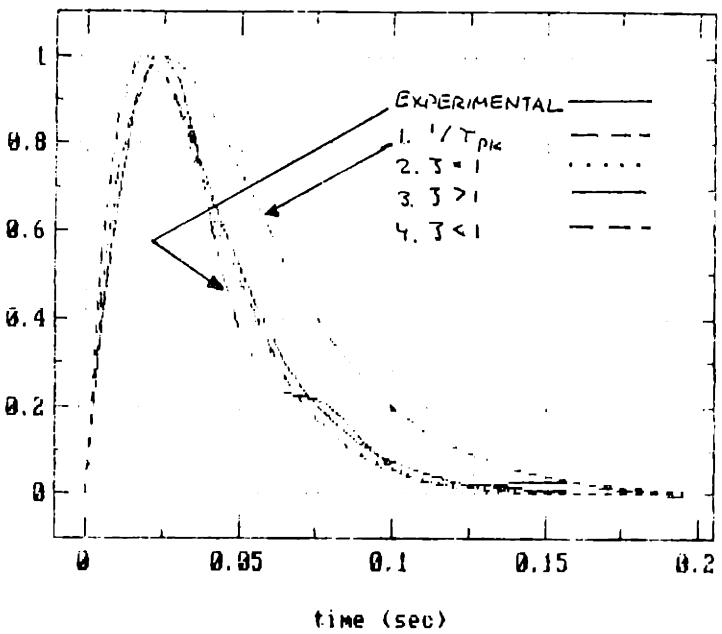

Figure 4.14: Experimental and simulated impulse responses for DLS model assumptions. Data from (a) TA and (b) MG, C11.

time histories were not typical second-order underdamped responses, it was thought that an underdamped, optimized model might improve the fit of model to data.

Using each of these four DLS models, poles were estimated from an impulse response function which was the average of four responses to maximal impulse stimulus inputs to the TA and MG of subject C11, and which had been shifted according to the measured time delay.

Results are illustrated in Figure 4.14, where the averaged, shifted experimental impulse response ($\mathrm{dls}(t)$) is compared with closed form solutions ($\widehat{\mathrm{dls}}(t)$) calculated using poles estimated using the indicated DLS model assumption. Estimated root locations ($\hat{\sigma}$,$\hat{\omega}$) and a χ^2 error parameter,

$$\chi^2 = \frac{1}{N}\sum_{i=1}^{N}\left[\mathrm{dls}(t) - \widehat{\mathrm{dls}}(t)\right]^2, \tag{4.3}$$

are listed in Table 4.2, where N is the number of points over which the impulse response function is measured or optimized.

It is clear that while using the first, critically damped model ($\hat{\sigma} = 1/\tau_{peak}$) guarantees that the simulated impulse response will have the same time-to-peak as the experimental one, this is at the cost of a poor match to the experimental response's tail. The problem does not appear to be in the assumption of critical damping. For both muscles, the critically damped, parametrically optimized model lies closer to the experimental response over its entire length and has a smaller χ^2 value than does the overdamped model. The model which permitted $\varsigma < 1$ (an underdamped system) arrived at a $\hat{\sigma}$, $\hat{\omega}$ pair where ς was indeed less than unity, and improved the χ^2 fit slightly over both the critically damped and overdamped models. The improvement was of a similar magnitude for both muscles; apparently the underdamped degree of freedom was not more of an asset for the MG with its non-second order oscillation.

The most plausible explanations for the inability of any second order, closed form model to perfectly describe the experimental impulse response are either that the system is not second order or it is nonlinear. This conclusion is supported qualitatively

Method	TA				MG			
	ς	a	b	$\chi^2 \cdot 10^3$	ς	a	b	$\chi^2 \cdot 10^3$
1. $1/\tau_{peak}$ ($a = \hat{\sigma}$)	1.00	50.0	—	8.03	1.00	40.0	—	22.84
2. optimized: critically damped ($a = \hat{\sigma}$)	1.00	57.5	—	4.90	1.00	55.6	—	3.69
3. optimized: underdamped ($a = \hat{\sigma}_1$, $b = \hat{\sigma}_2$)	1.00	53.7	54.3	5.44	1.00	52.3	53.1	3.96
4. optimized: underdamped ($a = \hat{\sigma}$, $b = \hat{\omega}$)	0.95	52.8	16.8	4.40	0.95	51.4	16.2	3.44

Table 4.2: Pole locations estimated by each DLS model. Subject C11. All values in rad/sec; N = 40.

and visibly by the shape of the MG's experimental impulse response which demonstrates a possibly nonlinear oscillation about an otherwise second order response. Th underdamped, simulated response falls off more quickly than the critically and overdamped responses, and this characteristic is permitting it to match the experimental response most closely.

The open loop testing carried out later in this study spotlighted the inadequacies of this dynamic system model, both for DRRM deconvolution and as a component of the OLC feedforward block. It is probable that a higher order model could fit the experimental impulse response more closely, and possible that employment of this model could significantly improve performance in either task (deconvolution or OLC). It is not clear whether these benefits would outweigh the increased complexity and consequent development and computation time required to implement the model, without actually doing so. Such an investigation was not performed here.

The second order, critically damped dynamic model was used for the DRRM's implementation here. Being much more amenable to streamlined automation in the DRRM, the $1/\tau_{peak}$ approximation to σ was used rather than the Marqhardt-Levinson parametric optimization, with the exception of a few cases where the $1/\tau_{peak}$ approach gave a particularly unsuccessful, *i.e.* noise-polluted, deconvolution.

Note that in general, the dynamic system does not change with time as markedly as the static nonlinearity does. In a routine implementation, it might prove cost-effective to perform a precise, high order identification once and then use this model repeatedly on the same subject without verifying it each time. This would probably be the situation for a muscle such as the MG represented in Figure 4.14 (b); its pronounced non-second order morphology is poorly described by the $1/\tau_{peak}$ criterion.

It was desirable to assess the sensitivity of the critically damped dynamic system model to root location and its effect on DRRM IRC estimation. The experimental and $1/\tau_{peak}$ synthetic impulse responses were bracketed by responses computed with faster and slower roots, such that the χ^2 error between the experimental and $\hat{\sigma} = 1/\tau_{peak}$

responses was approximately matched by the error between the $\hat{\sigma} = 1/\tau_{peak}$ response and $\hat{\sigma} = 1/tpk \pm \delta$ responses (Figure 4.15 (a),(c)). It was theorized that the difference in deconvolution error among the latter would be a reasonable estimate of the error imposed by using the $1/\tau_{peak}$ approximation instead of a "perfect" model of the dynamic system. The IRCs produced by each of the three synthetic models ($\hat{\sigma} = 1/\tau_{peak}$, $\hat{\sigma} = 1/\tau_{peak} \pm \delta$) are shown in Figure 4.15 (b) and (d).

For both muscles, the TA and the MG, the sensitivity to $\hat{\sigma}$ manifests itself as deconvolution noise rather than in overall IRC shape or position. The sensitivity is more pronounced for the MG than for the TA, as might be expected after a visual inspection of the corresponding impulse responses. Observe that in the MG's case, a value of $\hat{\sigma} = 1.5 \cdot 1/\tau_{peak}$ was far more successful in deconvolution that was $\hat{\sigma} = 1/\tau_{peak}$, bearing out the need for a better way to choose $\hat{\sigma}$ than the $1/\tau_{peak}$ approach. The TA also experienced an improved deconvolution in the direction of faster roots, such that the best was $\hat{\sigma} = 1.2 \cdot 1/\tau_{peak}$.

Dynamic System Linearity: The success of any of the IRC ID methods considered here hinged on the validity of the assumption that the stimulated muscle system could be separated into static nonlinear and dynamic linear parts. A test of this assumption was to verify the actual linearity of the DLS by considering the degree to which impulse response shape changed with stimulus strength. Impulse trains were applied to several muscle preparations, and normalized responses were compared for shape variation and root movement.

The linearity of the relation of impulse response shape to impulse stimulus strength is demonstrated with experimental data from subject animal C11 in Figure 4.16. An impulse train consisted of four repetitions each of ten SS levels, ranging uniformly from 10% to 100% of the current stimulus zone, ZZ. Impulse amplitudes were randomized before application and the four responses to each amplitude were averaged. The forty impulse commands were interspersed by 1.7 seconds with amplitudes randomly ordered. Total record duration was approximately 80 seconds. Results for the 10% and 20%

(a)

TA
IMPULSE
RESPONSES

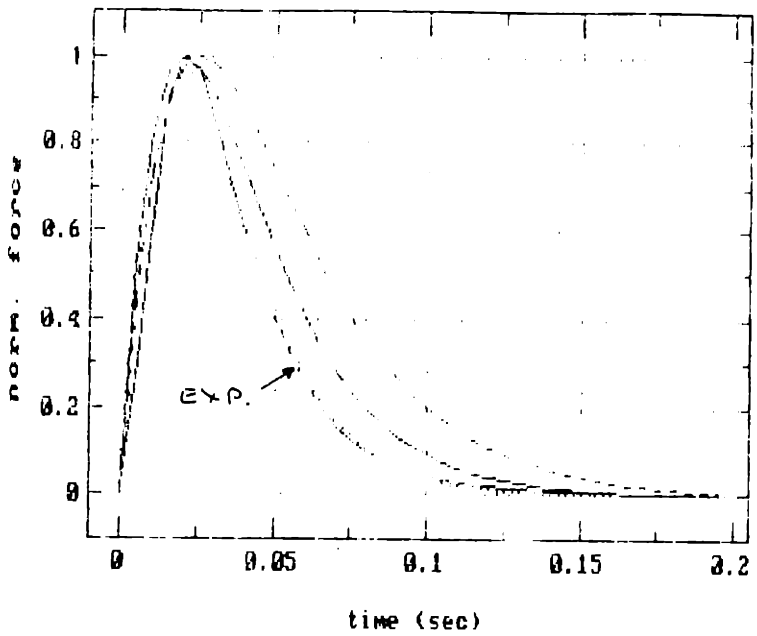

—— experimental
– – – δ = 0.80 (1/tpk) = 40 r/s
—— δ = 1.00 (1/tpk) = 50 r/s
····· δ = 1.20 (1/tpk) = 60 r/s

(b)

TA
IRCs

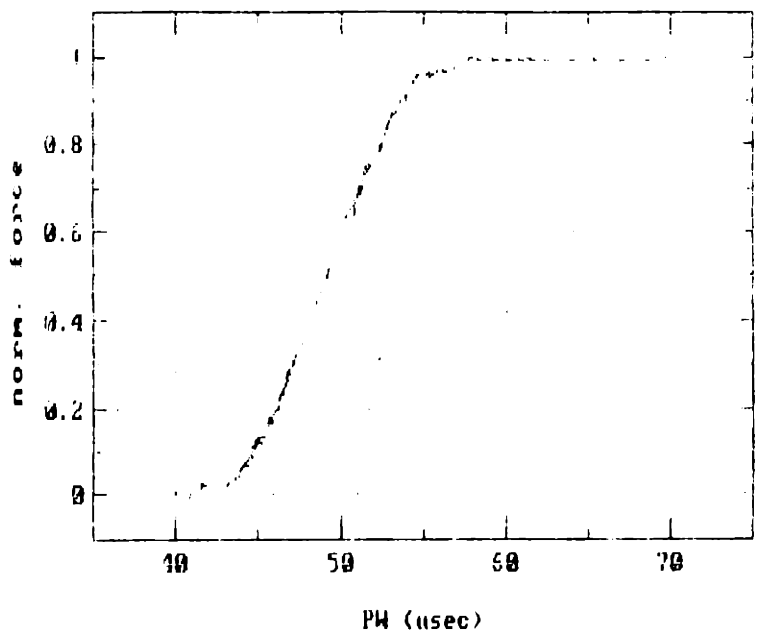

(c)

MG
IMPULSE
RESPONSES

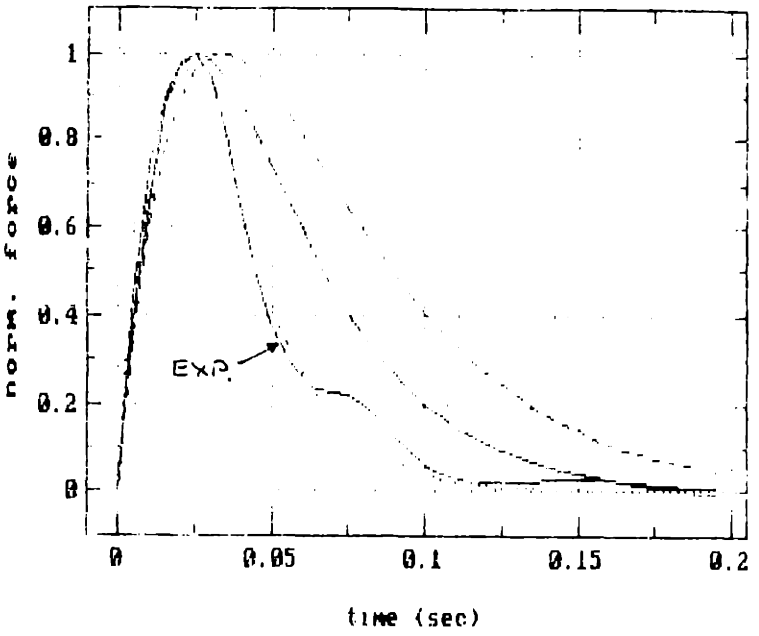

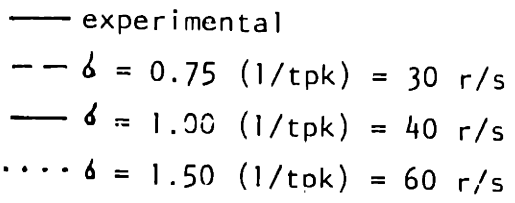

(d)

MG
IRCs

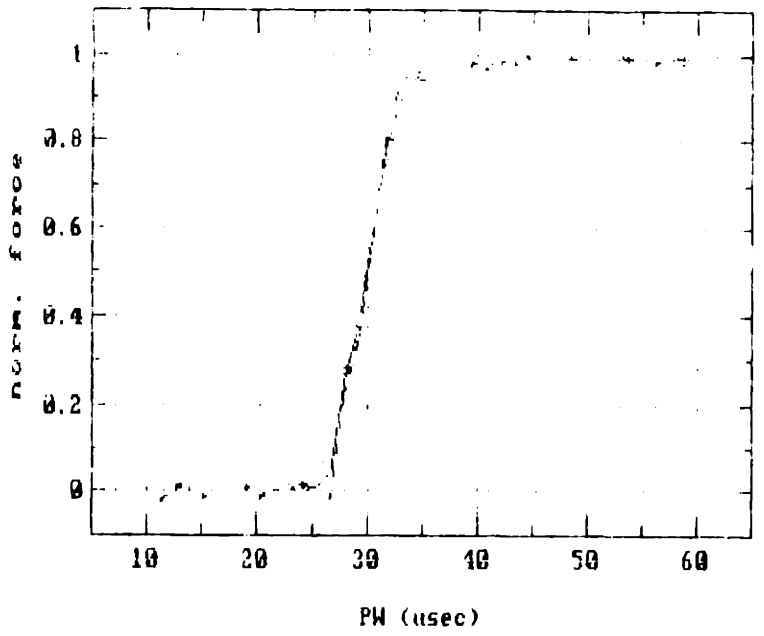

Figure 4.15: Sensitivity of deconvolution to root placement: experimental and synthetic impulse responses with their DRRM IRCs. C11.

(a) TA

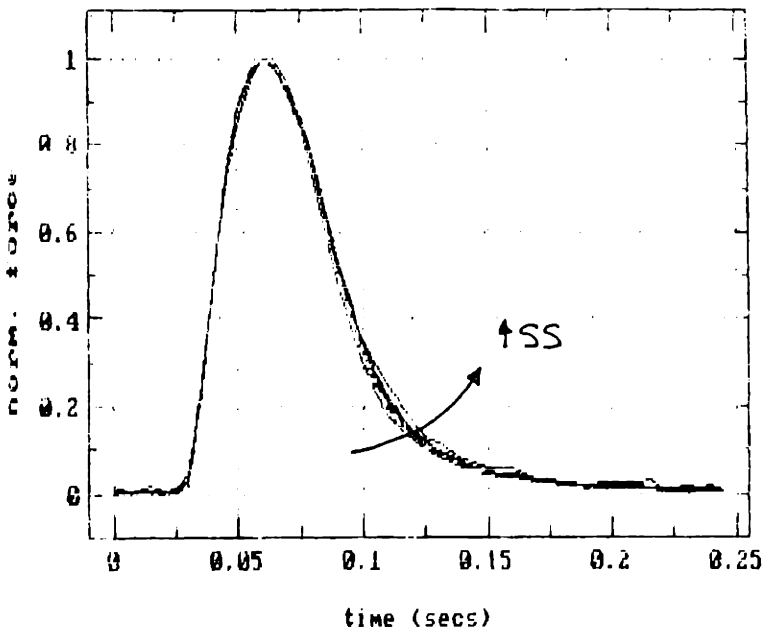

(b) MG

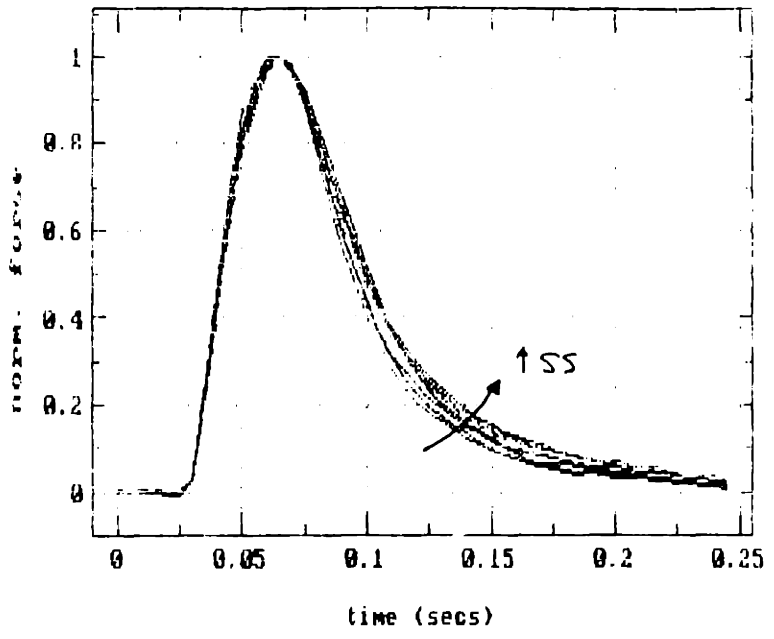

Figure 4.16: Eight peak-normalized impulse responses showing shape as a function of stimulus strength. (a) TA and (b) MG, subject C11.

Stimulus Strength (fraction of zoom zone)	$\hat{\sigma} = 1/\tau_{peak}$	
	TA	MG
0.30	33.33	40.00
0.40	28.57	40.00
0.50	28.57	33.33
0.60	28.57	33.33
0.70	28.57	33.33
0.80	28.75	33.33
0.90	28.57	33.33
1.00	28.57	33.33
range	4.76	6.67
mean	29.10	34.82
std. dev	1.50	2.77

Table 4.3: Estimated root location ($\hat{\sigma}$) statistics as a function of stimulus strength Subject C11. All values in rad/sec.

commands were discarded because those muscle responses were not discernible from background noise.

Pole location was used to quantify impulse response shape. The dynamic subsystem was modeled as second order with repeated real roots ($\zeta = 1$), and σ was approximated by $\hat{\sigma} = 1/\tau_{peak}$. Table 4.3 lists $\hat{\sigma}$ values for the impulse responses of Figure 4.16.

The arrows in Figure 4.16 indicate the direction of increasing stimulus strength associated with the responses shown: the response widens as the stimulus increases.

This variation does not extend to the time-to-peak parameter at the resolution permitted by the 5 msec sampling period. τ_{peak} is constant for each muscle over the bulk of the stimulus range, dropping measurably only at the lowest activation levels. It is clearly not a perfect estimator of dynamic linearity, since it does not reflect a visible nonlinearity.

Despite dissatisfaction with these efforts at quantifying the dynamic response's linearity with respect to stimulus strength, it seems safe to claim that the impulse response's time-to-peak is linear and that its tail-off region is less so. These observations are consistent with the aphysiological recruitment order typically observed for FES. A similar fast-twitch fiber population is being activated at all stimulus levels, since by the size principle these fibers are the first to be recruited and with a nonfatiguing twitch input, they are also recruited by strong stimuli. Slow-twitch fibers increase their contribution with stimulus strength, giving the effect of an s-plane pole towards the origin.

It is difficult to discern the importance of this amount of dynamic nonlinearity, either through morphological shape differences in DRRM recruitment curves generated using dynamic systems based on the various impulse responses of Figure 4.16, or through open loop control tests using a feedforward system consisting of those same IRCs in conjunction with the dynamic estimate[3]. The difficulty lies in the inadequate modeling. A synthetic DLS must be used for the reasons discussed previously, but the

[3]See Section 5.3 for an elaboration on open loop control testing.

discrepancies between a synthetic and an experimental response is greater than that between two experimental ones. Such tests are therefore pointless.

It is the author's judgement that this nonlinearity is insignificant compared to other modelling error, such as non-second-order dynamic behaviour and, most prominently, the time varying characteristics of the so-called static nonlinear subsystem. When these problems have been dealt with more precisely, it may be worthwhile to again approach the issue of dynamic nonlinearity in order to achieve very fine control. Until then, such an effort would be misplaced. It is further suggested that when a quick estimate of the dynamic system is desired, little error would be introduced by using 2 to 4 averaged maximal twitch responses, rather than a longer series of responses to stimuli distributed over the stimulus range.

Input

It was conjectured that the DRRM would perform better with a smooth input function than with a sharp-edged ramp[4]. The input X need not have smooth derivatives, since the response is not expected to follow it precisely. However, response to an input smoother than a ramp might be less artifact ridden and hysteresis prone because a discontinuity in the input sequence could distort the output and complicate the deconvolution process. A further benefit of one type of smooth input, the inverted cosine bell curve, could be the higher threshold- and saturation-region resolutions of its IRC estimates where the input changes more slowly.

The two input types that will be discussed in Section 5.3, the sawtooth ramp and cosine bell shown in Figure 4.17 as

$$(a)\ x(t) \equiv \left\{ \begin{array}{ll} a(t - \mathrm{T}_{on}), & \mathrm{T}_{on} < t \leq \mathrm{T}_{on} + \mathrm{T}_{hr} \\ a\left[2 \cdot \mathrm{T}_{hr} - (t - \mathrm{T}_{on})\right], & \mathrm{T}_{on} + \mathrm{T}_{hr} < t \leq \mathrm{T}_{off} \end{array} \right\}$$

[4]More insight on the role of input signal smoothness may be found in the forthcoming discussion of dynamic OLC task design (Section 5.3, Input). Note that DRRM's requirements differ from those of the dynamic OLC task, in that the stimulus input X is constructed directly rather than by inverting a command or desired output sequence $\mathrm{U} = \mathrm{Y}_{d}$ through an estimate of the dynamic subsystem.

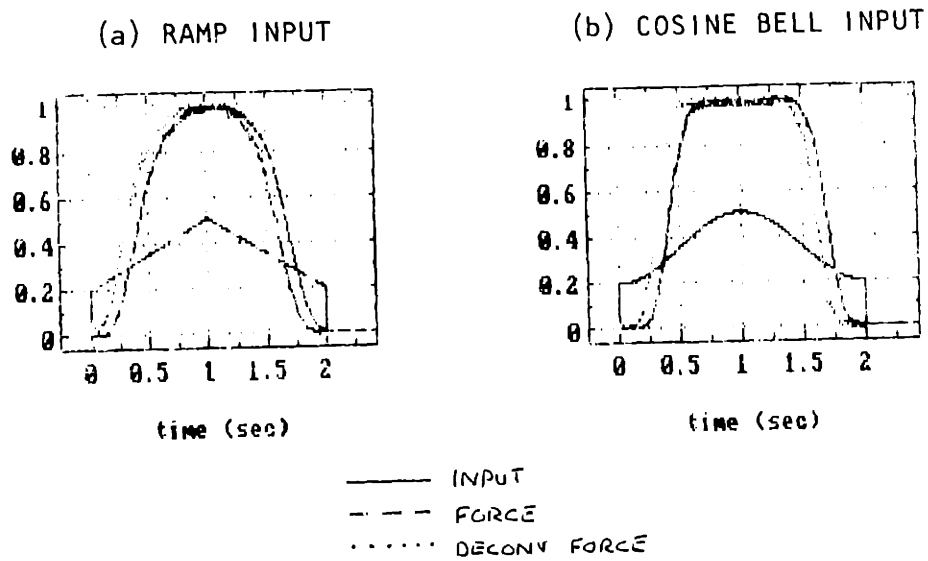

Figure 4.17: I/O time histories for DRRM inputs investigated, showing normalized stimulus input and force response. TA, subject C8.

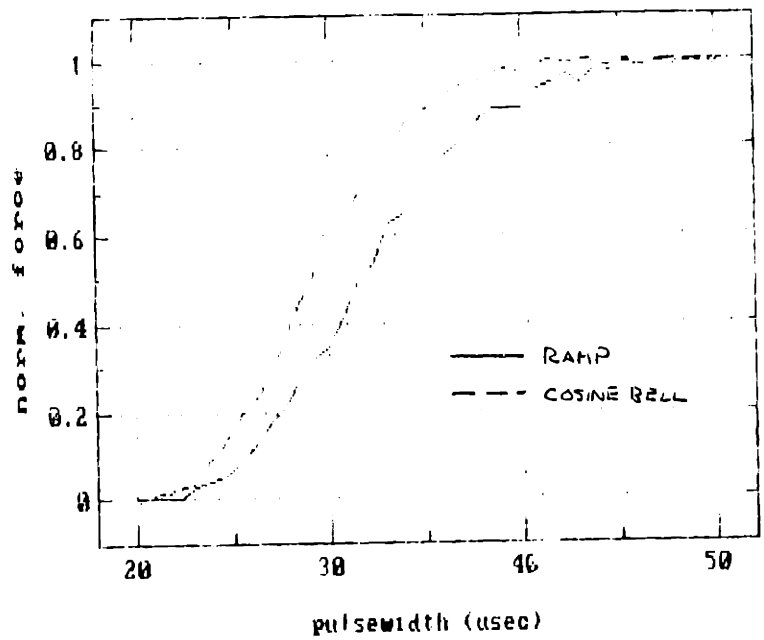

Figure 4.18: Estimated IRCs for ramp and cosine bell inputs. TA, subject C8.

$$(b)\ x(t) \equiv 1 - \cos\left[\omega(t - T_{on})\right], \quad T_{on} < t \leq T_{off},$$

were applied to the same muscle preparations with half-ramp periods (T_{hr}) of 1.0 seconds. I/O time histories and corresponding estimated recruitment curves are shown in Figures 4.17 and 4.18 for the TA of subject animal C8, where the cosine bell data set was taken 35 minutes after the ramp data.

The time history records exhibit the risk of concentrating map points at low and high commands. It can be a good idea when the zoom zone is chosen very closely to the threshold and saturation stimulus levels, but otherwise the resolution is wasted. No information is gained from the large plateau in the cosine bell history, which takes up half of the total stimulus time. If threshold and saturation are not known precisely (and in general they are not; that is why the IRC is being estimated), then in this respect the ramp input is a more sensible way to go.

The two deconvolved sequences show that hysteresis has been reduced by about the same amount in both cases. However, the maps themselves (Figure 4.18) are not quite alike. The invervening 35 minutes between the records' acquisition could explain the apparent shift in active zone, but there still remain differences in shape. The bell map has a narrower active zone with a steeper slope, and it is smoother than the ramp map, presumably a benefit of the smoother input. The discrepancy in active zone width is potentially serious, but it is impossible to tell which version is more correct without testing both in open loop control.

Since time and resources were limited, more extensive comparisons were not made and the DRRM was used with a ramp input for the remainder of the study on the basis of its uniform resolution. Later, after completion of the open loop control tests for all of the identification methods, the concept of a smooth DRRM input was resurrected as a possible means of improving the deconvolution step; this will be discussed in Chapter 7. The non-uniform resolution problem/benefit mentioned above would still exist. It might be worthwhile to devise another input with smooth corners, but which rises faster and levels off later than does the cosine bell.

Input Ramp Period

Since the overriding objectives of the DRRM were accuracy closely followed by speed and fatigue minimization, it was worthwhile to look at the effect of input frequency, in terms of half-ramp period (T_{hr}), on quality of IRC estimation in order to choose the minimim T_{hr} which would turn in a satisfactory performance. While a small T_{hr} was more efficient from the standpoint of time and fatigue minimization, it also decreased the IRC estimate's resolution (fewer data points were taken at the same sampling frequency) and increased hysteresis effects (a steeper ramp slope made dynamics more significant). Neither the minimum adequate resolution level nor the degree to which deconvolution could in practice overcome hysteresis were clear without reference to experimental results.

Shown in Figure 4.19 are raw and deconvolved force response vs. stimulus input crossplots obtained for single-repetition ramp inputs with T_{hr} values of 0.5 and 5.0 seconds. Records were taken taken from MG of C8 within 40 minutes of each other. Figure 4.20 compares the DRRM isometric recruitment curves for T_{hr} values of 0.5, 2.0 and 5.0 seconds.

The data demonstrates that fatigue becomes an issue as T_{hr} increases, with the 5.0 second force response dropping more quickly than it rose. On the other hand, this deconvolution technique has difficulty accomodating the sever hysteresis and more abrupt corners of a steep ramp, as is evidenced by the bumpier deconvolved sequence in Figure 4.19 (a).

The higher resolution provided by a slow ramp ($T_{hr} \cdot f_{stm} = 200$ points for the 5.0 second ramp, as opposed to 20 points for the 0.5 second ramp) is a dubious advantage, since it appears in map form mostly as increased noise. This is because noise occurring with the same frequency content in both records is compressed in the output/input crossplot and appears to have a higher frequency there.

Choice of a cutoff frequency is complicated for fast ramps because the more abrupt corners are responsible for more high-frequency noise in the output. Further, the

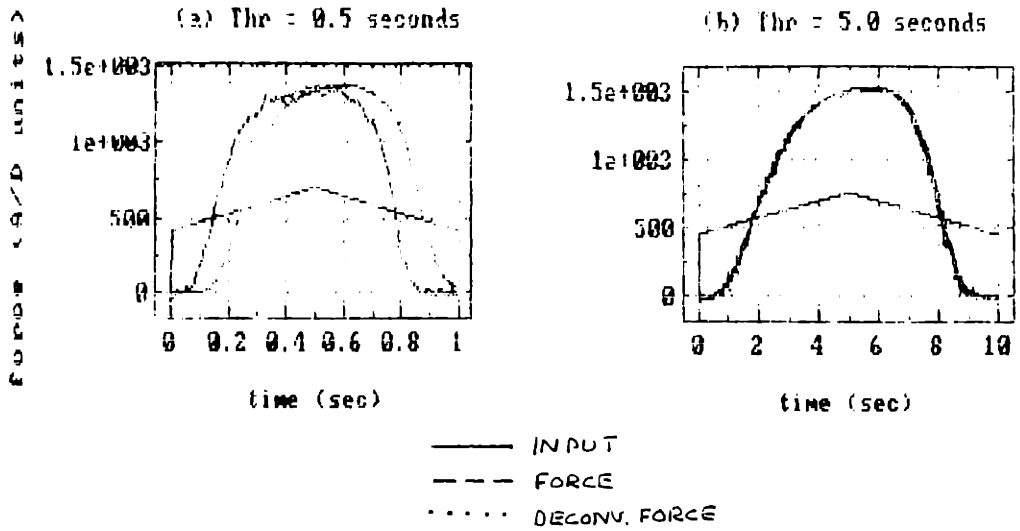

Figure 4.19: DRRM normalized force and deconvolved force time histories for different T_{hr} values. MG, subject C8.

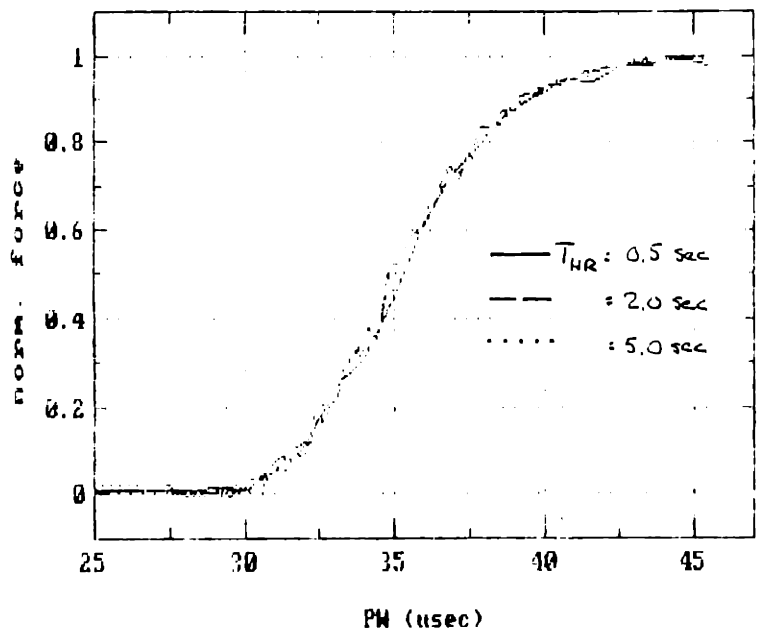

Figure 4.20: DRRM IRC estimation as a function of T_{hr}. MG, subject C8.

decreased resolution effectively makes the nonlinearity harder so that careless filtering will easily obscure its details. However, the shapes of the various IRC estimates of Figure 4.20 are quite similar for most of the active zone, suggesting that the filtering has not been too harmful.

The 1.0 second half ramp period was chosen for this study as the best compromise between resolution, speed and fatigue.

Number of Ramp Repetitions

Deconvolution, even of a filtered or smoothed experimental ramp response through a synthetic and noiseless transfer function, will amplify any remaining noise. One means of noise reduction explored, the averaging of multiple, tandem ramp responses after their deconvolution was considered promising because it would smooth uncorrelated noise while retaining information common to all repetitions. On the other hand, repeated ramps took longer to apply and process while the additional fatigue degraded IRC estimation quality, undermining the DRRM's chief advantages of speed and low fatigue rate. A compromise in the number of repetitions could be arrived at only after examination of real data and IRCs estimated from different numbers of repetitions.

DRRM data sets with four ramp repetitions were taken and processed with the parameters stated in the preceding section on general implementation. IRCs estimated from an average of the first one, two and four deconvolved ramp responses, shown in Figure 4.21 for the TA of subject C11, were compared for progressive fatigue and relative noise content.

The effects of noise reduction are more evident than those of fatigue in the maps shown, since the normalization has disguised the scaling influence of fatigue. Remember that for use with a normlaized control command, the map's unscaled amplitude is irrelevant. Shape, however, is critical; and it seems here that the DRRM IRC's *shape* changes very little with fatigue.

Although it is difficult to tell from the plot shown, it was found here that there

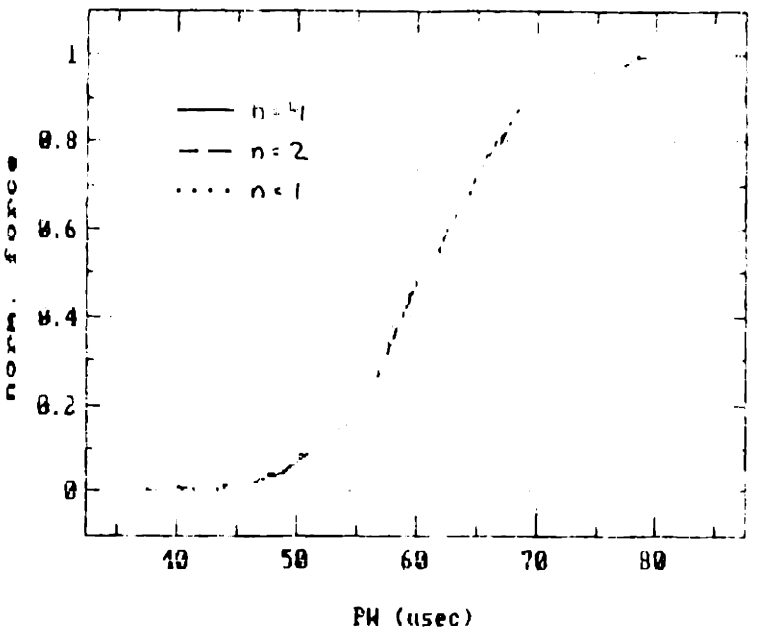

Figure 4.21: DRRM IRC estimation as a function of number of ramp repetitions. TA, subject C11.

was little additional benefit in increasing n from two to four unless the deconvolution was particularly difficult (for example, deconvolution of data from a muscle with an impulse response exhibiting non second-order behavior). Four ramps were used for the remainder of this study, but two or three would probably have been sufficient.

Zoom Zone

A convenient test of the agility of the DRRM in accomodating oddly shaped and hard nonlinearities as well as gentle sigmoid curves was to vary the stimulus zoom range (ZZ) from close to the current active range (maximizing IRC resolution) to the maximum stimulus range available. In this manner even the smoothest of IRCs becomes a hard nonlinearity.

Several low-resolution DRRM data sets were taken in close proximity to zoomed sets, and IRC estimates compared for threshold and saturation estimation and for shape differences. Figure 4.22 demonstrates the dependency of DRRM IRC estimates on the

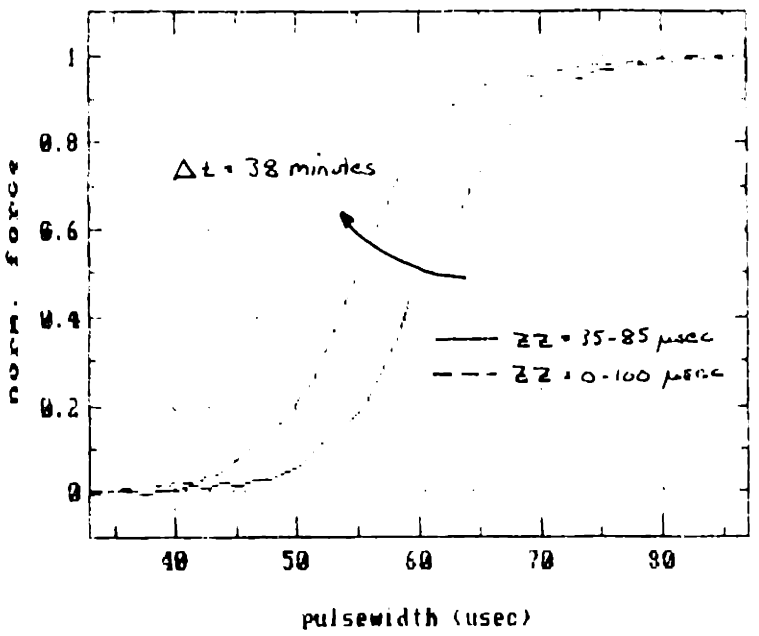

Figure 4.22: DRRM IRC estimation as a function of zoom zone. MG, C11.

ZZ and their loss of resolution when the ZZ is increased. For the first of the two IRC estimates, taken from the MG of subject C11, the SS input covered the entire available range, 0.0 to 100.0 μsec. The second used a zoom zone with edges chosen close to the estimated current threshold and saturation stimulus levels, 35 to 85 μsec. Only this region is displayed, for the sake of resolution. Each curve has the same number of points (40) spread uniformly in their respective zoom zones, between which straight lines were interpolated. The second curve therefore gains resolution at the cost of the effort of finding threshold and saturation stimulus strengths. The two data sets were taken 38 minutes apart, with significant intervening threshold drift.

Because of threshold drift, the two IRC active zones are shifted. The IRC estimate shapes are similar, however, increasing confidence in the DRRM's robustness. Further insight will be gained by comparing its results with those of other ID methods, particularly the discrete ones (Chapter 6).

4.2.4 Stochastic Response Method

Several routes were explored in the search for the most appropriate implementation of the StoRM's general algorithm. Each StoRM iteration consists of two separate tasks: (a) estimation of the best fit $\hat{H}$ to the DLS between $\hat{V}_x$ and Y, followed by deconvolution of Y through $\hat{H}$; and (b) determination of the best fit $\hat{Q}$ to the SNLS between X and $\hat{V}_y$, with subsequent evaluation of $\hat{V}_x$ from $\hat{Q}(X)$. These tasks will be considered separatedly in the ensuing discussion.

The final StoRM implementation used here was found to work well on simulated, noiseless Hammerstein systems with blocks similar to those believed to describe the stimulated muscle, and less well on simulated Hammerstein systems with additive periodic or random noise. Figure 4.23 displays a typical noiseless simulation, where reasonable convergence was achieved after 5 iterations. (a) shows the static nonlinearity (SNL_{act}) along with the systems predicted backwards through the DLS (SNL_y) and after smoothing and recomputing (SNL_x). (b) shows the actual and predicted dynamic system frequency responses, DL and DL_{est}, which are nearly identical. In (c) is shown the actual output sequences y with additive noise (y_{nn}), before addition of noise (y), and the estimated sequence y_e. In this simulation there was no noise so $y_{nn} = y$[5]. (d) tracks the normalized convergences of the indicated quantities over 5 iterations.

The parameters used for this simulation were: a 1330-point input sequence x with an approximately white frequency response and uniform probability distribution. The static nonlinearity was smoothed by bin-sorting into 30 bins. The dynamic system was optimized in the frequency domain, using a spectral window of length 256 points with wrapawound protection of 25 points, the length of the simulated impulse response. The meaning of these parameters will become clear shortly in the detailed discussion of the StoRM's implementation here. Note that for both real and noisy, simulated systems,

[5] Were $y_{nn} \neq y$, the algorithm would have been performed using the noisy sequence y_{nn}. In a successful procedure, y_e should reject the noise and converge $y_e \rightarrow y$, rather than $y_e \rightarrow y_{nn}$. The latter would be impossible (at least for these simulated systems) since the model does not include additive noise.

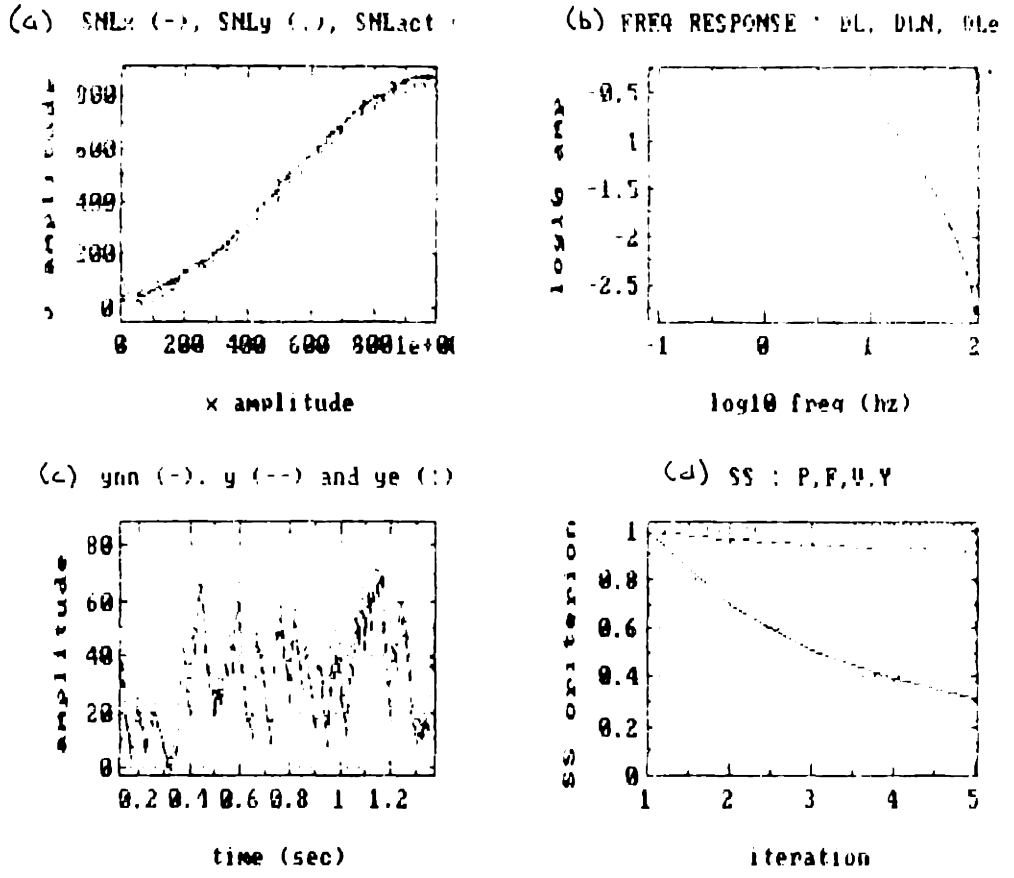

Figure 4.23: StoRM identification based on a simulated, noiseless system which otherwise resembles that of a stimulated muscle.

much longer sequences (up to 2500 points) were necessary to achieve even marginal success in convergence, by permitting more windows to be averaged in the frequency domain step.

At this writing StoRM success using experimental systems has not been satisfactory, but it is difficult to say whether the problem is poorly characterized noise, dynamic nonlinearity or other deficiencies in the Hammerstein model. The author believes that with further development the problems can be resolved, and that the StoRM remains a potentially powerful identification method. After such refinement, it still must be tested in realtime feedforward control systems as have the other ID methods presented in this thesis, to see if it offers more or better information than they do. Such tests of the StoRM's IRCs were not conducted in this study.

Fitting of the Dynamic Linear Subsystem

Hunter and Korenberg [23] suggest filtering the DLS entirely in the time domain, using autocorrelation techniques [22] to find the best-fit dynamic system and time deconvolution to estimate the intermediate sequence, $\hat{V}_z$. It was found here that the time-domain approach gave good results for simulated systems, but that for long ($>$ 1500 points) I/O sequences it made excessive computational time and space demands on the available processing resources. Also, StoRM's ability to correctly identify a simulated system degenerated rapidly with the addition of either periodic or white output noise, a situation that will certainly be encountered in real systems, and time domain options for treating the noise were limited and cumbersome.

Techniques of spectral analysis offered greater speed, smaller space requirements and more options for dealing with noise. The frequency-domain algorithm that was used here is outlined below:

(i) The dynamic system transfer and coherence functions, T_{ab} and C_{ab}, were estimated (optimal or Wiener filtring, [6,7]) with

$$T_{ab} = \frac{| P_{aa} P_{ab} |}{P_{aa} P_{bb}} \tag{4.4}$$

$$C_{ab} = \frac{|P_{aa}P_{ab}|}{P_{aa}P_{bb}}, \tag{4.5}$$

where T_{ab} approximates the linear part of the best-fit relation between the frequency domain states $A(f)$ and $B(f)$, and C_{ab} the nonlinear (noisy) part. P_{aa} is the power spectrum of $A(f)$, and P_{ab} is the cross-spectrum of $A(f)$ and $B(f)$.

(*ii*) The transfer function estimate, $\hat{H} = T_{ab}$, was then used to deconvolve the output segment by segment, after conditioning with the coherence function estimate C_{ab} to remove the parts of Y not linearly related to $\hat{V}_x$ such that

$$\hat{V}_y = \frac{\left[\begin{matrix} Y \\ C_{ab} \end{matrix}\right]}{T_{ab}}. \tag{4.6}$$

(*iii*) The real intermediate sequence, $\hat{v}_y(t)$, was finally constructed by inverse transforming $\hat{V}_y(f)$.

StoRM results with experimental data suggest that stronger weapons than the coherence function must brought to bear on system noise. Some filtering schemes cursorily investigated, including one similar to that used successfully for the DRRM (Section 4.1.3), show promise.

Number of Segments: The quality of DLS estimation is closely linked to the number of transform windows or segments (N_{seg}); 8-12 are commonly employed. The need for a large N_{seg} increases with a noisy system, since the "averaging" effect of multiple windows helps to reject uncorrelated system noise from T_{ab}. For the sake of transfer function estimation, a good strategy would be to divide the real I/O sequences into many small segments before Fourier transformation, *i.e.* to maximize N_{seg} while allowing M (window length) to be small.

Window Length: Of course, there is another side to the story. Once $\hat{H}$ is estimated between $\hat{V}_x$ and Y, it must be used to deconvolve Y. To convolve or deconvolve a real sequence in the frequency domain, each real segment must be protected form end-effects

by zero-padding it with N_h points[6] prior to transformation, where N_h is the length of the system impulse response. This places a lower limit on the window length, M, since M must at least be greater than N_h. Also, a small M slows the convolution process since more segments must be used. Impulse responses for this system typically lasted 0.25-0.50 seconds; with an f_s of 200 Hz, N_h had to be 50-100 points. The smallest practical window was therefore 128 or 256 points.

Fitting of the Static Nonlinear Subsystem

There exist innumerable ways of reducing an overdetermined, static relation between two vectors, in this case $x(t)$ and $\hat{v}_y(t)$. The Hunter approach [22] is to fit a high-order polynomial using least-squares parameter optimization, and compact N_s values (the sequence length) into a few polynomial coefficients. This may be viewed either as marvelously efficient or as exorbitantly wasteful, depending on the amount of scatter in the relation and in how well the actual static nonlinearity can be described by a polynomial. Numerical instability often becomes severe in fitting polynomials of order greater than three or four, because the high order coefficients dominate the lower order ones. Conversely, low-order polynomials are limited in the variety of shapes they can accomodate. They were unable to closely approximate the recruitment curves estimated by other identification methods here.

The next obvious approach was to smooth the raw, overdetermined $\hat{Q}$, obtained by sorting the stochastic X sequence by magnitude and plotting $\hat{V}_y(X)$ against the sorted X. Since points on the abscissa (X axis) are not necessarily spaced uniformly after sorting, the most convenient smoothing method was to sort X into bins and average all $\hat{V}_y(X)$ for each bin (Figure 4.24). The bin size could be adjusted with input length and degree of scatter to ensure enough $\hat{V}_y$ values in each bin for good averaging. A longer sequence thus permitted a finer resolution for $\hat{Q}$.

[6] In practice, improved performance was found when *both* ends of the real segment were padded with N_h zeros, although this theoretically should not be necessary. When the strategem was used, it increased the mininum M constraint to $M > 2 \cdot N_h$.

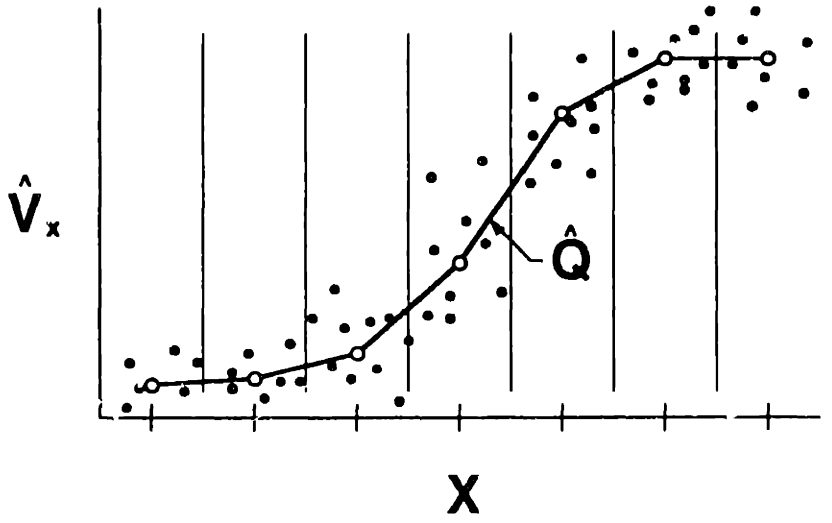

Figure 4.24: Bin-sorting of Q.

This strategy was much more successful with both simulated and experimental data, and is the one in current use. However, it would be worthwhile to investigate other smoothing techniques.

Effect of Input Duration

Long stochastic I/O sequences are useful in the StoRM because they contain more information than do short ones. However, they fatigue the muscle and because of fatigue, the responses themselves sometimes degrade with continued stimulation. Figure 4.25 show experimental stochastic responses with examples of worst- and best-case fatigue degradation from the TA (b) and MG (c), respectively, of subject C11. The input (a) has a uniform PDF, but doesn't look like it because the spikes are so close together. It is uncertain why some muscle preparations are able to sustain response to a stochastic input better than others, although muscle fiber population is the most likely explanation.

To see how prediction quality improves with sequence length, the StoRM was ex-

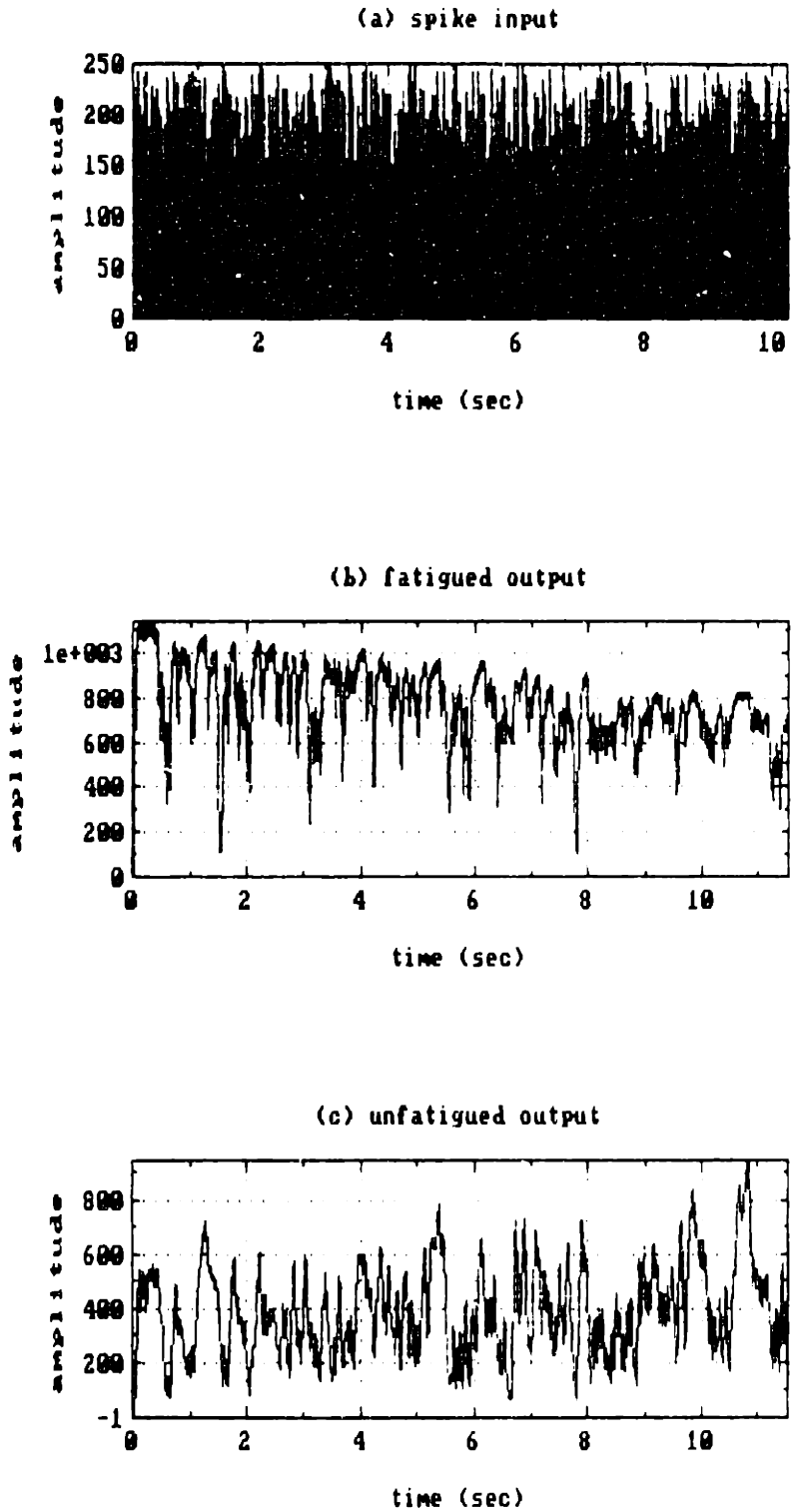

Figure 4.25: Stochastic spike input (a) and experimental force responses exhibiting (b) worst- and (c) best-case fatigue degradation.

ecuted using data subsets of succesively increasing duration. In order to distinguish sequence length effects from those of response degradation, the comparisons were performed using data from a time-invariant, simulated system resembling the real one. Data sets were of length (N_s) 256, 512, 1024 and 2048 for frequency domain estimation, filtering and deconvolution using N_{seg} of one, two, four and eight segments, each length 256 points (M).

For the simulated systems, one segment was inadequte for estimation and good estimation was achieved only with 4-8 segments or 1024-2048 sequence points. At a 200 Hz sampling frequency, this decrees real sequence durations of at least 6-11 seconds. Re-inspection of Figure 4.25 reveals a complication: fatigue-related time variation in the worst-case real system is evident well within the minimum sequence length. Even if the output were noiseless and the muscle a perfect Hammerstein system in all other respects, this compbination of input length, segment length and number of segments might not allow good estimation of this system.

Further investigation should be able to uncover a way around this problem. Several parameters (M, N_s, N_{seg}, f_s, N_h) are being simultaneously optimized and while this particular issue's optimal value for N_{seg} — apparently the limiting factor here — just happens to conflict with the best ones from other considerations, there is room for juggling and compromise. Also, all real systems are not as bad as the one in Figure 4.25(b); that of (c) exhibits little degradation at 12 seconds. Unfortunately, the identification method must be reliable for use in *any* system likely to be encountered.

Effect of Input Nature

It was conjectured that the StoRM would be sensitive to input determinism, bandwidth, autocorrelation function (ACF) and probability density function (PDF), and that some or all of these characteristics could be manipulated to increase the amount of useful information yielded from a given sequence length.

However, other factors and sources of error needed to be resolved first. When they

have been, a sensitivity analysis should be designed using simulated and real data to evaluate the effects of these factors.

Chapter 5

Methods: IRC Estimate Comparisons and OLC Testing

Since there is no correct answer to which an IRC estimation method may be compared, any judgement as to the relative merits of each IRC ID method must be based first on its consistency or repeatability — if applied to a muscle five times in five minutes, will the method give the same answer each time? — and second on whether the method enables one to improve the control of artificially stimulated muscle.

The IRC identification methods were refined and their products compared and tested with these objectives in mind. This section describes specifically how the identification methods were assessed, and results are presented and discussed in counterpart sections in Chapters 6 and 7.

5.1 Experimental Design

5.1.1 Study Requirements

The project's aims were (a) to develop alternative means of characterizing a muscle, and quantitatively assess the relative merits of each for different conditions and tasks, and (b) to investigate the validity and limitations of the Hammerstein muscle model. The IRC identification methods were evaluated on the basis of the following criteria:

1. **Identification Method Consistency:** Study the variation among IRCs estimated by a single method with respect to time, fatigue, muscle (fiber type, muscle/tendon length ratio), preparation (apparatus calibration parameters) and individual.

2. **Divergence in IRCs Estimated by Different Methods:** Quantify the variation among IRCs estimated by different methods, other variables held constant. Identify and account for magnitude of IRC estimate differences and the conditions under which they are maximized.

3. **Performance and Appropriateness:** Test the effectiveness of each identification method by using its estimated IRC in open loop control tasks designed to determine how well it characterizes the muscle plant.

5.1.2 Protocol Design of Individual Experiments

Because of the exploratory nature of the study, new questions, unforeseen problems and possible solutions were continually being discovered. Therefore instead of repeating or systematically varying a standardized protocol for each experiment, a less rigorous approach was taken in designing each protocol. This imposed sufficient commonality of structure in data taken from different individuals to permit some important cross comparisons and collective analysis, while retaining enough flexibility to pursue new issues as they arose.

Long-term time variation (hours or minutes, as opposed to periods of the order of individual data record durations) was the dominating force in experiment protocol design. Since some aspects of muscle response were found to vary significantly in the timeframe of a single experimental day, data intended to be compared independently of long-term time variation in the system had to be obtained during a relatively short time.

Conversely, it was desirable to periodically obtain data modules of similar structure in order to analyze the effects of long-term time variation.

The protocols therefore made use of modular data blocks of the following types:

Drift Check Block: A standardized data set which quantitatively tracked the drift of several muscle parameters over the course of the experimental day, a Drift Check Block (**DCB**) was taken periodically during an experiment, ideally every 30 to 90 minutes. For each muscle it consisted of measurement of

1. current maximum isometric force;
2. current stimulus strength ranges and exact threshold values to provide a measure of real muscle IRC horizontal shift; and
3. data for IRC estimates by at least one identification method, generally the Deconvolved Ramp Response Method, as an approximate measure of real IRC shape change.

Recruitment Curve Block: The Recruitment Curve Block (**RCB**) was intended to compare time variations for a given method within a single muscle preparation, and to compare variations for that method across muscle preparations. Its data was used to compare IRCs estimated by different identification methods for the same muscle in the same preparation, time and fatigue states, and provide a complete data pool with which to develop and evaluate the identification methods.

An RCB was composed of the data required for each ID method to estimate an IRC for both muscles, and was taken several times (2–3) in an experimental day.

Open Loop Control Block: The Open Loop Control Block (**OLCB**) compared the open loop control performances of IRCs recently estimated by different methods. Responses to both step and dynamic commands were recorded where the stimulus input sequence was created by passing a command or desired output sequence through an inverted IRC estimate and, in the case of a dynamic command, through an inverted estimate of the dynamic subsystem as well. A detailed OLCB protocol and a description of inversion procedures may be found in Section 5.3.

The OLCB was taken several times in an experimental day, in conjunction with an RCB to provide IRC estimates. It was employed only in the latter part of the study, when most of the recruitment curve identification methods had been developed sufficiently to permit realtime implementation.

Method Specific Block: The Method Specific Block (**MSB**) was a flexibly structured data set reserved for exploration of questions relating to specific identification methods. Its contents and frequency varied with the question.

...

In general, the same protocols were conducted on both muscles. Stimulation alternated between the TA and the MG, with at least 5 minutes between tests on a single muscle to reduce fatigue effects. Also, in an attempt to minimize contamination of the

results by post-tetanic potentiation [11,13], a 2.0 second conditioning pulse of maximal stimulation followed by 10.0 seconds of rest was applied before each stimulation sequence.

A comment on the vincibility of protocol before reality is in order here. Ideally, an RCB and OLCB pair would be carried out on a muscle whose state was constant during the period of data collection, *i.e.* a muscle whose "real" recruitment curve had not changed. However, even a faultlessly executed RCB required 60 minutes of stimulation and rest time, and an OLCB as long as 120 minutes. Complications inevitably stretched the data blocks out even longer. For a muscle whose state changes significantly after an hour or two of steady muscle activity, an IRC estimated at the beginning of a tandem RCB-OLCB pair would be obsolete by the time it was tested.

When IRC estimates are to be examined for ID method dependency by direct comparison of their shapes, it makes sense to apply all the ID methods close together and test them in open loop control later. To compare them indirectly through their OLC performances, however, the OLC tests for each IRC should be executed immediately after the IRC is estimated. Without retreating to a protocol that was much less ambitious in either the number of ID methods tested or the extent of OLC testing — which in retrospect might have been the wisest approach — both demands could not be satisfied at once. In practice, at least one contiguous RCB was taken from each subject animal, and other RCB/OLCB pairs were integrated by following IRC estimation for each ID method imediately with OLC testing of that method. Direct comparisons of IRC estimates from the interspersed RCB/OLCB units were made with caution.

5.2 IRC Time Variation and ID Method Consistency

In evaluating the identification methods, it was desirable to (a) distinguish method-caused IRC estimation error from genuine time variation in muscle response, (b) to assess the consistency or repeatability of each method, and (c) to unearth and if pos-

sible correct method trends, idiosyncrasies and outright errors through comparisons of IRCs estimated by different ID methods. In some cases the ID methods measured or estimated different quantities, so comparisons had to be made with care and justifications for discrepancies sought.

The aim of this study was to develop a control tool and not to catalogue system properties. However, data collected with this end could occasionally do double duty. It was helpful to have some awareness and expectation of the nature and magnitude of real system changes, chiefly long-term time variation in muscle response, in order to distinguish them from modelling errors. This need will be encountered on a larger scale in the future implementation of these and other identification methods in clinical control situations.

Some quantitative indices were needed to pinpoint sources of temporal IRC estimate changes and to provide an objective basis for verifying and comparing the different identification methods. Two IRCs, true or estimated, may differ in two orthogonal aspects. First, they may be offset as a whole to the left or the right, and second, their profiles may diverge independently of x-axis position. The first difference was characterized here by position of an IRC's leftmost or threshold stimulus strength value, THR. IRC profile is completely described by active zone width (independent axis scaling), peak force (dependent axis scaling), and normalized shape. The parameter of peak force was discarded as being too badly contaminated by genuine system changes to be useful here, since muscle fatigue within a data block introduced the additional variable of dependency of IRC peak force on order of ID method execution. The other parameters are elaborated on below.

5.2.1 Threshold

It is imperative that a controller know correctly the threshold input level which first excites a response, defined here as THR. While an IRC estimate's shape might be ID method-related without necessarily compromising its usefulness, its threshold is a

system parameter which a successful identification must get right. The problem is complicated by the fact that a muscle's threshold stimulus value drifts over time, with an unpredictable direction and rate [18]. It was therefore important to find both how accurately each ID method could be expected to track THR, and how much THR actually drifts in a typical system.

Tracking of Real Threshold Time Variation

Distinguishing real system time variation from ID method estimation error demanded a consistent, accurate and nonfatiguing means of locating the threshold stimulus strength. An independent record of this threshold estimate as a function of time could be compared with ID method predictions.

An algorithm which quickly and nonfatiguingly estimated THR to the stimulator's resolution of 0.1 μsec of pulsewidth (PW) was developed for this purpose. There being no ultimate standard of comparison, the accuracy of this procedure could only be inferred from its consistency and repeatability (Section 6.3). Its underlying principle is illustrated in Figures 5.1 and 5.2. The lowest stimulus strength eliciting a measurable response, the threshold boundary (THR_{TB}), was found after an incremental search by scanning the force record following an impulse input for a maximum value exceeding the defined force threshold.

A train of such impulses were applied to the muscle at 0.20 second[1] intervals, with initial stimulus strength (SS, in PW) of 0.0 μsec and successively increased by 10.0 μsec increments. When a threshold force was detected, the current PW was decremented by 10.0 μsec to give the new low stimulus amplitude, and the increment was divided by 10. After waiting an additional 0.25 seconds (the length of the muscle's impulse response) for the muscle response to die out completely, the process was repeated twice more beginning with the new low stimulus amplitude and increments of 1.0 and 0.1 μsec, successively. When the final threshold stimulus level, THR_{TB}, was found at an

[1] The impulse response maximum occurs at $t = \tau_{peak}$, and the muscles investigated here all had a $\tau_{peak} \ll 0.20$ seconds.

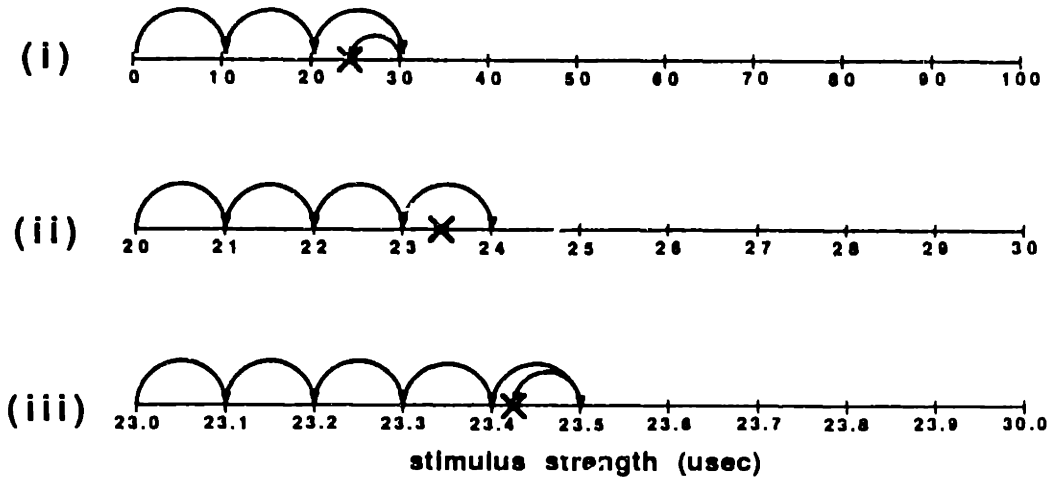

Figure 5.1: A modified bisection search to bracket a stable THR between stimulus strengths of 23.4 and 23.5.

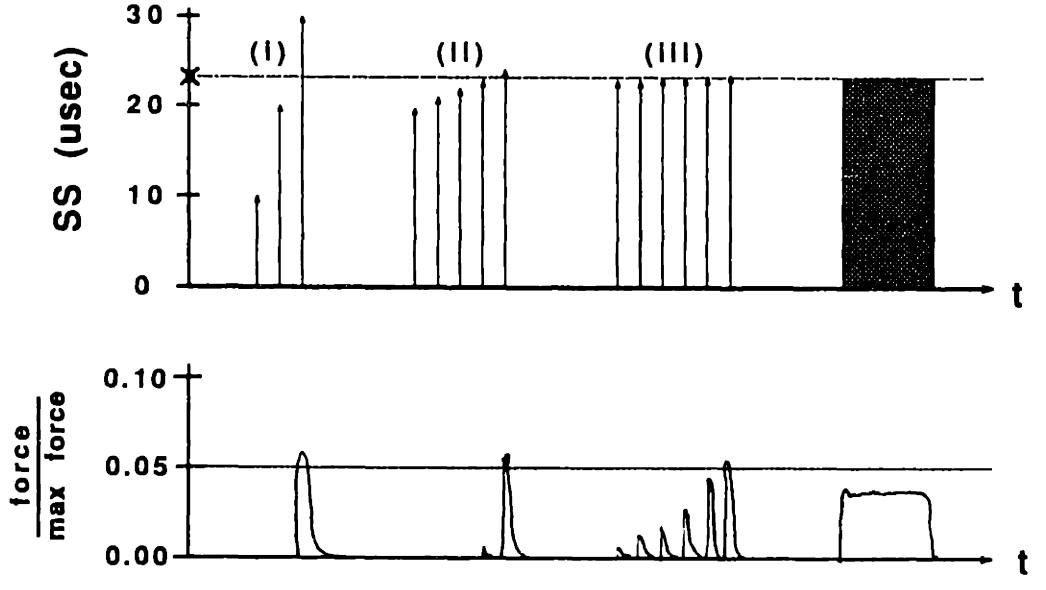

Figure 5.2: Time history for the search of the previous figure.

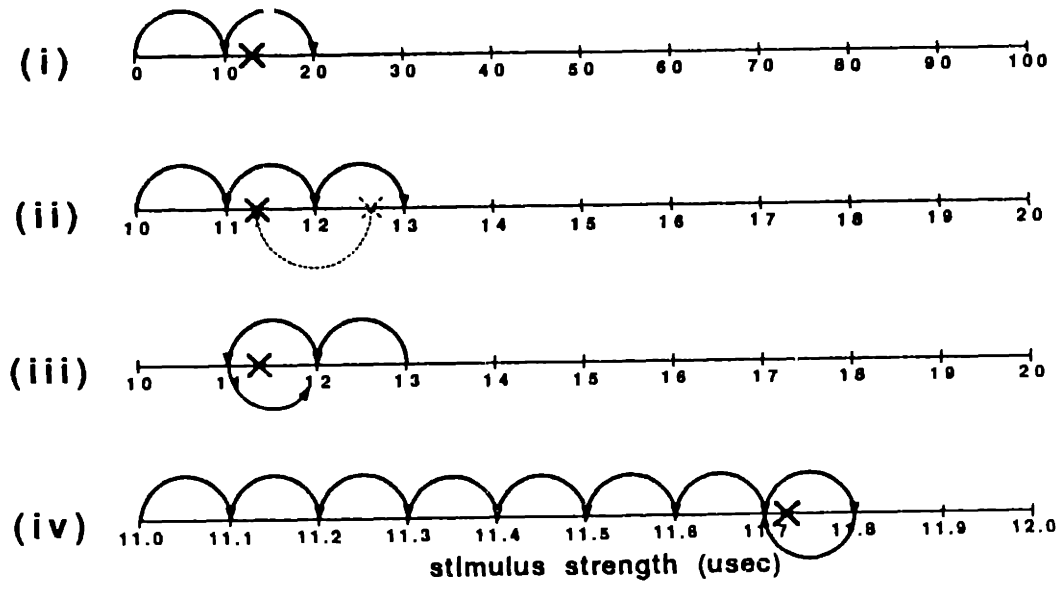

Figure 5.3: Search for a shifting THR.

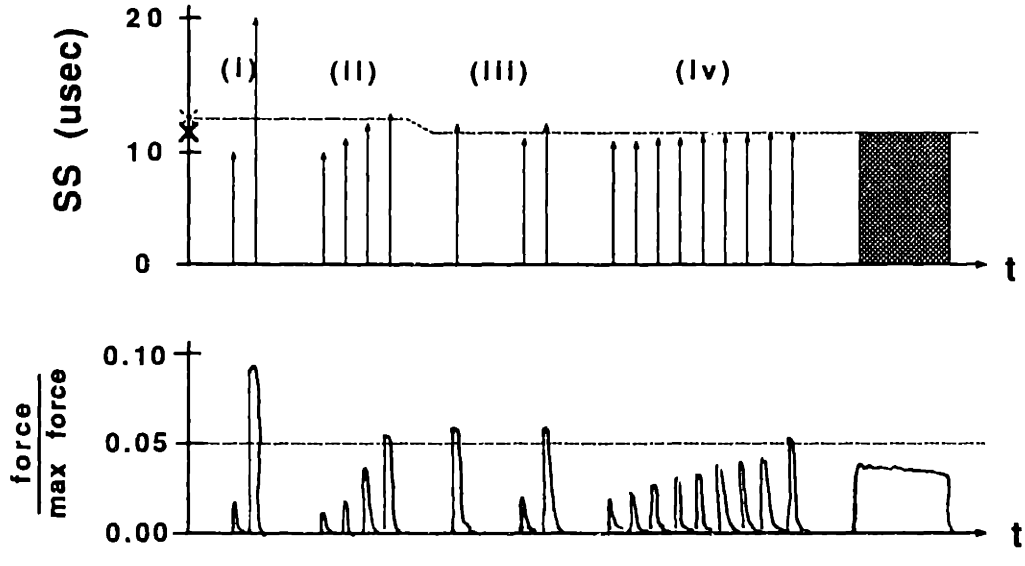

Figure 5.4: Time history for the search of the previous figure.

increment of 0.1 μsec, it was verified with a 1.0 second step input of amplitude THR_{TB} = 0.1 μsec. If no threshold force was seen in the step's response, that PW was returned as the current THR_{TB}; otherwise the test was repeated. Additional provisions were made for a threshold which shifted during the detection process (Figures 5.3 and 5.4).

THR_{TB} was measured at the beginning, end, and periodically throughout (ideally every 60 to 90 minutes) each data acquistion block (DCB, RCB and OLCB). It was recorded as a function of time for each muscle to provide an estimate of real muscle threshold drift and, as a relatively reliable and consistent threshold estimation method, a yardstick of permissible ID method threshold estimation error.

Accuracy of Threshold Estimation by Identification Method

The precision with which each ID method was able to pinpoint stimulus threshold was estimated by comparing THR_{meth}, the threshold indicated by a particular method, with the value of THR_{TB} found at the beginning of each RCB. An error criterion,

$$\varepsilon(\mathrm{THR}_{meth}) \equiv \mathrm{THR}_{TB} - \mathrm{THR}_{meth} \tag{5.1}$$

was constructed, where both threshold estimates were taken from the same data block and THR_{TB} was assumed *a priori* to be the more reliable estimate of the two, and as such a better measure of actual system changes. The ZZ (zoom zone) normalization was included to diminish bias due to variable stimulation resolutions, and was roughly set by calibrating pulse amplitude (PA) at the experiment's initiation. The normalization was still imperfect since neither PA tuning and ZZ choice were system properties, but performed at user discretion.

An approximation of real threshold drift was formed by replacing THR_{meth} in Eq. 5.1 with a second value of THR_{TB} taken at the end of the block, to bracket a reasonable range for $\varepsilon(\mathrm{THR}_{meth})$.

The relative performance of each ID method was generalized with an average over all the IRCs estimated by that method during the study, from data representing a spectrum of time, muscles and experimental subjects.

5.2.2 Active Zone Width

Active zone width (AZW) was the width of the stimulus range between threshold and saturation, defined here as

$$\mathrm{AZW} \equiv \mathrm{SAT} - \mathrm{THR}, \tag{5.2}$$

where SAT and THR were time-varying system properties, in general imprecisely known. AZW was different from AZ, defined in Section 1.3, which was a vector quantity referring to the position of the active zone within the total available SS range as well as to its width. The related number

$$\mathrm{AZW}_{meth} \equiv \mathrm{SAT}_{meth} - \mathrm{THR}_{meth} \tag{5.3}$$

was taken from an IRC estimated by a particular ID method, and consequently might exhibit method-dependency.

Ascertaining AZW's stability was important from the standpoint of both plant characterization and verification of ID method consistency. AZW defines a stimulus dynamic range, the region within which the IRC must be known for effective muscle control. The significance of a relatively constant AZW is that an elusive SAT can then be computed from the more easily determined threshold level. An IRC estimate could be swiftly recalibrated simply by shifting it to the left or the right after checking the stimulus threshold with a algorithm like the one described above.

Sources of AZW changes were harder to attribute to system time variation or estimation error than were those of threshold shifts, because the indistinct and highly fatigue sensitive saturation stimulus strength (SAT) was not measured as reliably or independently as THR was. They had to be assessed indirectly by comparing the temporal drift in AZW estimated by a single IRC ID method. Only temporal shifts significantly greater than cross-method ranges would imply the presence of real system changes.

AZW_{meth} was tracked by method over the experimental day. To facilitate cross-

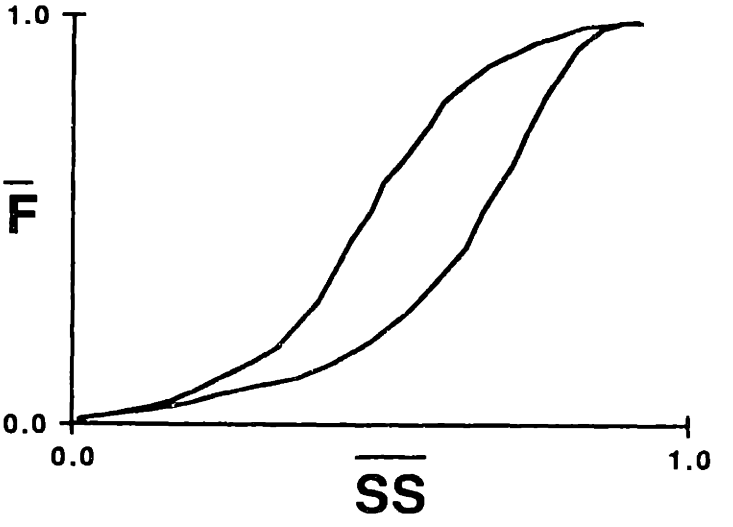

Figure 5.5: Example of normalized estimated IRC shape variation.

preparation comparisons, the percent change was also calculated:

$$\Delta\text{AZW} \equiv \frac{\text{AZW}_b - \text{AZW}_a}{\text{AZW}_a}, \tag{5.4}$$

where the subscripts may refer either to the parent recruitment curves' times of creation for single method comparisons, or to method of estimation for multiple method, same-time studies. In the former, division by the elapsed time $\Delta t = (t_b - t_a)$ provided an approximation of rate of AZW change and allowed an average change rate to be calculated for each ID method.

5.2.3 Shape

When recruitment curves were normalized on their independent (SS) axes to distinguish shape from active zone width differences, as well as on their dependent (force) axes to

eliminate magnitude variation,

$$\overline{SS} \equiv \frac{SS - THR_{meth}}{SAT_{meth} - THR_{meth}} \tag{5.5}$$

$$\overline{F} \equiv \frac{F}{F_{peak}} \quad . \tag{5.6}$$

the curves were still generally not identical, as may be seen in Figure 5.5[2].

A parameter was needed to quantify this final category of IRC divergence, and to ascertain whether time variation or ID method error was responsible for it.

For two recruitment curves generated by the same method, it was straightforward to formulate and discretize the percent shape difference:

$$\Delta SHAPE \cong \frac{1}{n_{rc}} \sum_{i=1}^{n_{rc}} | \bar{F}_a(i) - \bar{F}_b(i) | \tag{5.7}$$

where n_{rc} is the number of IRC points estimated by that particular ID method. Variation in values of ΔSHAPE for IRCs estimated by a single ID method at different times which exceeded that of values estimated by different methods at the same time could be attributed to actual IRC temporal drift. ΔSHAPE was also normalized to elapsed time $(t_k - t_0)$ to clarify trends in shape change.

Differences between IRCs estimated by different ID methods were cumbersome to quantify, since the various ID methods generated curves of differing resolutions. Each curve had to be linearly interpolated to the finest resolution present in the set being compared, before evaluation of ΔSHAPE according to Eq. 5.7. To reduce the dependency of variation on time, cross-method comparisons were restricted to recruitment curves generated from a single data block, the RCB defined in Section 5.1. Since ΔSHAPE is a difference, not an absolute quantity, it must refer to a standard. The Step Response Method was chosen for this purpose because it is the technique most used, so $\Delta SHAPE_{SRM}$ was zero by definition. Time normalization was less helpful here as than it was in temporal ΔSHAPE tracking, because the time elapsed during data collection was insignificant.

[2] $\bar{F}$ does not need to be shifted before normalization, since the entire range from 0 to F_{peak} is of interest.

ΔSHAPE was also averaged by time and method for all IRCs estimated in the study.

5.3 IRC ID Method and Open Loop Control

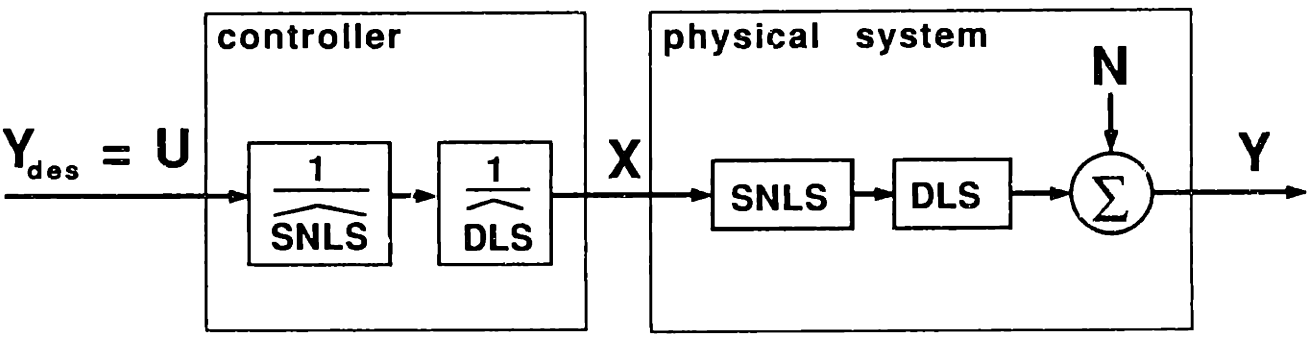

Figure 5.6: General open loop control scheme.

IRCs estimated by all the identification methods examined here were tested in open loop control (OLC) situations, closed loop control (CLC) being beyond the scope of this study. OLC tests, based on the general OLC scheme of Figure 5.6, consisted of either static or dynamic command following, tasks encountered in both physiological and clinical situations. The two types of commands had to be processed differently to create stimulus input sequences. Dynamic system cancellation is unnecessary when the goal is only to attain a specified steady state output value, but accurate tracking of a continous command requires inversion of an estimate of the dynamic system roots.

Only two of the methods, DRRM and StoRM, estimated the dynamic system in tandem with the static nonlinearity, and the remaining methods were tested with DRRM's estimate of the muscle dynamics. All the methods do not estimate the same quantity, so this hybridization was expected to be a source of error in the OLC test results, causing some methods to perform better at one type of task than at another. Comparison of ID method showings in the two categories yielded insight into their strengths and weaknesses.

OLC tests were conducted in the Open Loop Control Blocks (OLCBs) mentioned in Section 5.1 and detailed below. Each OLCB was taken in conjunction with a Recruitment Curve Block (RCB), from which the IRC estimate for each ID method was taken.

Two-Point IRC Estimation

In addition to the IRC identification methods described in Chapter 4, OLC tests were conducted using two-point IRC estimates consisting of zero deadzone and unity saturation regions separated by a linear active zone. The two-point IRC estimate's strength is simplicity and speed of construction and update. If its OLC performance proved to be comparable to those of more precisely measured IRC's, it could be useful in control of rapidly changing plants.

The two breakpoints defining the three segments may be chosen in a variety of ways. Threshold and saturation stimulus strengths may be measured independently or from another, higher resolution IRC estimate, and used regardless and/or in ignorance of actual IRC shape (Figure 5.7(a)). Alternatively, they may be chosen so that the center segment is a best-fit line through the active zone region of another IRC estimate (b). The two approaches, or hybridizations of them, are appropriate in different situations. If knowledge of muscle turn-on or saturation is more important than fine control over the active region, the former should be used. The choice of breakpoints also may be influenced by the availability of a high-resolution IRC estimate.

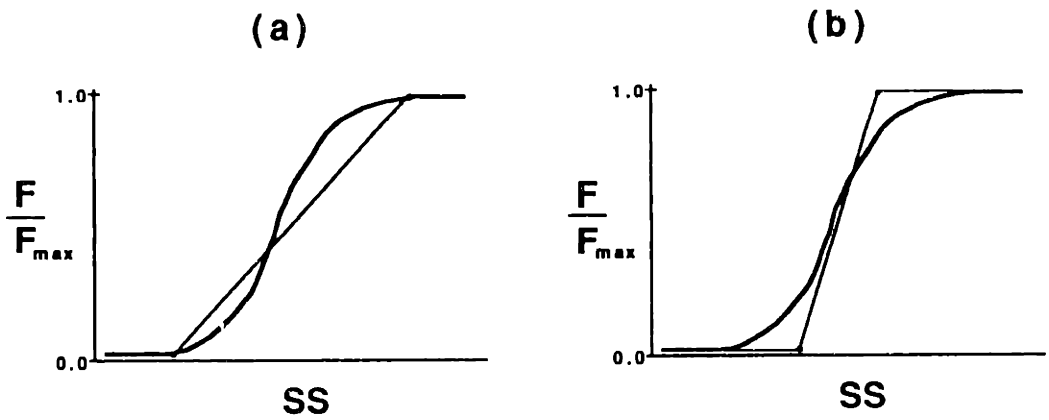

Figure 5.7: Two ways of estimating a two-point IRC. (a) THR/SAT breakpoints; (b) best-fit of active zone region.

Here, both approaches were explored and a systematic strategy was not developed until late in the study. The two-point "identification method" is consequently less consistent than it might be, and this should be kept in mind when considering experimental results.

$\widehat{\text{SNLS}}$ Inversion

Inversion of an estimated SNLS is illustrated in Figure 5.8. Command (U) could vary between 0.1 and 1.0, representing the corresponding desired fraction of maximum isometric force. A command of 0.0 became 0.0 μsec, while commands $0.0 < U < 1.0$ were inverted through an SNLS (IRC) estimate interpolated to the stimulator resolution, 0.1 μsec.

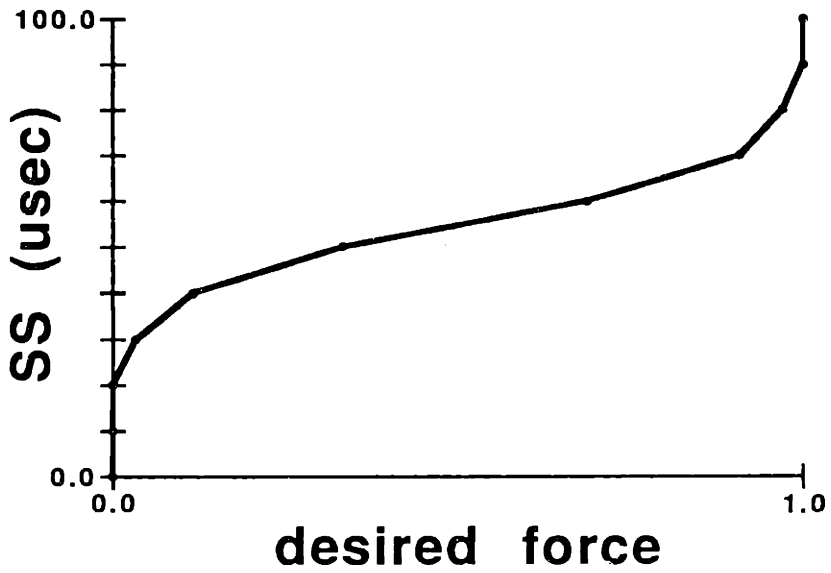

Figure 5.8: Inversion of a typical 10-point recruitment curve.

$\widehat{\text{DLS}}$ Inversion

Inversion of an estimated DLS began with the definition of $\widehat{\text{DLS}}$ in terms of its real, repeated poles, $\hat{\sigma}_{1,2}$. The procedure for this step depended on the ID method and is described in the corresponding discussion in Chapter 4.

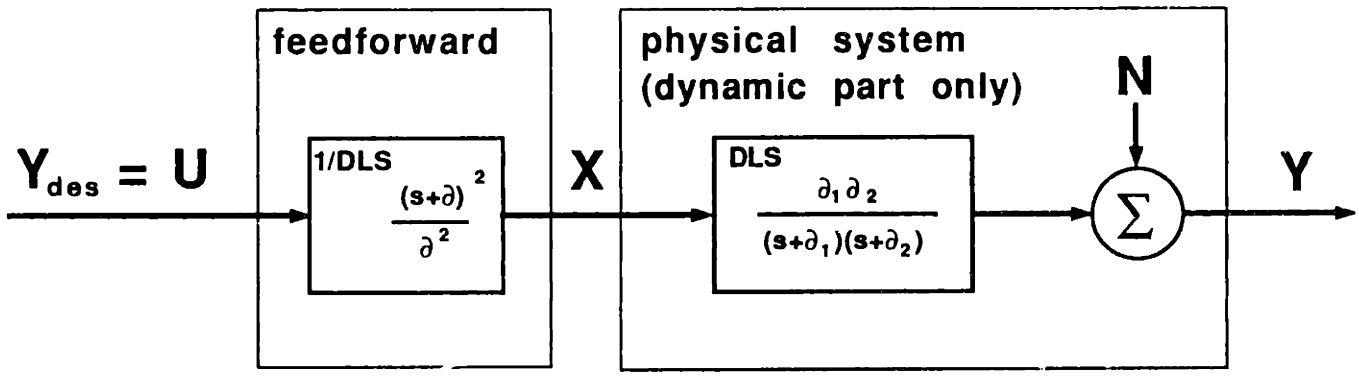

Figure 5.9: Dynamic subsystem (DLS) inversion process. SNLS not shown.

The modelled $\widehat{\text{DLS}}$ was then inverted as in Figure 5.9 to construct an X corresponding to the desired output U=Y_d. This could be done in a number of ways for an arbitrary Y_d. When Y_d was known, the most direct approach (and the one used here) was to transform $\widehat{\text{DLS}}^{-1}$ to the time domain such that[3]

$$\widehat{\text{DLS}}(s) \equiv \frac{\hat{\sigma}^2}{(s+\hat{\sigma})^2}$$

$$\widehat{\text{DLS}}^{-1}(s) = \frac{(s+\hat{\sigma})^2}{\hat{\sigma}^2}$$

$$X(s) = \widehat{DLS}^{-1}(s) \cdot U(s)$$

$$X(s) = \frac{(s^2 + 2\hat{\sigma}s + \hat{\sigma}^2)}{\hat{\sigma}^2} U(s)$$

$$x(t) = \frac{\ddot{u}(t)}{\hat{\sigma}^2} + \frac{2\dot{u}(t)}{\hat{\sigma}} + \frac{u(t)}{1} \quad . \tag{5.8}$$

Observe that it is possible for $x(t)$ to be nonpositive for some combinations of $\hat{\sigma}$ and $u(t)$, although a negative SS input has no meaning for this system. Simulations demonstrated that for the range of $\hat{\sigma}$ applicable here, a negative $x(t)$ rarely occurred and when it did, negligible error was incurred by clipping negative values to zero.

5.3.1 Static Command Following

Subsystem Inversion and I/O Processing

Steady state muscle force response to a discrete series of inverted step commands was measured. Muscle dynamics were neglected for steady state control, resulting in the simplifed controller configuration of Figure 5.10.

The time history for this test (Figure 5.11) resembled that used in the Step Response Method, Section 4.2.1, with the addition of $\widehat{SNLS}$ inversion. Four commands of decreasing amplitude evenly spaced from 1.0 to 0.25, with a fifth of amplitude 0.01 (a command U of 0.0 would have yielded no information, while one of 1% provided a check on threshold tracking) were applied, each of duration T_{on} of 1.0 seconds and separated by rest periods of duration T_{off} 10.0 seconds. The last 0.5 second of force response to each step input was averaged to obtain the steady state response, the first 0.5 second being sufficient to permit transients to die out while incurring minimal fatigue. The

[3] Eq. 5.8 does not include $\widehat{SNLS}$ inversion. In general, $u(t)$ would be passed through an inverted IRC estimate prior to application of this relation to obtain $x(t)$.

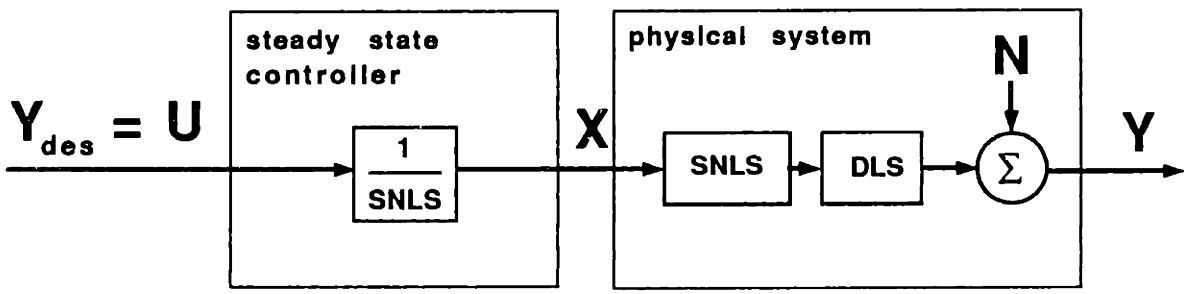

Figure 5.10: Inverted step command following scheme.

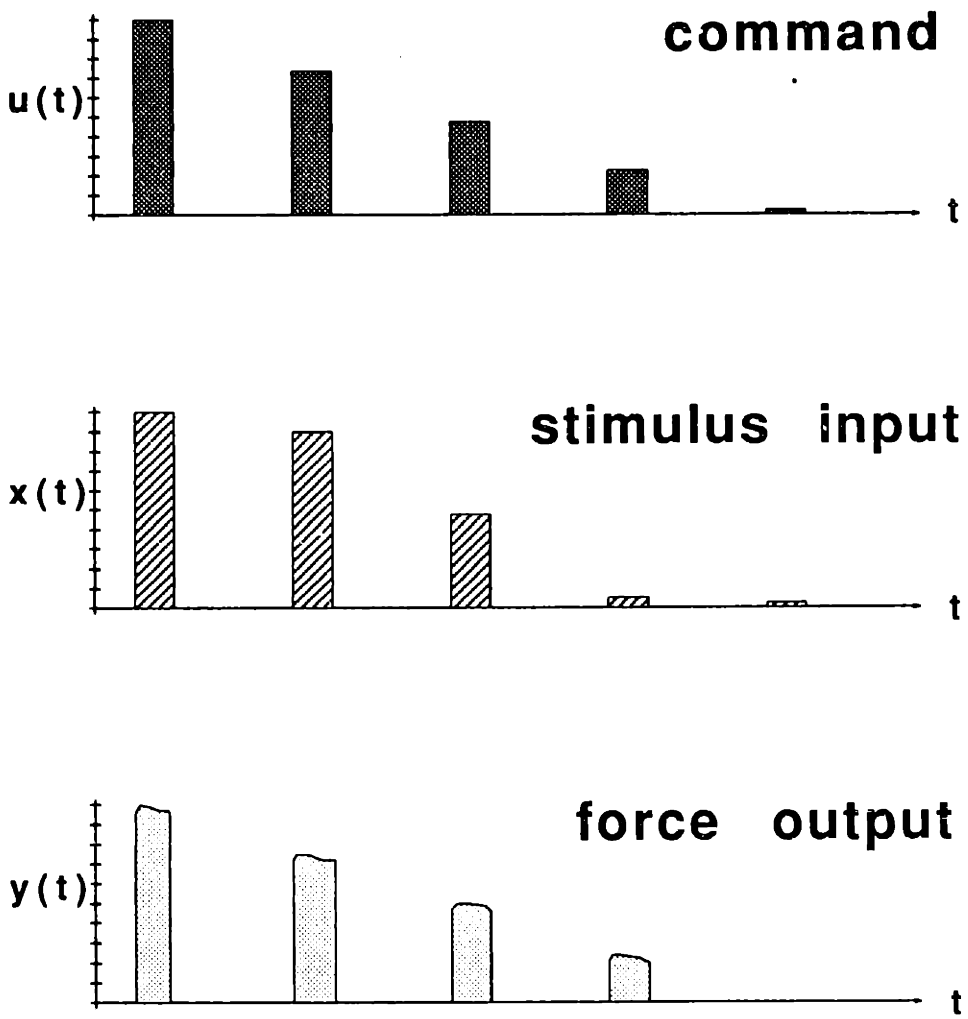

Figure 5.11: Inverted step command following time history for the inverted recruitment curve above.

average force was then normalized to the peak average force in the record to obtain $\bar{F}_{avg}$ as a function of U.

Evaluation

An error criterion for the static inverse response,

$$\varepsilon(\text{SOLC}) \equiv \frac{1}{n_s} \sum_{i=1}^{n_s} | \, U_i - \bar{F}_i \, | \tag{5.9}$$

was calculated for each IRC estimate tested, where n_s is the number of discrete step commands applied. ε(SOLC) was averaged by method for all IRC estimates tested in static OLC during the study.

5.3.2 Dynamic Command Following

Subsystem cancellation

Four permutations of subsystem cancellation (refer to Figure 5.6) were considered:

(a) no cancellations: $\quad X = U$

(b) DLS cancellation: $\quad X = \widehat{DLS}^{-1} \cdot U$

(c) SNLS cancellation: $\quad X = \widehat{SNLS}^{-1}(U)$

(d) DLS+ SNLS cancellation: $\quad X = \widehat{SNLS}^{-1}(\widehat{DLS}^{-1} \cdot U)$

where U was the command, X the stimulus input and Y the measured force output. $\widehat{DLS}$ and $\widehat{SNLS}$ are the estimated versions of the dynamic subsystems described in Chapter 2; $\widehat{SNLS}$ is here equated to the IRC estimate. Note that the nonlinearity of SNLS and $SNLS^{-1}$ institute order dependence in the inversion process, *i.e.*,

$$\left\{\widehat{SNLS}^{-1}(\widehat{DLS}^{-1} \cdot U)\right\} \neq \left\{\widehat{DLS}^{-1} \cdot \widehat{SNLS}^{-1}(U)\right\} .$$

The ID methods which did not estimate the DLS as well as the SNLS, namely the Step, Impulse and Raw Ramp Response Methods, were tested with the dynamic system estimate from DRRM for that block.

Input

It can be seen from the preceding discussion on DLS cancellation that a physically realizable inversion of the second-order $\widehat{DLS}$ requires a command sequence with finite first and second derivatives. An $x(t)$ constructed from a ramp by Eq. 5.8 could not have been successfully implemented. Perfect following of the ramp's sharp edges would demand the muscle to change its velocity instantaneously which, having inertia, it is incapable of doing. This is illustrated in Figure 5.12(a) in the discontinous first and infinite-valued second derivatives of a ramp $x(t)$. The inverted cosine bell of Figure 5.12(b), described by

$$u(t) = 1 - cos(\omega t),\ (0 \leq t \leq \frac{2\pi}{\omega}) \text{ and } (\omega = 1/2T_{hr}) \ , \tag{5.10}$$

has two finite derivatives and was thus satisfactory for force command following.

Note, however, that if muscle velocity or position were being controlled in place of force, (b) would also be inappropriate. The only directly controllable output quantity in this system is muscle contractile force via modulation of stimulus strength. Control of muscle length (position) or velocity of shortening or lengthening are possible only by controlling muscle force in conjunction with a knowledge of the muscle load's static and dynamic characteristics. Therefore a U_{vel} referring to desired velocity, for instance, would have to be differentiated to find the desired force output U_{force} corresponding to U_{vel}, and $U_{force} = d(U_{vel})/dt$ then manipulated as in Eq. 5.8. This means one component of X would be the original U_{vel}'s third derivative, or for position control, U_{pos}'s fourth derivative. The third and fourth derivatives of the cosine bell of Eq. 5.10 have infinite initial and final values. Therefore in the cases of position or velocity command following a different command sequence must be found, such as the first or second integral of the cosine bell.

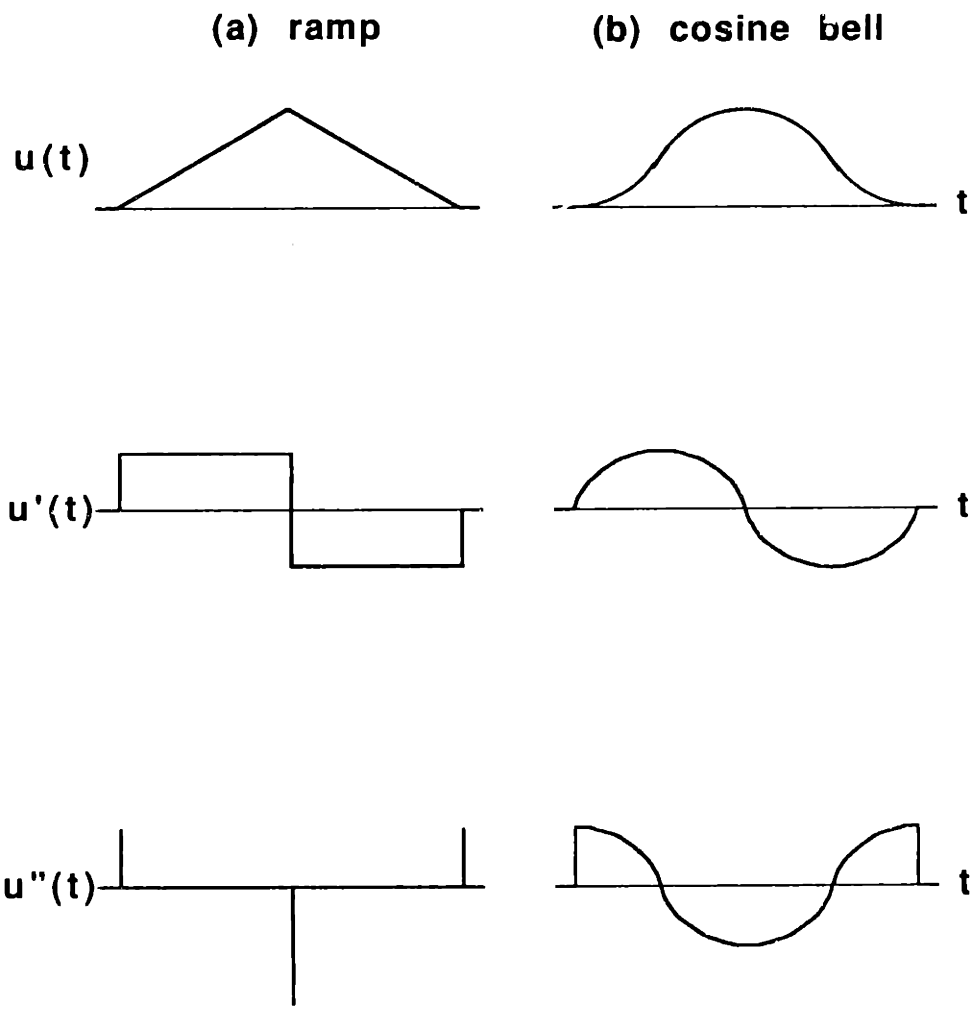

Figure 5.12: Dynamic OLC input candidates and their derivatives: (a) ramp and (b) cosine bell.

Evaluation

To measure the accuracy with which the actual output Y matched the desired output $Y_d = U$, an error criterion was constructed for the continuous inverse response:

$$\varepsilon(\text{DOLC}) \equiv \frac{1}{n_d} \sum_{i=1}^{n_d} \mid u_{t_k} - y_{t_k} \mid \tag{5.11}$$

where $n_d = 2 \cdot T_{hr} \cdot f_s$ was the number of data points in the dynamic I/O sequence. $\varepsilon(\text{DOLC})_{avg}$ averaged the continuous inverse response error for all the IRC estimates tested in dynamic OLC during the study.

Chapter 6

Results: IRC Estimate Comparisons and OLC Testing

This chapter contains the recorded and reduced results of open loop control (OLC) tests, taken to evaluate the recruitment curve identification methods. The experimental data relevant to ID method development may be found in Chapter 4.

The last two animals, C10 and C11, were devoted largely to testing of the ID methods in open loop control. The protocols for these two animals were structured according to the section on experimental design, 5.1, each containing two Recruitment Curve Block (RCB) / Open Loop Control Block (OLCB) pairs. For both subjects, the first RCB/OLCB pair was taken in tandem, *i.e.* the RCB was completed before the OLCB was begun. It was found that system changes during the combined block were so large that the IRCs estimated in the RCB no longer described the muscle well enough to be useful for control purposes. The OLCB data had to be discarded, but the RCB data was particularly valuable since the various IRC estimates were made within a short timespan.

The second RCB/OLCB pair was interspersed as described in Section 5.1. Its OLCB data was valid, but direct comparisons of the IRC estimates themselves should be made with skepticism since they are separated by significant periods of time and muscle activity.

6.1 System Time Variation

6.1.1 Tracking of Real Threshold Time Variation

Estimated muscle stimulus threshold (THR_{TB}) was recorded as described in Section 5.2.1 for all DCBs and RCBs, and used to construct a record of threshold variation over the day. Figure 6.1 plots THR_{TB} as a function of time for the TA and MG of subject C11. This steady and occasionally precipitous temporal decrease in stimulus threshold was observed consistently in all subjects of this study. The TA's threshold dropped so far during this experiment that the stimulus pulse amplitude (PA), usually held constant throughout an experiment, had to be decreased after 8 hours, explaining the discontinuity in the TA record of Figure 6.1(b).

(a) C10

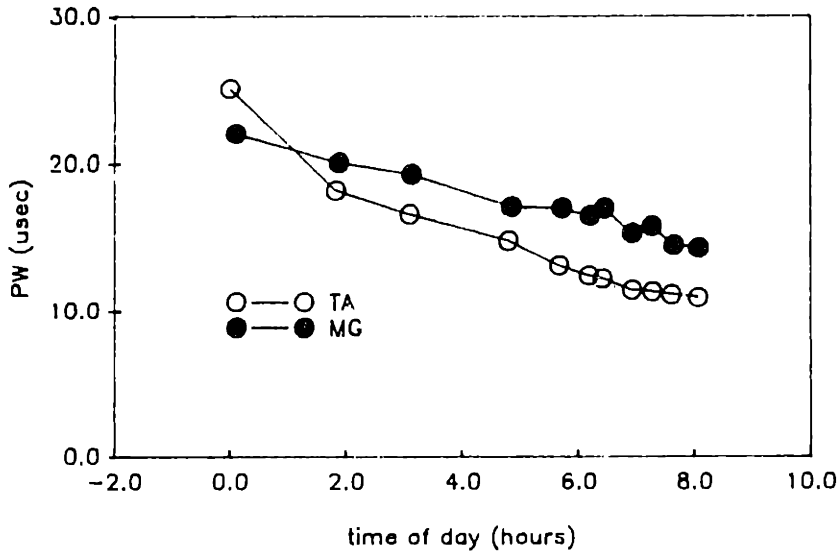

(b) C11

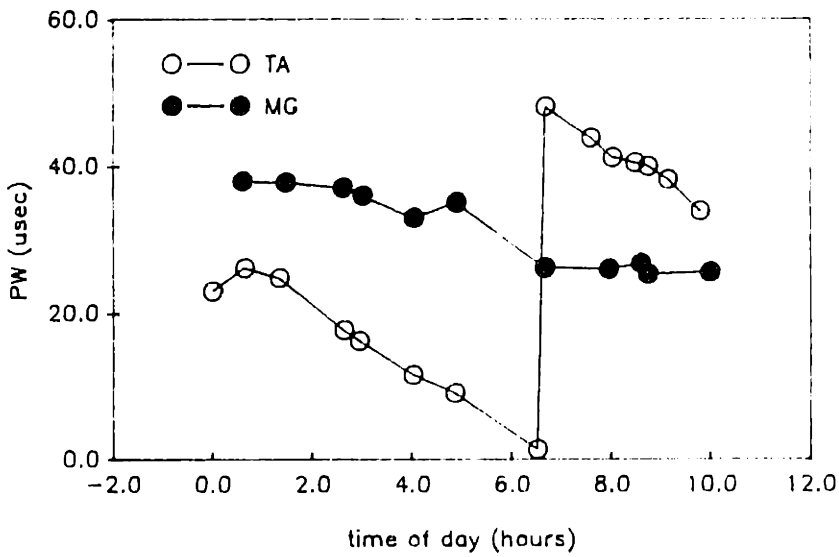

Figure 6.1: THR_{TB} as a function of time. TA and MG of subject animals (a) C10 and (b) C11.

If the PA were not reset to reduce the total amount of current passing through the electrode at a given pulsewidth (PW), stimulus threshold would drop to a very small value and the active zone width and effective stimulus input resolution would decrease as well.

6.1.2 Effect of Delay Between IRC Estimation and Use

To demonstrate the degradation of IRC effectiveness with the passage of time, OLC command-response records taken from the first and second RCB/OLCB pairs are compared. The first data block pair was taken in tandem, the RCB completed before the OLCB was begun. The second pair was interspersed by immediate testing of each IRC estimate.

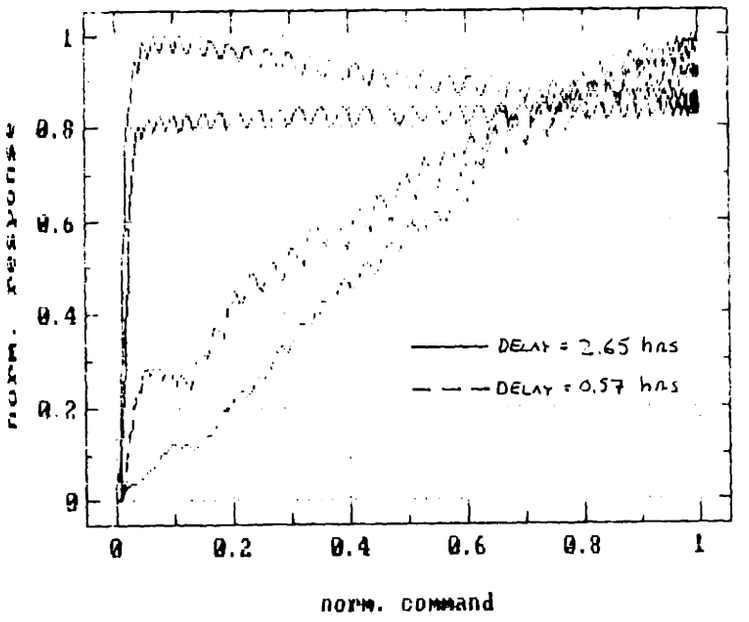

Figure 6.2: Effect on OLC of delay between DRRM IRC estimation and use. TA, subject C11.

Figure 6.2 plots TA response vs. inverted $\left[\widehat{\mathrm{DLS}} + \widehat{\mathrm{SNLS}}_{DRRM}\right]$ dynamic command from each of the two data sets. Time elapsed between estimation and testing of

the first curve (in RCB1 and OLCB1, respectively) was 2.65 hours; for the second (RCB2/OLCB2), 0.57 hours.

6.2 Isometric Recruitment Curves

Figure 6.3 shows a set of typical IRCs estimated by each identification method, as well as two-point maps, for the TA and the MG of subject animal C11. Data for all maps shown were taken with the same zoom zone (ZZ) during the second RCB, as an RCB/OLCB pair of total elapsed time 135 minutes.

Each IRC estimate was normalized to its own peak for ease of comparison; without normalizition, peaks vary widely because the ID methods use different kinds of input. For example, a steady-state response to a step input in general has a greater magnitude than does the response to either an impulse or a ramp of the same peak amplitude. In the case of the DRRM, the IRC estimate is the result of a deconvolution with arbitrary gain; for the StoRM, a linear system gain may be absorbed by either the $\widehat{\text{SNLS}}$ or the $\widehat{\text{DLS}}$ blocks, diminishing the significance of the amplitude of the estimated intermediate V sequence.

The IRCs were estimated over a period of time, and estimates were separated by periods of the steady muscle activity of OLC testing. Times of estimation relative to that for the first IRC (SRM's) are listed in Table 6.1, and may be compared to the curves in Figure 6.3.

Direct comparison analyses were carried out on StoRM estimates for the sake of completeness. Because of their obvious crudity, however, they were not tested in open loop control.

Variation Among Muscles

Although the TA and MG were chosen for their dynamic similarity (similar populations of fast and slow-twitch fibers), their dynamic responses were not identical. This is illustrated by Figure 6.4(a) with the normalized impulse responses of each muscle of

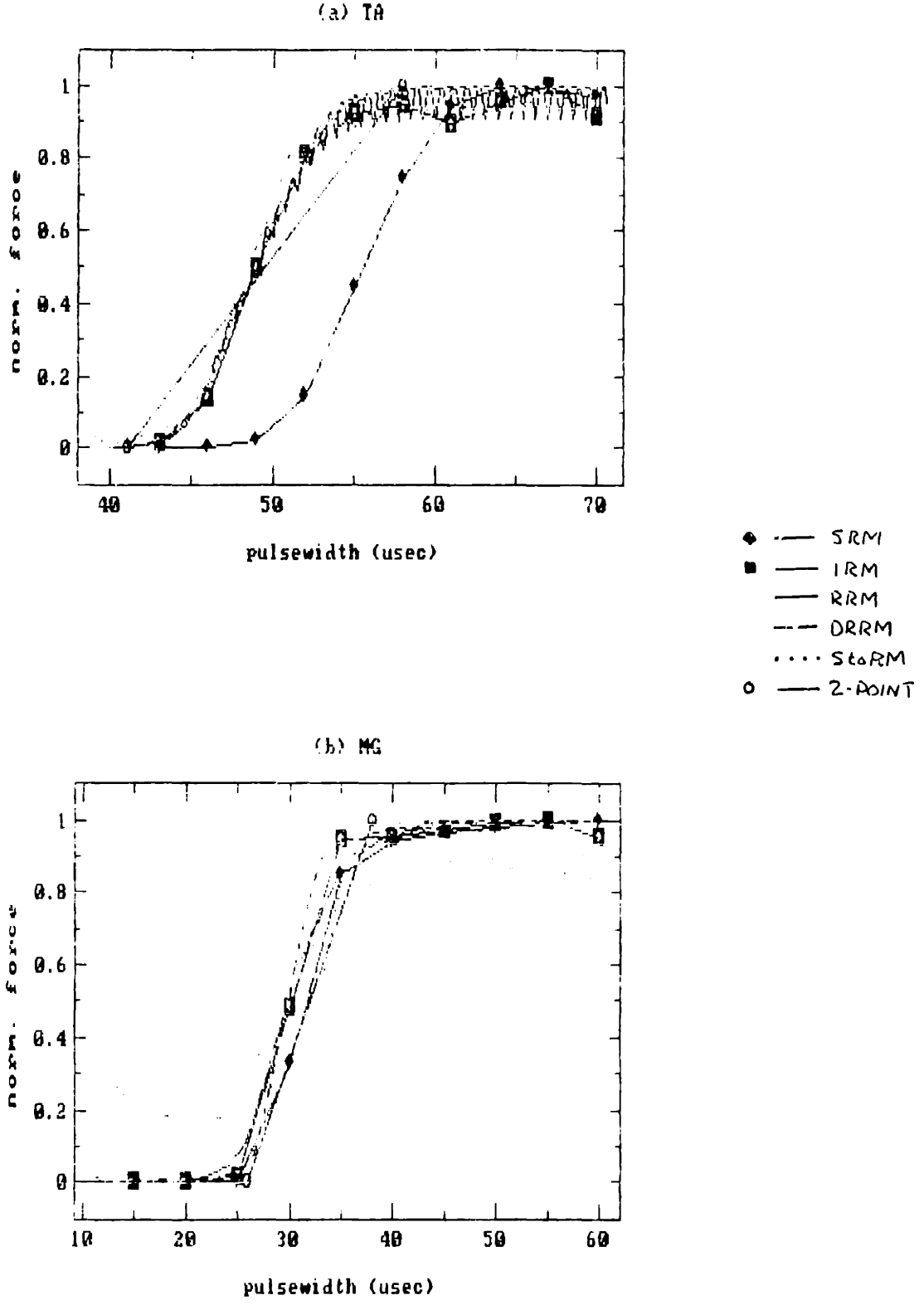

Figure 6.3: Typical normalized IRC estimates for each ID method. RCB2/OLCB2, subject C11.

			identification method					
	muscle	parameter	SRM	IRM	RRM	DRRM	StoRM	2-point
time of estimation (hours)	TA	T	0.00	0.50	0.95	0.95	1.68	1.83
		Δt	—	0.50	0.45	0.45	0.73	0.15
	MG	T	0.00	0.42	0.88	0.88	1.57	1.70
		Δt	—	0.42	0.46	0.46	0.69	0.13

Table 6.1: Times of estimation for the IRC estimates of Figure 6.1. t_0 is the start of the RCB/OLCB pair.

subject C11, and in 6.4(b) by their ramp response/input crossplots (T_{hr} = 1.0 seconds). The time-to-peaks (τ_{peak}) of the impulse responses are 0.015 and 0.030 seconds, respectively, corresponding to poles at 66.67 and 40.00 rad/sec for linear, critically damped second-order systems. These records were taken from the DRRM data set of the second RCB/OLCB pair, the source of the IRC estimates plotted in Figure 6.3.

6.3 IRC Estimate Morphology

The consistency, accuracy and sources of variation in the IRCs estimated by the different ID methods were evaluated with the aid of the three criterion defined and discussed in Section 5.2: estimated IRC threshold (THR_{meth}), active zone width (AZW), and shape (SHAPE). For all three criterion, the "typical" results shown summarize data which span two Recruitment Curve Blocks (RCBs) taken from the TA or MG of a single animal, C11, during one experiment. The duration of each RCB (time elapsed from threshold measurement to completion of data acquisition for last method) was less than or equal to 110 minutes. The "average" results are based on IRCs estimated

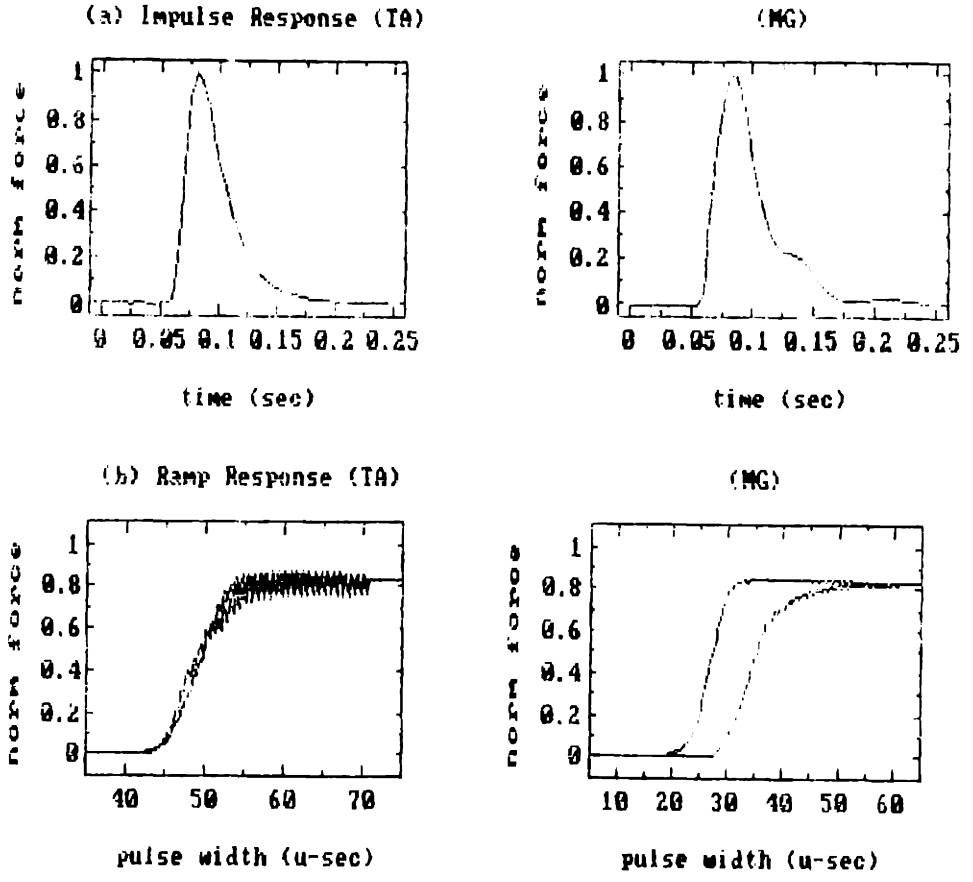

Figure 6.4: Difference in the (a) impulse responses and (b) ramp responses of the TA and MG of C11.

from a total of four RCBs, taken from two animals (C10 and C11), and using both the TA and MG.

6.3.1 Threshold Estimation

THR_{TB} was used to calculate $\epsilon(THR_{meth})$ (Eq. 5.1), the divergence of the THR_{meth} estimated by each IRC ID method from THR_{TB}, for recruitment curves estimated by each ID method during a particular RCB. $\epsilon(THR_{meth})$for a single data set (RCB2, subject C11), as well as the average $\epsilon(THR_{meth})$ for all the recruitment curves estimated for each method from subjects C10 and C11 is displayed by method in Figure 6.5 ($n = 8$). Table 6.2 lists statistics for $\epsilon(THR_{meth})$, with the statistical pool complete and also subdivided by muscle and animal.

Method-predicted stimulus threshold was defined as the interpolated SS value which first excited an interpolated force value equal to the force threshold, which was in turn defined as a percent of maximum force. The interpolation was necessary to compare how low-resolution methods such as the SRM and IRM, each with 11 points, with the higher-resolution methods. The error criterion $\epsilon(THR_{meth})$ was calculated using a THR_{TB} value interpolated between the two closest values bracketing a given ID method data set, since THR_{TB} changed so rapidly.

For a smooth curve with a steep active zone, THR_{meth} is not very sensitive to the value of force stimulus used. However, some of the methods did not produce completely smooth IRCs. The DRRM curve in particular was characterized by low amplitude noise in the deadzone region, an artifact of imperfectly filtered deconvolution of a noisy output. Stimulus threshold was evaluated at a force threshold of 2% of the curve's maximum, so that THR_{meth} for the DRRM would reflect the initiation of the curve's active zone rather than a spurious noise value.

$\epsilon(THR_{meth})$ shows substantial variation for all the methods. Two factors must be noted here. First, the zoom zone for the first RCB (curves not shown) was not chosen conservatively enough to allow for the drop in threshold which occurred during the

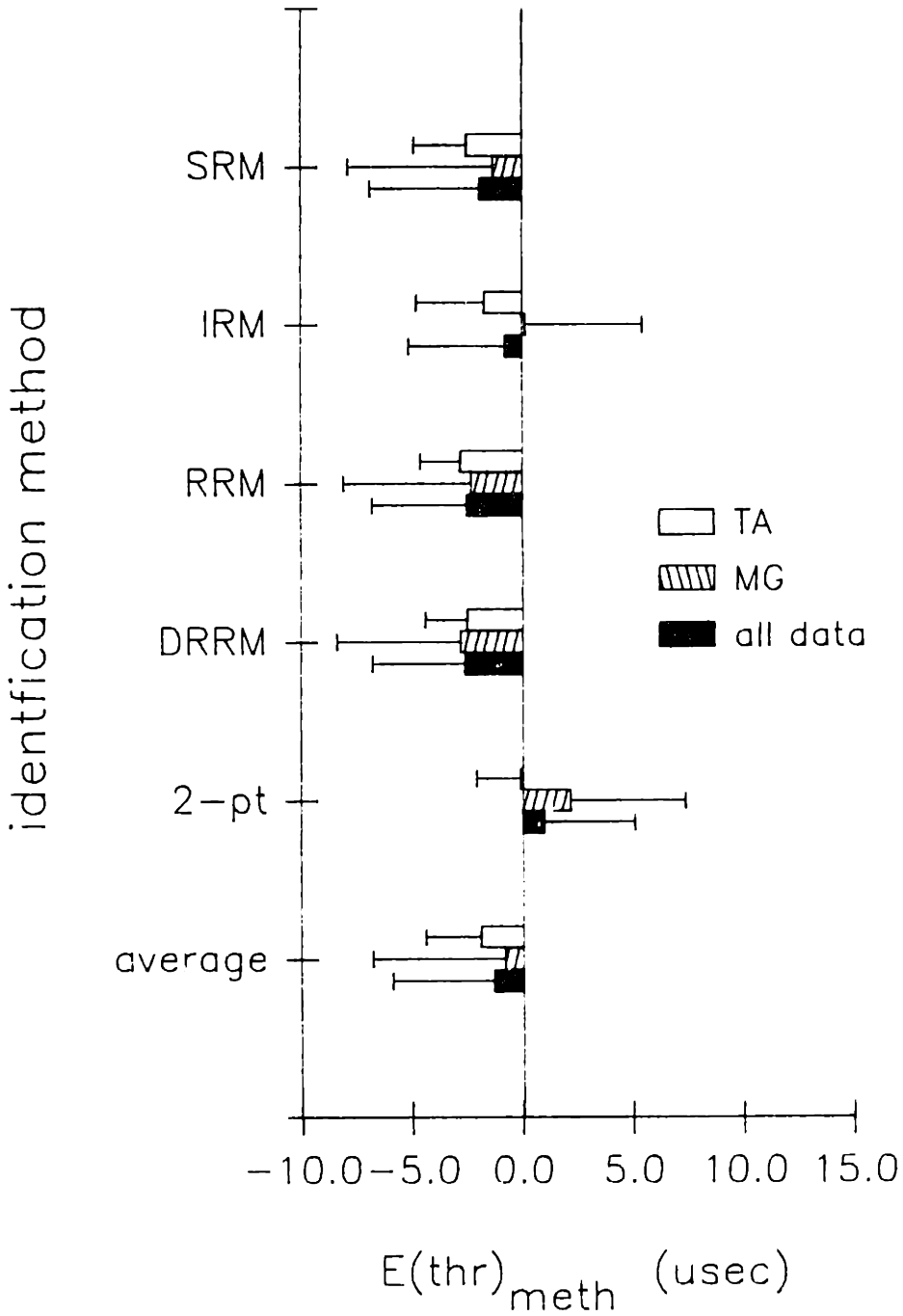

Figure 6.5: Average threshold-finding error ($\varepsilon(\mathrm{THR})_{avg}$) for each ID method. All data: average if TA and MG, C10 and C11 ($n = 8$).

data block. Some of the IRCs were estimated from data which did not include the deadzone and turn-on region; *i.e.*, the lowest stimulus strength used in estimation was higher than the actual threshold, so the ID methods had no way of finding the correct value and were forced to overestimate it. This problem was encountered whenever it was desirable to hold the zoom zone constant; it was difficult to predict how far the threshold would drop during a given period of time.

Secondly, THR_{TB} as a function of time (Figure 6.1) is neither smooth nor monotonic, so that $\varepsilon(\mathrm{THR}_{meth})$ values may be colored by error due to THR_{TB} interpolation.

6.3.2 Active Zone Width

Recruitment curve active zone width (AZW) as estimated by each IRC ID method was monitored over the experimental day. SAT_{meth} was found in the same way as was THR_{meth}, *i.e.* as the interpolated SS first giving an interpolated force greater than the defined saturation level, here 97% of the curve's peak. The percent change in the AZW predicted by each ID method from the value estimated at start of the experiment was calculated for each method and corrected for elapsed time $(t_k - t_0)$. Averaged values of this parameter, $\Delta\mathrm{AZW}/\Delta t$, are plotted by ID method for the TA and MG of subjects C10 and C11, in Figure 6.6 and listed in Table 6.3. Since only two RCBs were taken from each animal, only one value of $\Delta\mathrm{AZW}/\Delta t$ could be evaluated per muscle for each ID method.

Figure 6.7 and Table 6.4 show averaged percent change in AZW estimated by each ID method ($\Delta\mathrm{AZW}_{meth}$, Eq. 5.4), calculated for the same population with respect to the chosen standard, SRM, in the same RCB.

In Figures 6.6 and 6.7, recall that ΔAZW is calculated with respect to the first IRC's or the SRM's active zone width, respectively. A positive value indicates that that ID method predicted an active zone narrower than standard's.

6.3.3 Shape

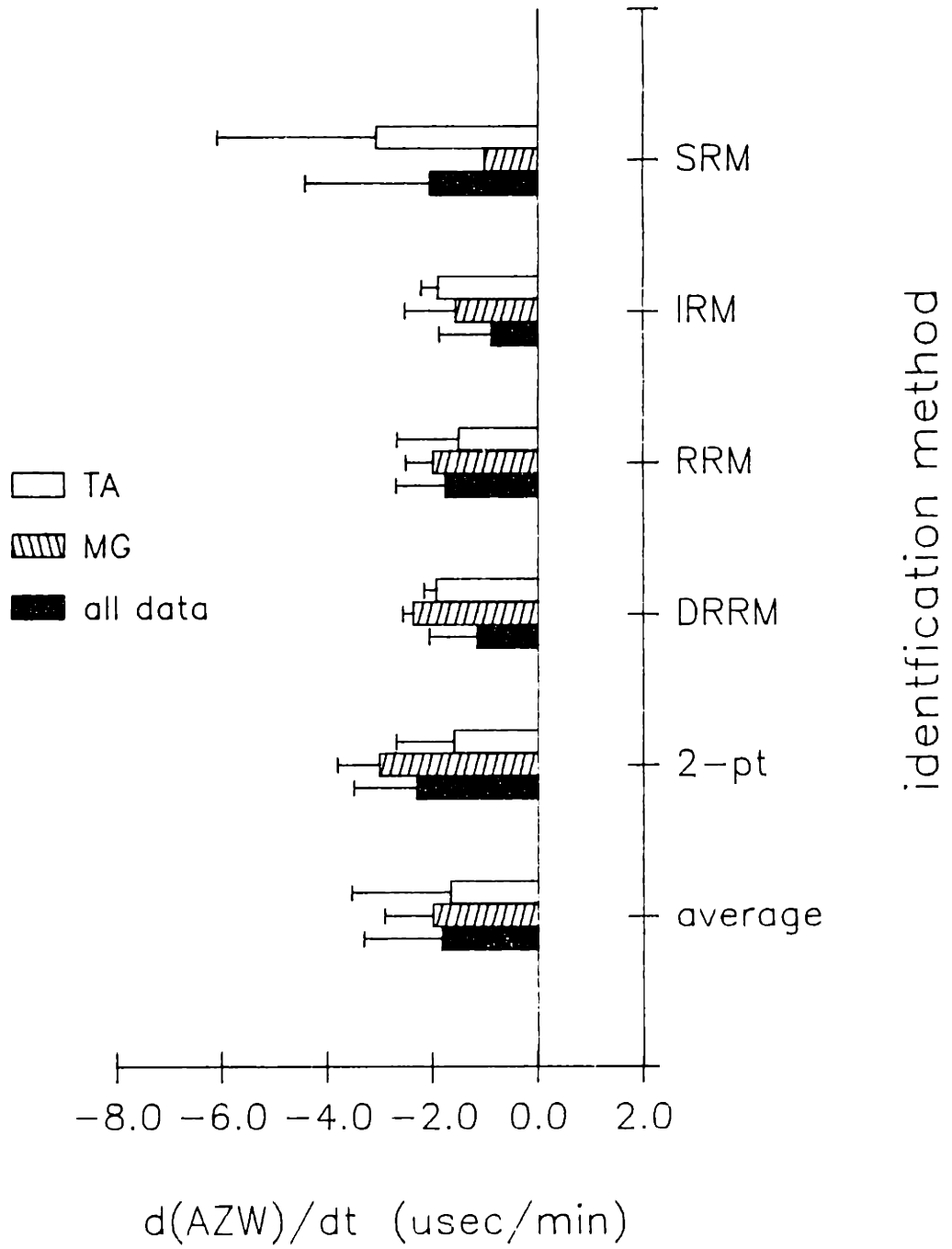

Figure 6.6: Averaged AZW % change over time ($\Delta AZW/\Delta t$), normalized by elapsed time. All data: average of TA/MG, C10/C11 ($n = 4$).

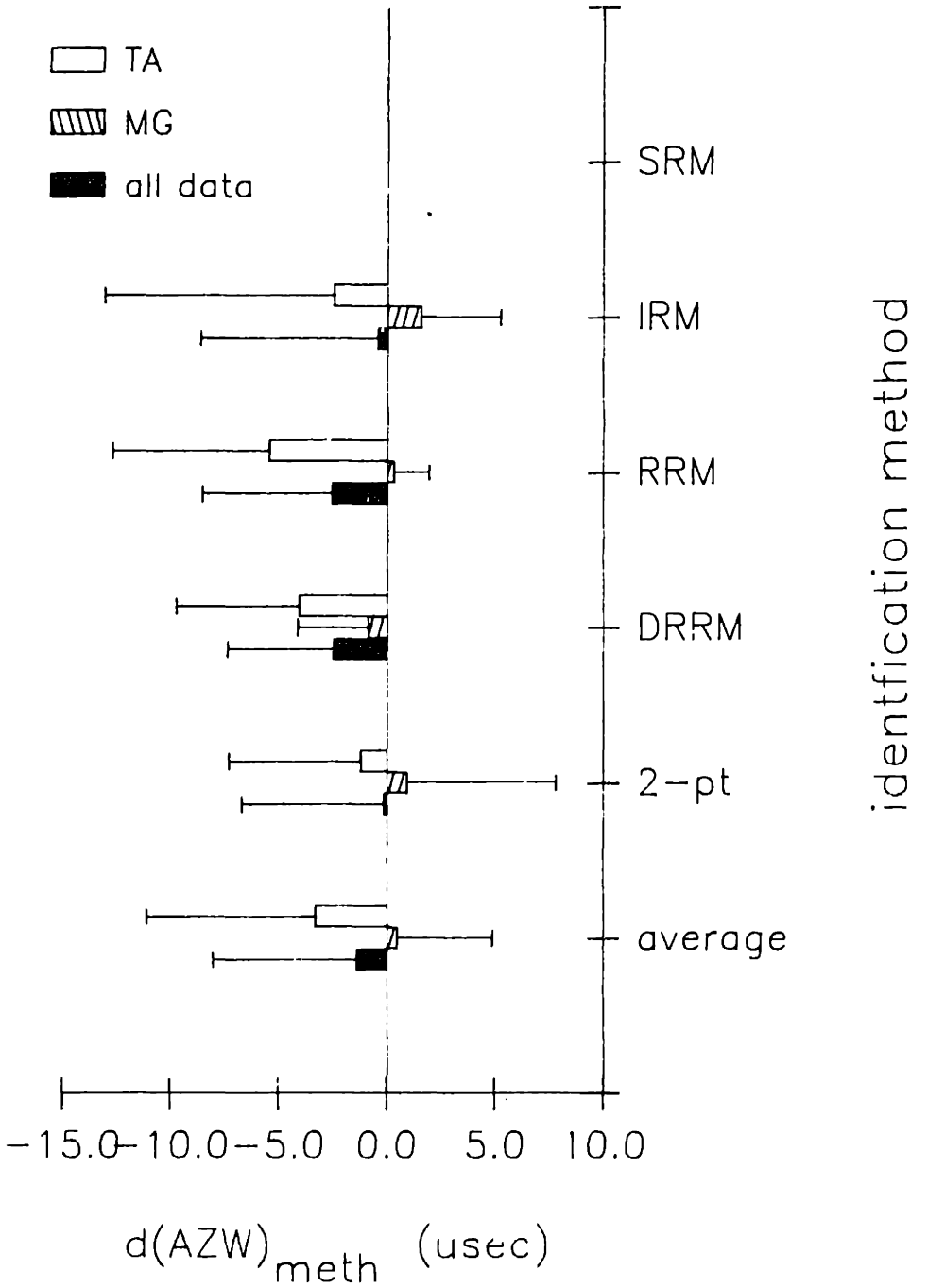

Figure 6.7: Averaged AZW % change from that of the SRM IRC estimated in the same data set (ΔAZW_{meth}). All data: TA/MG, C10/C11 ($n = 8$).

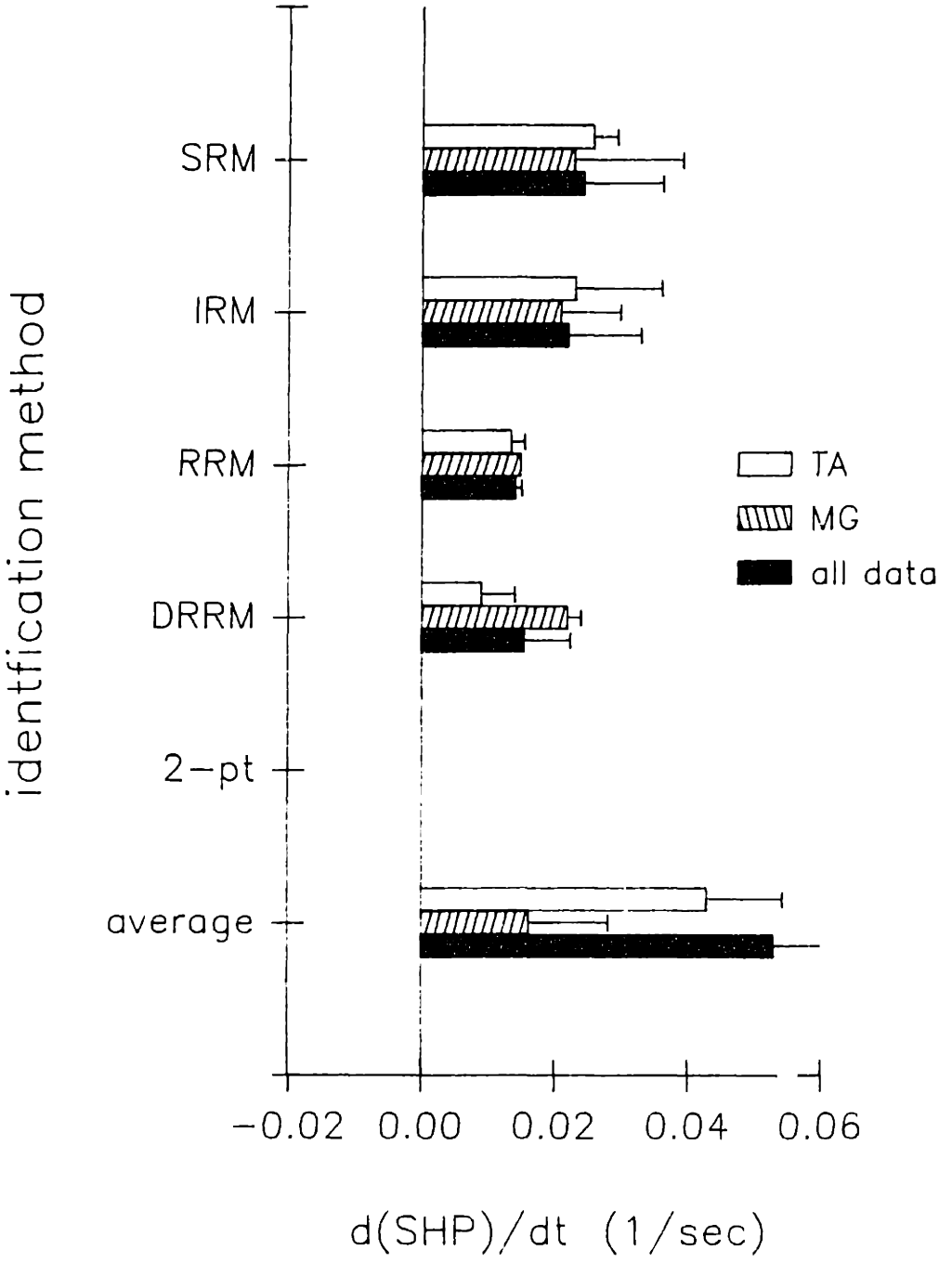

Figure 6.8: Averaged SHAPE % change over time (ΔSHAPE/Δt), normalized by elapsed time. All data: average of TA/MG, C10/C11 ($n = 4$).

(a) TA

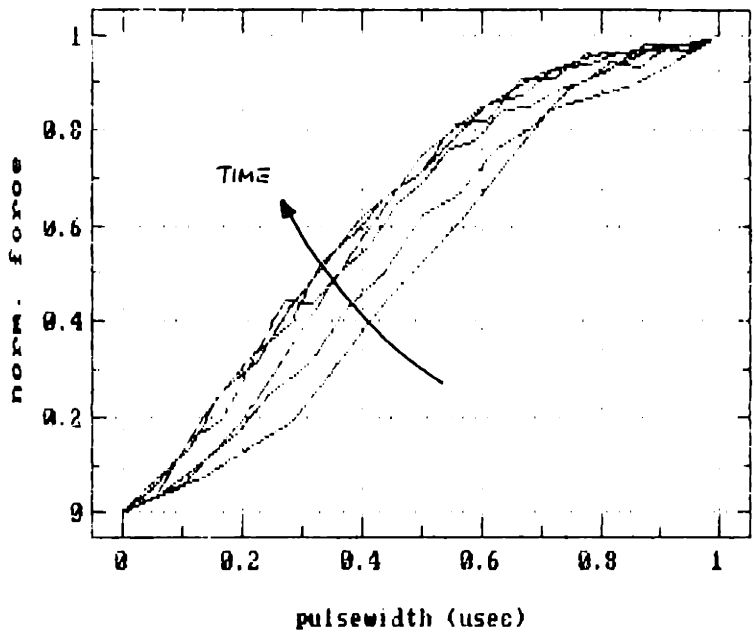

(b) MG

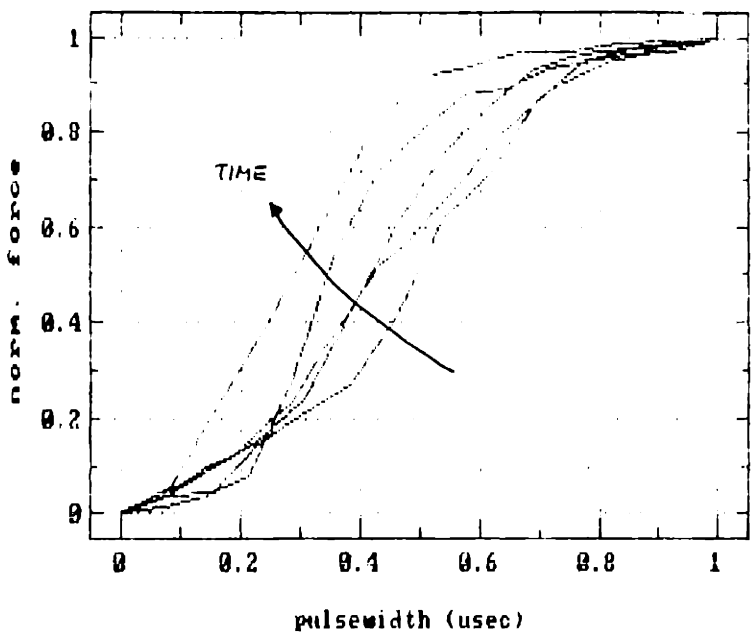

Figure 6.9: Biaxially normalized DRRM IRC estimates from the same muscles, showing temporal shape change. (a) TA and (b) MG, subject C11.

Temporal drift in normalized recruitment curve shape was tracked with the parameter ΔSHAPE/Δt (Eq. 5.7), the percent change in estimated IRC shape after biaxial normalization from the first IRC estimated by that ID method during that experiment.

Figure 6.8 shows averaged ΔSHAPE/Δt as a function of ID method, calculated from the temporal difference between the recruitment curves estimated by each method in two RCBs from each of subjects C10 and C11. Statistics for ΔSHAPE/Δt are tabulated by ID method, muscle and individual in Table 6.5.

To convey the magnitude of divergence represented by the values of Figure 6.8, the actual high-resolution DRRM recruitment curve estimates from which ΔSHAPE values were calculated for the TA and MG of subject C11 are plotted in order of estimation in Figure 6.9, after biaxial normalization. The additional curves in each plot are from DRRM's execution during DCBs as well as RCBs. Values of ΔSHAPE are plotted by method in Figure 6.10 as an average of TA and MG shape differences found in two RCBs taken from each of two subjects, C10 and C11, and listed in Table 6.6. Cross-method shape differences are illustrated in Figure 6.11, with examples of biaxially normalized TA and MG IRCs estimated at the same time by each ID method. Data was taken during a single RCB from subject C11; the IRC estimates are the same as those shown without normalization in Figure 6.3.

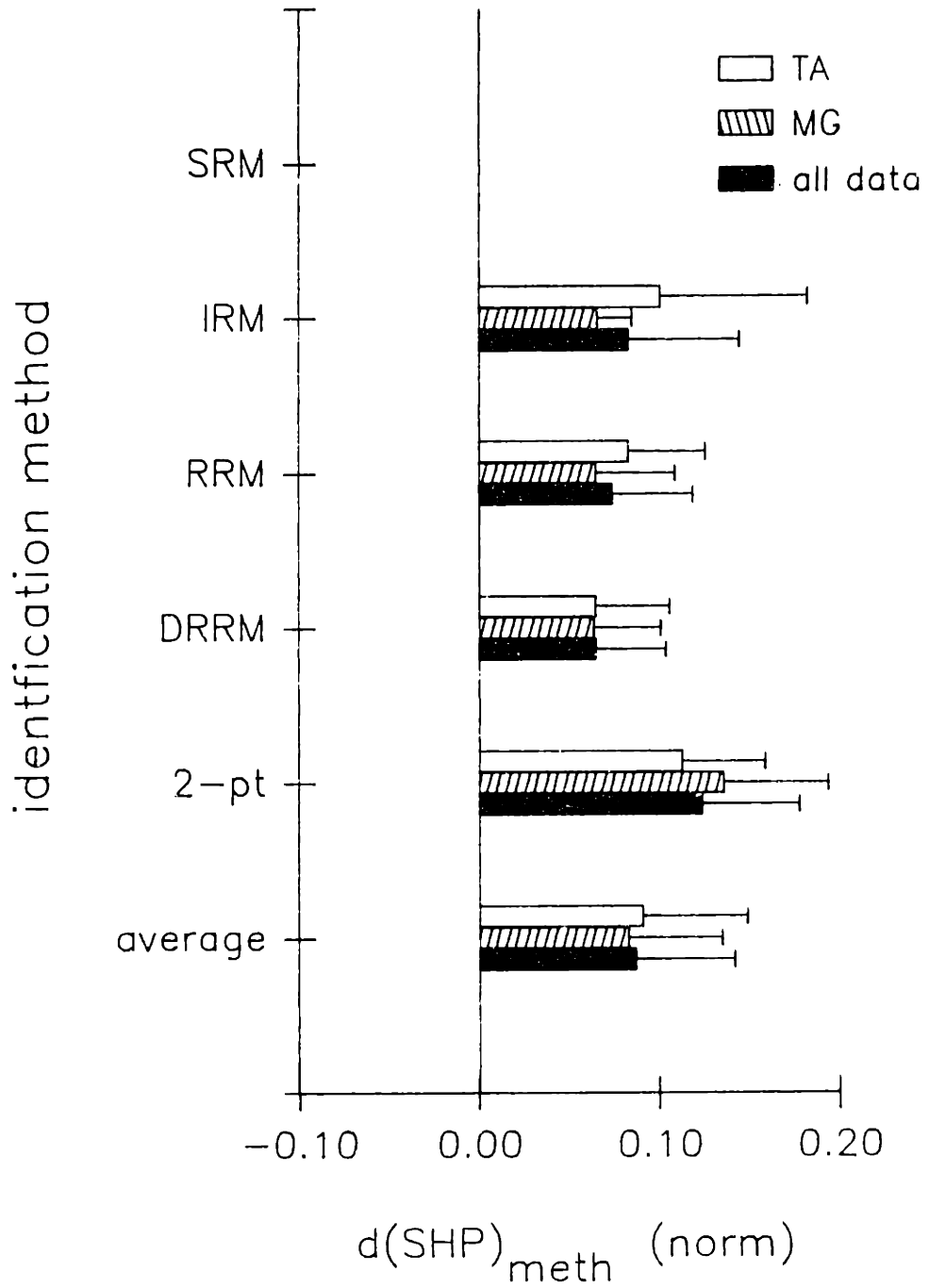

Figure 6.10: Average cross-method ΔSHAPE by method. The SRM is the standard for comparison. All data: TA/MG, C10/C11 ($n = 8$).

(a) TA

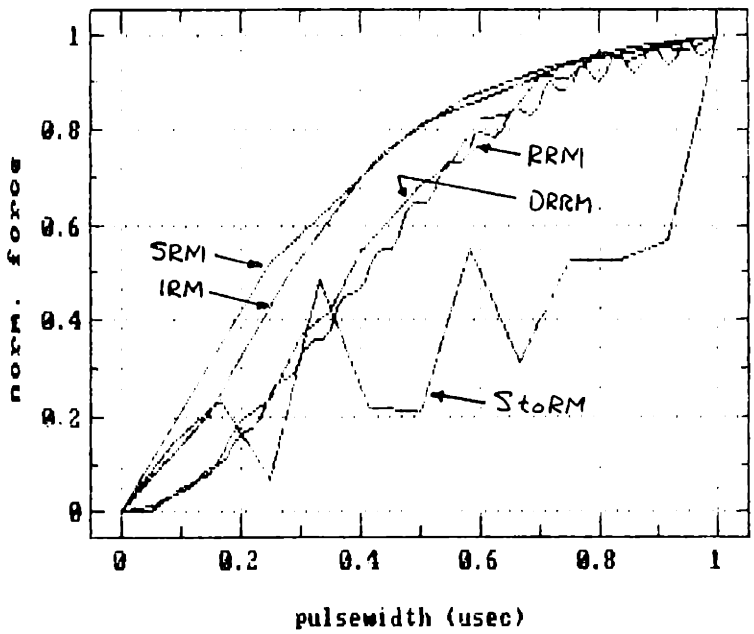

(b) MG

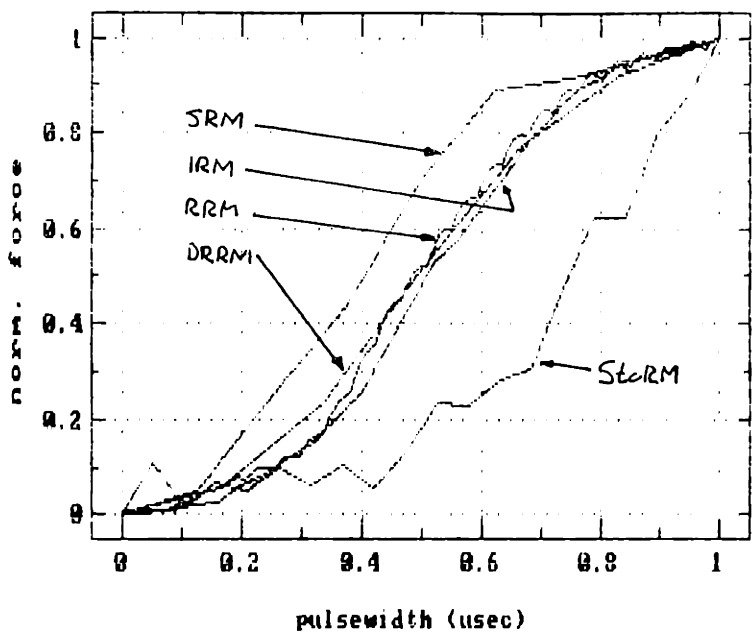

Figure 6.11: Cross-method variation in estimated IRC shape: normalized IRCs from each method for (a) TA and (b) MG of a single C11 RCB.

$\varepsilon(\mathbf{THR}_{meth})$

ID Method	muscles	subject	n	range	mean	med	std. dev.
SRM	TA	C10, C11	4	6.3	-2.5	-1.4	2.4
	MG	C10, C11	4	18.4	-1.3	-1.1	6.6
	TA, MG	C10	4	10.4	0.8	-0.9	4.0
	TA, MG	C11	4	11.2	-4.6	-4.1	4.4
	TA, MG	C10, C11	8	18.4	-1.9	-1.4	5.0
IRM	TA	C10, C11	4	7.7	-1.7	-0.1	3.1
	MG	C10, C11	4	14.4	0.2	-0.8	5.3
	TA, MG	C10	4	10.6	1.6	0.2	4.0
	TA, MG	C11	4	7.6	-3.1	-3.0	3.5
	TA, MG	C10, C11	8	15.4	-0.7	-0.1	4.4
RRM	TA	C10, C11	4	4.5	-2.8	-2.2	1.8
	MG	C10, C11	4	14.5	-2.3	0.2	5.8
	TA, MG	C10	4	4.1	-0.4	-1.3	1.7
	TA, MG	C11	4	13.8	-4.6	-4.3	5.0
	TA, MG	C10, C11	8	14.5	-2.5	-1.5	4.3
DRRM	TA	C10, C11	4	4.7	-2.5	-1.8	1.9
	MG	C10, C11	4	14.6	-2.8	-0.8	5.6
	TA, MG	C10	4	4.1	-0.3	-0.9	1.6
	TA, MG	C11	4	12.3	-5.0	-3.9	4.6
	TA, MG	C10, C11	8	14.6	-2.6	-1.4	4.2
Two-Point	TA	C10, C11	4	4.7	-0.1	-0.2	2.0
	MG	C10, C11	4	13.1	2.2	-0.1	5.2
	TA, MG	C10	4	9.9	4.0	1.8	4.1
	TA, MG	C11	4	1.1	-1.9	-1.9	0.4
	TA, MG	C10, C11	8	13.5	1.0	-0.1	4.1
All Methods	TA	C10, C11	20	9.3	-1.9	-1.4	2.5
	MG	C10, C11	20	23.2	-0.8	-0.6	6.0
	TA, MG	C10	20	13.8	1.1	-0.4	3.7
	TA, MG	C11	20	14.1	-3.8	-2.4	4.1
	TA, MG	C10, C11	40	23.2	-1.3	-1.3	4.6

Table 6.2: $\varepsilon(\mathrm{THR}_{meth})$ statistics. TA and MG, taken from two subject C10 and two C11 RCBs. All values are μsec.

ΔAZW = function of time

ID Method	muscles	subject	n	range	mean	med	std. dev.
SRM	TA	C10, C11	2	6.1	-3.1	-3.1	3.0
	MG	C10, C11	2	0.0	-1.0	-1.0	0.0
	TA, MG	C10	2	1.0	-0.5	-0.5	0.5
	TA, MG	C11	2	5.1	-3.6	-3.6	2.5
	TA, MG	C10, C11	4	6.1	-2.0	-1.0	2.4
IRM	TA	C10, C11	2	0.6	-0.2	-0.2	0.3
	MG	C10, C11	2	2.0	-1.6	-1.6	1.0
	TA, MG	C10	2	0.7	-0.2	-0.2	0.3
	TA, MG	C11	2	2.0	-1.5	-1.5	1.0
	TA, MG	C10, C11	4	2.7	-0.9	-0.5	1.0
RRM	TA	C10, C11	2	2.4	-1.5	-1.5	1.2
	MG	C10, C11	2	1.0	-2.0	-2.0	0.5
	TA, MG	C10	2	2.1	-1.4	-1.4	1.1
	TA, MG	C11	2	1.2	-2.1	-2.0	0.6
	TA, MG	C10, C11	4	2.4	-1.7	-1.2	0.9
DRRM	TA	C10, C11	2	2.5	-1.9	-1.9	1.2
	MG	C10, C11	2	0.4	-2.4	-2.4	0.2
	TA, MG	C10	2	1.9	-1.6	-1.6	0.9
	TA, MG	C11	2	1.0	-2.7	-2.7	0.5
	TA, MG	C10, C11	4	2.5	-2.1	-2.4	0.9
Two-Point	TA	C10, C11	2	2.2	-1.6	-1.6	1.1
	MG	C10, C11	2	1.6	-3.0	-3.0	0.8
	TA, MG	C10	2	1.7	-1.4	-1.4	0.9
	TA, MG	C11	2	1.1	-3.3	-3.3	0.6
	TA, MG	C10, C11	4	3.3	-2.3	-2.4	1.2
All Methods	TA	C10, C11	10	6.2	-1.6	-1.7	1.9
	MG	C10, C11	10	3.2	-2.0	-2.0	0.9
	TA, MG	C10	10	2.7	-1.0	-1.0	1.0
	TA, MG	C11	10	5.6	-2.6	-2.6	1.5
	TA, MG	C10, C11	20	6.2	-1.8	-1.8	1.5

Table 6.3: $\Delta AZW/\Delta t$ statistics for each ID method, relative to initial value for that method. TA and MG, subjects C10 and C11. All values are μsec.

ΔAZW = function of method

ID Method	muscles	subject	n	range	mean	med	std. dev.
SRM	TA	C10, C11	0	—	—	—	—
	MG	C10, C11	0	—	—	—	—
	TA, MG	C10	0	—	—	—	—
	TA, MG	C11	0	—	—	—	—
	TA, MG	C10, C11	0	—	—	—	—
IRM	TA	C10, C11	4	28.5	-2.5	0.8	10.6
	MG	C10, C11	4	9.3	1.6	-0.1	3.7
	TA, MG	C10	4	2.5	0.2	0.4	0.9
	TA, MG	C11	4	28.5	-1.0	3.7	11.5
	TA, MG	C10, C11	8	28.5	-0.4	0.4	8.2
RRM	TA	C10, C11	4	17.3	-5.4	-1.6	7.2
	MG	C10, C11	4	4.3	0.3	1.0	1.6
	TA, MG	C10	4	2.9	0.3	0.3	1.2
	TA, MG	C11	4	18.7	-5.4	-2.3	7.3
	TA, MG	C10, C11	8	19.8	-2.5	-0.8	6.0
DRRM	TA	C10, C11	4	13.6	-4.1	-1.1	5.7
	MG	C10, C11	4	8.1	-0.9	0.7	3.3
	TA, MG	C10	4	3.0	0.2	0.3	1.1
	TA, MG	C11	4	14.5	-5.1	-3.6	5.7
	TA, MG	C10, C11	8	15.4	-2.5	-0.5	4.9
Two-Point	TA	C10, C11	4	14.6	-1.2	2.0	6.1
	MG	C10, C11	4	18.6	1.0	1.9	6.9
	TA, MG	C10	4	5.1	2.0	2.1	1.9
	TA, MG	C11	4	21.0	-2.2	-3.2	8.6
	TA, MG	C10, C11	8	21.0	-0.1	2.0	6.6
All Methods	TA	C10, C11	16	28.5	-3.3	-0.7	7.8
	MG	C10, C11	16	18.6	0.5	0.7	4.4
	TA, MG	C10	16	5.9	0.7	0.6	1.5
	TA, MG	C11	16	29.3	-3.4	-1.4	8.8
	TA, MG	C10, C11	32	29.3	-1.4	0.1	6.6

Table 6.4: ΔAZW_{meth} statistics for each ID method relative to the SRM. TA and MG, subjects C10 and C11. All values are μsec.

ΔSHAPE = function of time

ID Method	muscles	subject	n	range	mean	med	std. dev.
SRM	TA	C10, C11	2	.007	.026	.026	.004
	MG	C10, C11	2	.033	.023	.023	.016
	TA, MG	C10	2	.023	.018	.018	.011
	TA, MG	C11	2	.017	.031	.031	.009
	TA, MG	C10, C11	4	.033	.024	.024	.012
IRM	TA	C10, C11	2	.026	.023	.023	.013
	MG	C10, C11	2	.019	.021	.021	.009
	TA, MG	C10	2	.024	.024	.024	.012
	TA, MG	C11	2	.020	.020	.020	.010
	TA, MG	C10, C11	4	.026	.022	.022	.011
RRM	TA	C10, C11	2	.003	.014	.014	.002
	MG	C10, C11	2	.000	.015	.015	.000
	TA, MG	C10	2	.000	.015	.015	.000
	TA, MG	C11	2	.003	.013	.013	.002
	TA, MG	C10, C11	4	.003	.014	.017	.001
DRRM	TA	C10, C11	2	.009	.009	.019	.005
	MG	C10, C11	2	.004	.022	.018	.002
	TA, MG	C10	2	.016	.012	.020	.008
	TA, MG	C11	2	.010	.019	.017	.005
	TA, MG	C10, C11	4	.020	.016	.017	.007
Two-Point	TA	C10, C11	2	.000	.000	.000	.000
	MG	C10, C11	2	.000	.000	.000	.000
	TA, MG	C10	2	.000	.000	.000	.000
	TA, MG	C11	2	.000	.000	.000	.000
	TA, MG	C10, C11	4	.000	.000	.000	.000
All Methods	TA	C10, C11	10	.036	.014	.013	.011
	MG	C10, C11	10	.039	.016	.015	.012
	TA, MG	C10	10	.036	.014	.013	.011
	TA, MG	C11	10	.039	.017	.014	.012
	TA, MG	C10, C11	20	.039	.015	.014	.012

Table 6.5: ΔSHAPE/Δt statistics for each ID method, relative to initial value for that method. TA and MG, C10 and C11. Normalized A/D units.

ΔSHAPE = function of method

ID Method	muscles	subject	n	range	mean	med	std. dev.
SRM	TA	C10, C11	0	—	—	—	—
	MG	C10, C11	0	—	—	—	—
	TA, MG	C10	0	—	—	—	—
	TA, MG	C11	0	—	—	—	—
	TA, MG	C10, C11	0	—	—	—	—
IRM	TA	C10, C11	4	.209	.101	.069	.082
	MG	C10, C11	4	.042	.066	.064	.019
	TA, MG	C10	4	.040	.066	.067	.017
	TA, MG	C11	4	.209	.101	.068	.082
	TA, MG	C10, C11	8	.209	.083	.087	.062
RRM	TA	C10, C11	4	.112	.083	.083	.043
	MG	C10, C11	4	.117	.065	.050	.044
	TA, MG	C10	4	.112	.067	.050	.043
	TA, MG	C11	4	.117	.082	.083	.045
	TA, MG	C10, C11	8	.118	.074	.054	.045
DRRM	TA	C10, C11	4	.108	.065	.067	.041
	MG	C10, C11	4	.095	.064	.051	.037
	TA, MG	C10	4	.108	.057	.051	.039
	TA, MG	C11	4	.095	.072	.067	.037
	TA, MG	C10, C11	8	.115	.065	.054	.039
Two-Point	TA	C10, C11	4	.121	.113	.114	.046
	MG	C10, C11	4	.159	.135	.124	.058
	TA, MG	C10	4	.087	.110	.124	.035
	TA, MG	C11	4	.160	.139	.131	.064
	TA, MG	C10, C11	8	.175	.124	.124	.054
All Methods	TA	C10, C11	16	.229	.091	.086	.058
	MG	C10, C11	16	.205	.083	.065	.052
	TA, MG	C10	16	.130	.075	.057	.041
	TA, MG	C11	16	.216	.099	.087	.065
	TA, MG	C10, C11	32	.229	.087	.074	.055

Table 6.6: ΔSHAPE statistics for each ID method, relative to the SRM. TA and MG, subjects C10 and C11. All values in normalized A/D units.

6.4 IRC ID Method and Open Loop Control

The recruitment curves generated by each of the recruitment curve identification methods were tested in open loop control (OLC) situations, using both static and dynamic command inputs. Performances were compared with those using noninverted command sequences (a linear estimated IRC) and two-point IRC estimates.

The following pages show typical OLC test results. For consistency, all example tests for both types of input were taken from the second RCB/OLCB pair of subject animal C11, the one illustrated in Figure 6.3. Commands were inverted through appropriate IRC estimates taken from that RCB. The examples may be compared with one another since they refer to the same muscle preparation in the same state.

The first OLCB for subject C11 was taken in tandem with its associated RCB, rather than interspersed with it. During the time elapsed between IRC estimation and use, the active zone for both muscles shifted so far to the left that their IRC estimates were ineffectual in control. These test records are not included in any of the averaged values, because presumably they fail through system time variation and not because of defective IRC estimation.

Static Command Following

Muscle force response to inverted step commands was measured as described in Section 5.3. Figure 6.12 displays the records of steady-state force as a function of command amplitude corresponding to the IRC estimates of Figure 6.3. The total elapsed time of the RCB/OLCB pair was 135 minutes.

Figure 6.13 shows ε(SOLC) (Eq. 5.9) as a function of IRC ID method for the command-response sequences of Figure 6.12. Figure 6.13 shows averaged ε(SOLC) vs. IRC ID method, taken from three static OLC tests taken from the TA and MG of subjects C10 and C11, while Table 6.7 lists statistics for the static OLC tests performed. Some of the test data sets were incomplete, so the population size (n) varies with ID

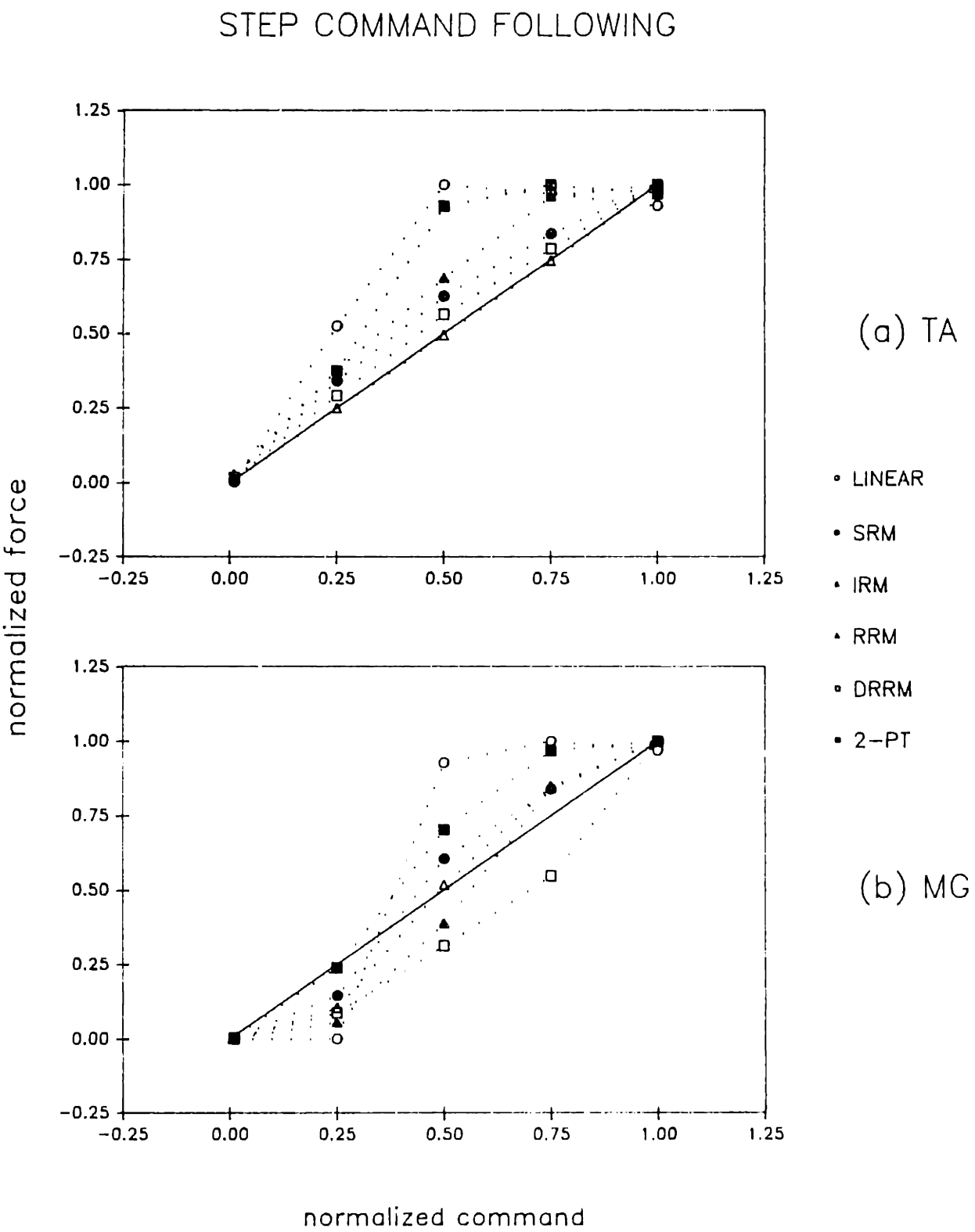

Figure 6.12: Typical static command following results. Commands were inverted through IRCs from each method. RCB2/OLCB2, C11.

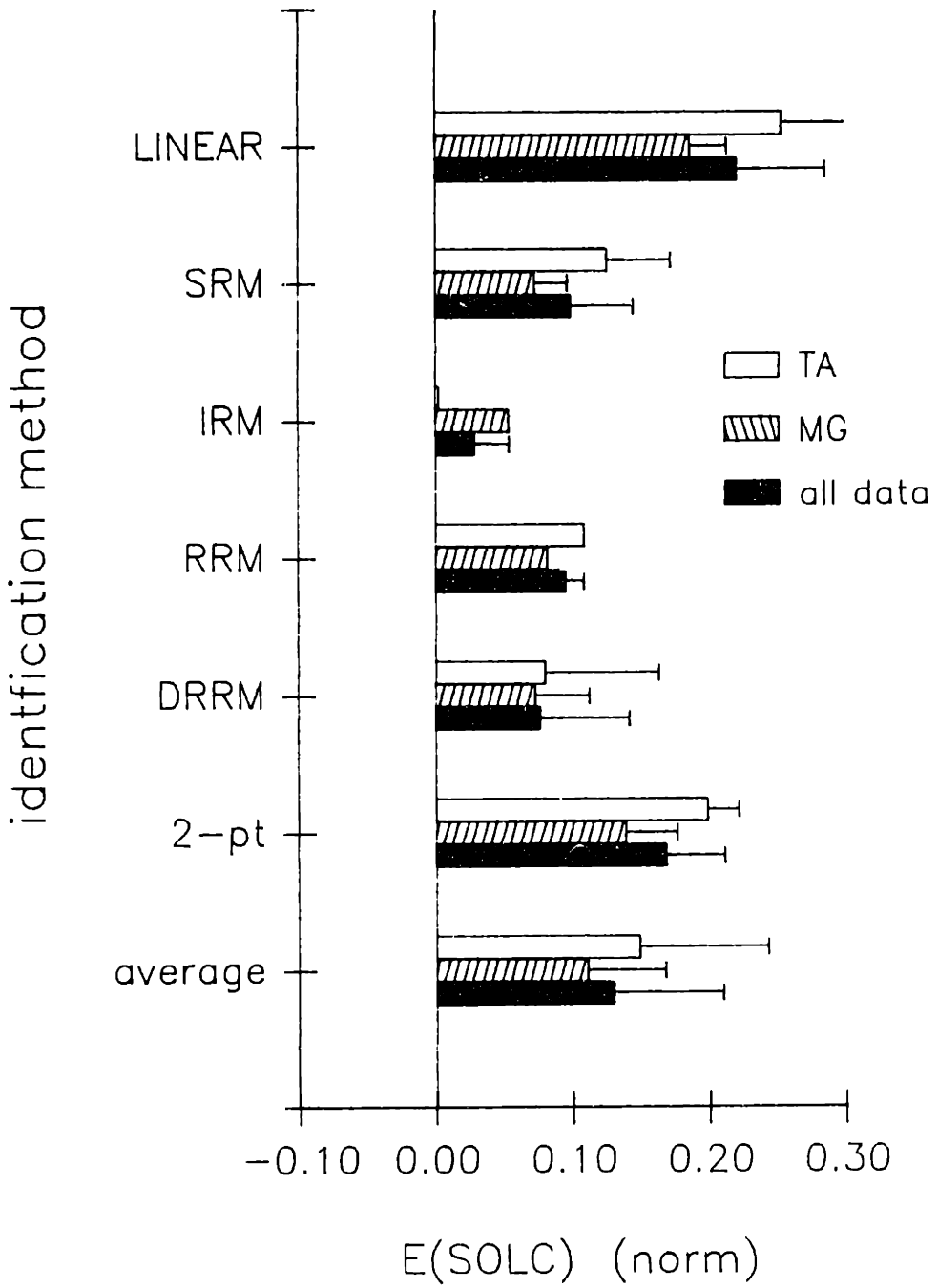

Figure 6.13: ε(SOLC) as a function of IRC ID method. All data: average of TA and MG, C10 and C11 ($n = 4$).

method.

ε(SOLC)

ID Method	muscles	subject	n	range	mean	med	std. dev.
linear	TA	C10, C11	3	.168	.254	.215	.074
	MG	C10, C11	3	.066	.187	.194	.027
	TA, MG	C10	4	.207	.229	.204	.078
	TA, MG	C11	2	.021	.204	.204	.011
	TA, MG	C10, C11	6	.207	.221	.204	.065
SRM	TA	C10, C11	3	.105	.126	.152	.047
	MG	C10, C11	3	.055	.073	.061	.024
	TA, MG	C10	4	.115	.119	.129	.045
	TA, MG	C11	2	.001	.061	.061	.001
	TA, MG	C10, C11	6	.115	.100	.084	.046
IRM	TA	C10, C11	1	.000	.003	.003	.000
	MG	C10, C11	1	.000	.054	.054	.000
	TA, MG	C10	0	—	—	—	—
	TA, MG	C11	2	.051	.029	.029	.026
	TA, MG	C10, C11	2	.051	.029	.029	.026
RRM	TA	C10, C11	1	.000	.109	.109	.000
	MG	C10, C11	1	.000	.082	.082	.000
	TA, MG	C10	0	—	—	—	—
	TA, MG	C11	2	.027	.095	.095	.014
	TA, MG	C10, C11	2	.027	.095	.095	.014
DRRM	TA	C10, C11	3	.184	.080	.029	.083
	MG	C10, C11	3	.094	.073	.086	.040
	TA, MG	C10	4	.184	.079	.053	.074
	TA, MG	C11	2	.085	.071	.071	.042
	TA, MG	C10, C11	6	.184	.077	.057	.065
Two-Point	TA	C10, C11	3	.055	.199	.204	.023
	MG	C10, C11	3	.089	.139	.152	.038
	TA, MG	C10	4	.071	.189	.191	.027
	TA, MG	C11	2	.080	.128	.128	.040
	TA, MG	C10, C11	6	.135	.169	.172	.043
all methods (excluding linear)	TA	C10, C11	14	.354	.149	.167	.094
	MG	C10, C11	14	.198	.111	.097	.057
	TA, MG	C10	16	.344	.154	.159	.084
	TA, MG	C11	12	.212	.098	.085	.063
	TA, MG	C10, C11	28	.354	.113	.132	.090

Table 6.7: Statistics for all static OLC tests performed. TA and MG, taken from two C10 and one C11 OLCBs. All values in normalized A/D units.

Dynamic Command Following

Muscle response to a continous command was measured, where the command input $u(t)$ was a cosine bell curve with half-ramp period (T_{hr}) of 1.0 second, and of amplitude 0.0 (zero response desired) to 1.0 (maximal response desired).

All tests displayed were conducted during the same (second) RCB/OLCB pair as were the examples of static open loop control tests shown in the previous section.

Figure 6.14 is a typical set of continuous command and force response time histories with complete plant cancellation, $X = \widehat{DLS}^{-1} \cdot \widehat{SNLS}^{-1}(U)$, where X is the stimulus input constructed by inverting the command U. The $\widehat{SNLS}$ was the IRC estimated by the indicated ID method, one of those shown in Figure 6.3. Force in all records was normalized to the record's maximum force so that closeness of command following could be seen clearly.

Figures 6.15 and 6.16 offer the same information from a different perspective, plotting force directly against command for the set of inverse plant permutations detailed in Section 5.3.2. They are composed of separate curves for each ID method because the inverse systems included the $\widehat{SNLS}$, and each ID method estimated a different $\widehat{SNLS}$. Figure 6.15 displays responses to commands passed only through an inverted $\widehat{SNLS}$ while muscle dynamics were neglected. In Figure 6.16, both static and dynamic estimated systems are cancelled and the command is shown with its elicited response for each kind of estimated IRC. The $\widehat{DLS}$ was obtained from the system impulse response in the manner of the Deconvolved Ramp Response Method, detailed in Section 4.1.3.

For both sets, the record which employed a linear IRC estimate serves as a control for the others. In the uninverted command-response sequence of Figure 6.15(a), the static subsystem is approximated as a straight line and muscle dynamics by a delta function (permutation (a) in Section 5.3.2), while Figure 6.16(a) shows the effect of neglecting static nonlinearity while inverting the linear dynamic system (permutation (b)).

Note that many of the TA time histories of Figure 6.14 show a glitch in force close

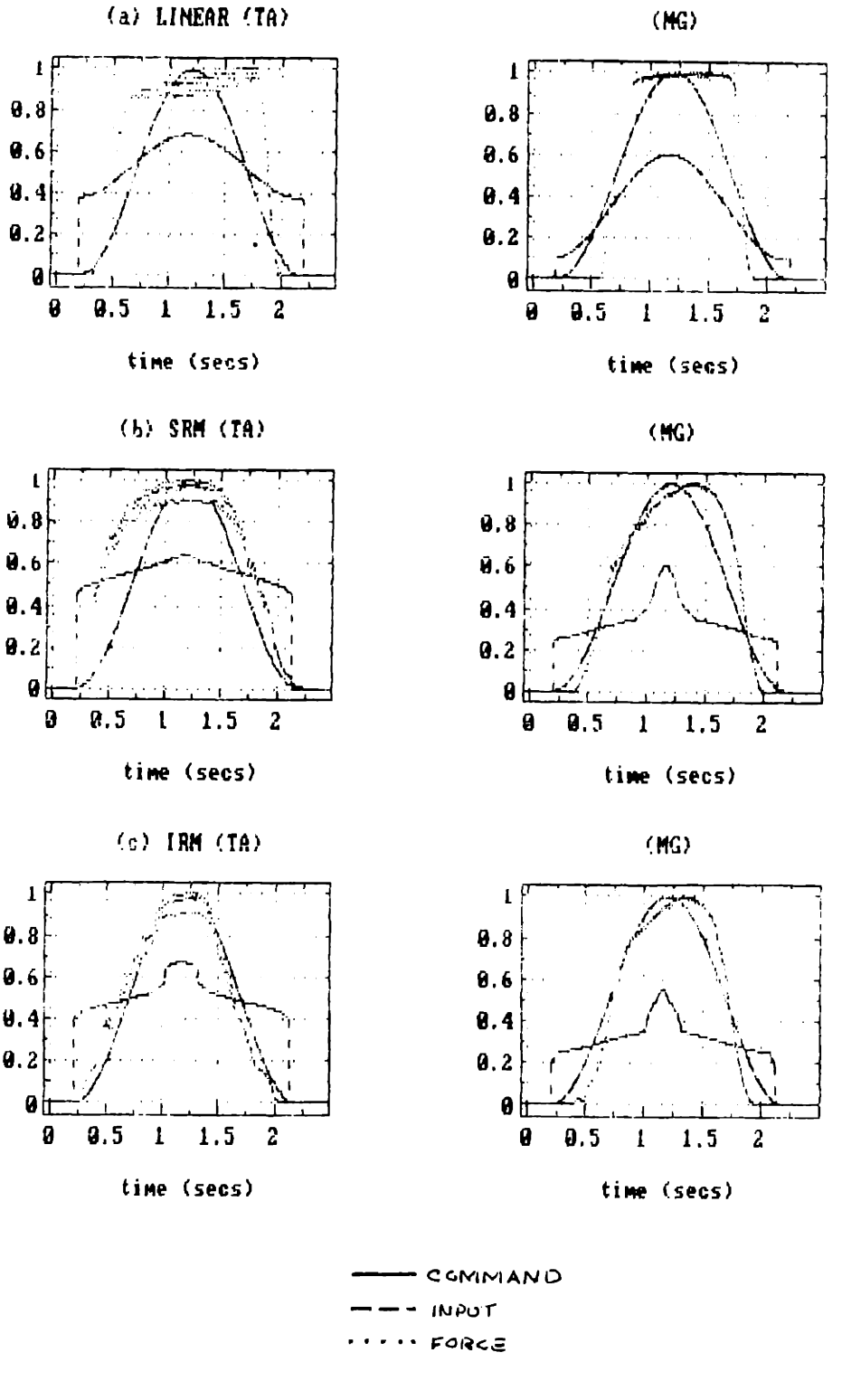
(a) LINEAR (TA)
(MG)
1
0.8
0.6
0.4
0.2
0
0 0.5 1 1.5 2
time (secs)
(b) SRM (TA)
(MG)
(c) IRM (TA)
(MG)
COMMAND
INPUT
FORCE

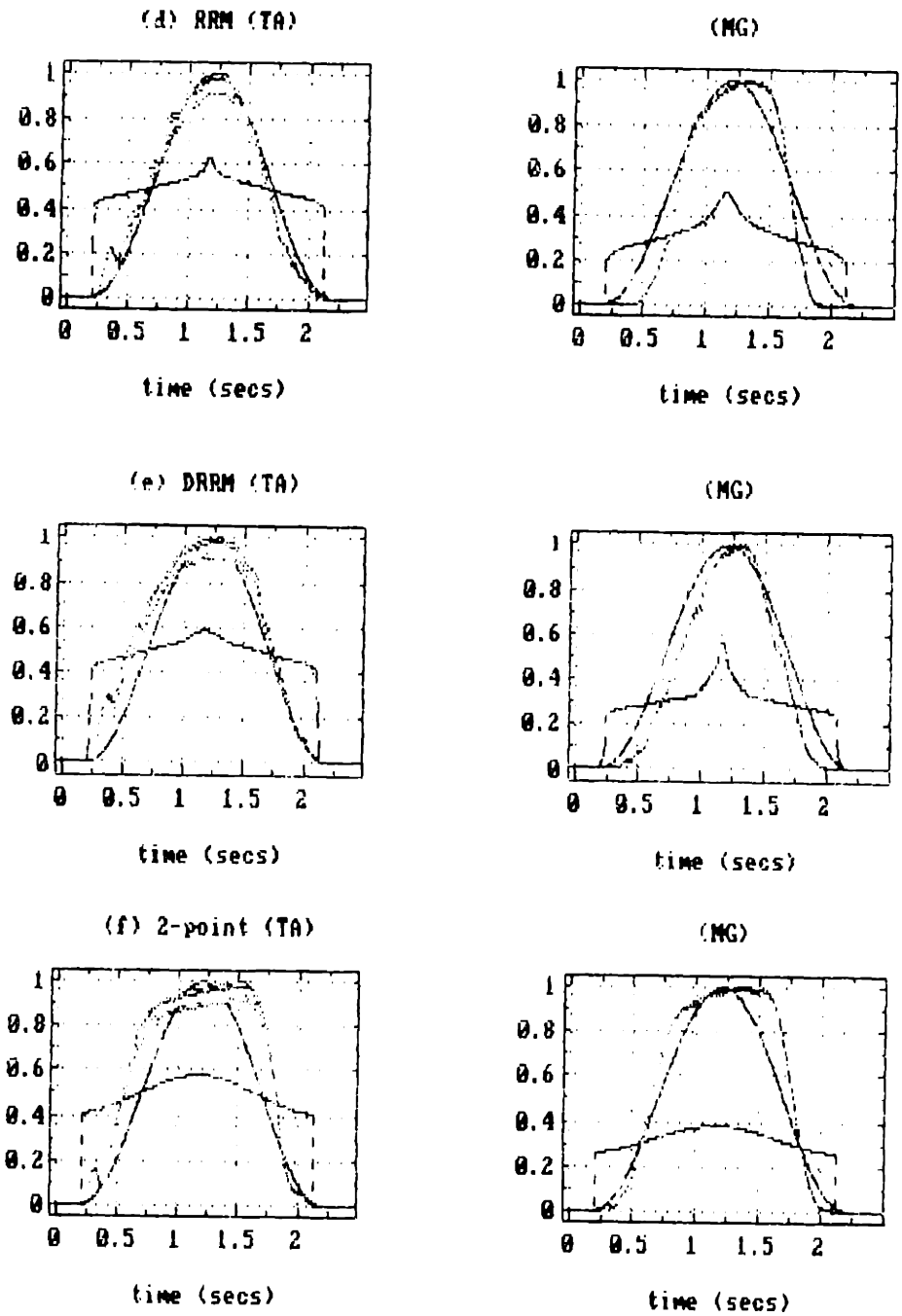

Figure 6.14: Command, stimulus input and force response time histories for feedforward block of $\widehat{\text{DLS}}$+ $\widehat{\text{SNLS}}$(meth). RCB2/OLCB2, C11.

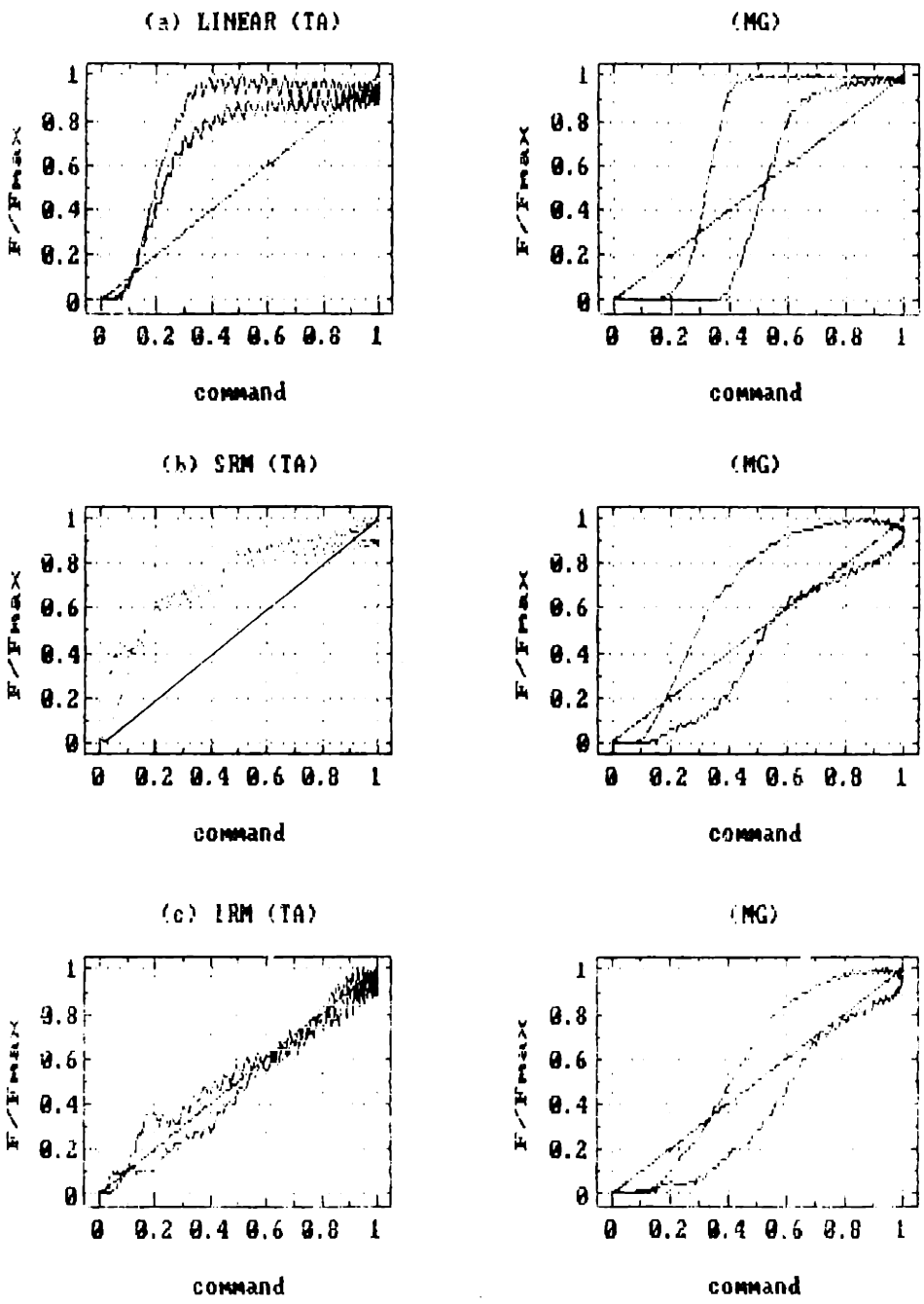
(a) LINEAR (TA)
(MG)
(b) SRM (TA)
(MG)
(c) IRM (TA)
(MG)
F/Fmax
command
0
0.2
0.4
0.6
0.8
1

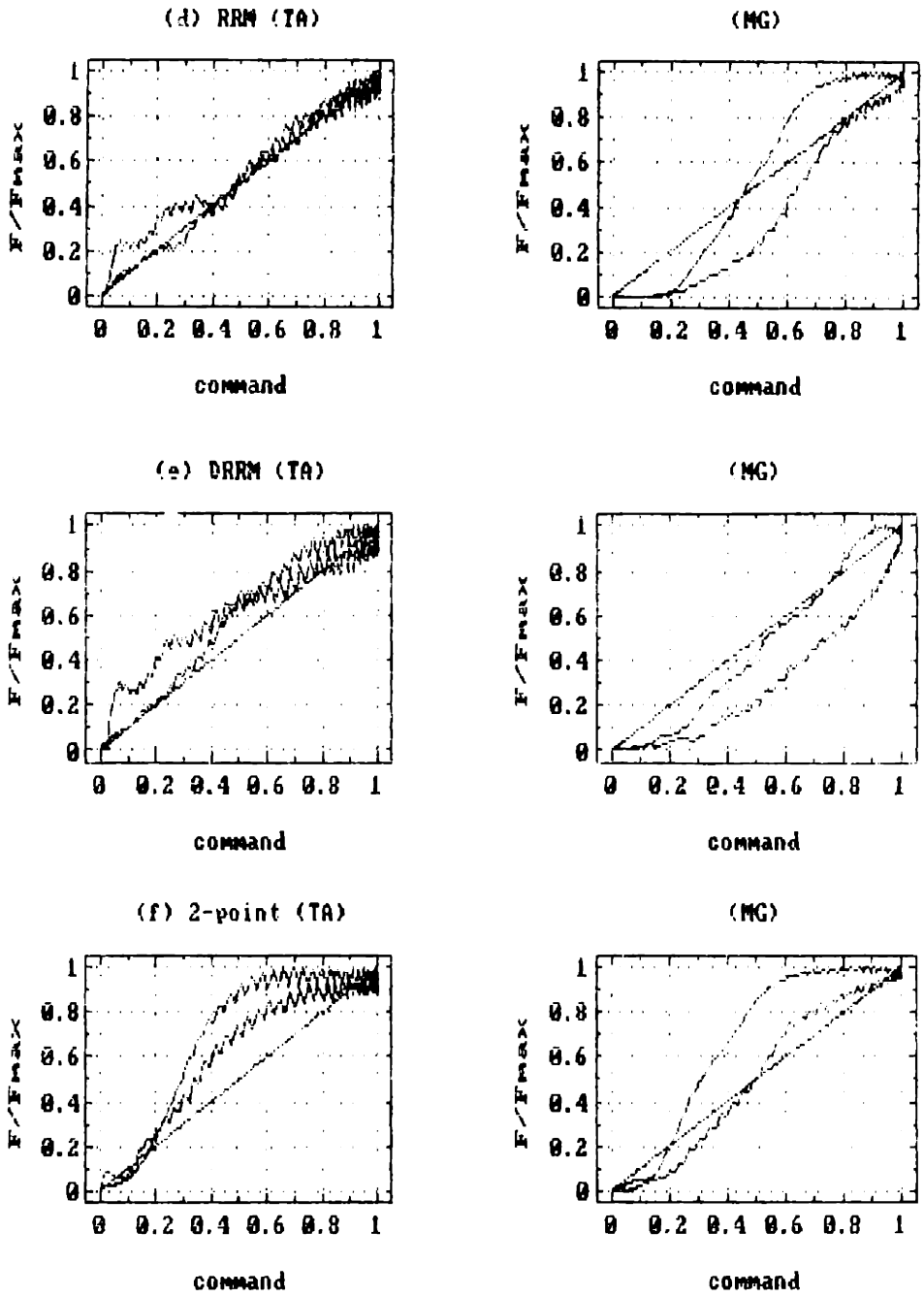

Figure 6.15: Effect of SNLS cancellation. Command for each plot is passed through an IRC estimated by the indicated ID method. C11.

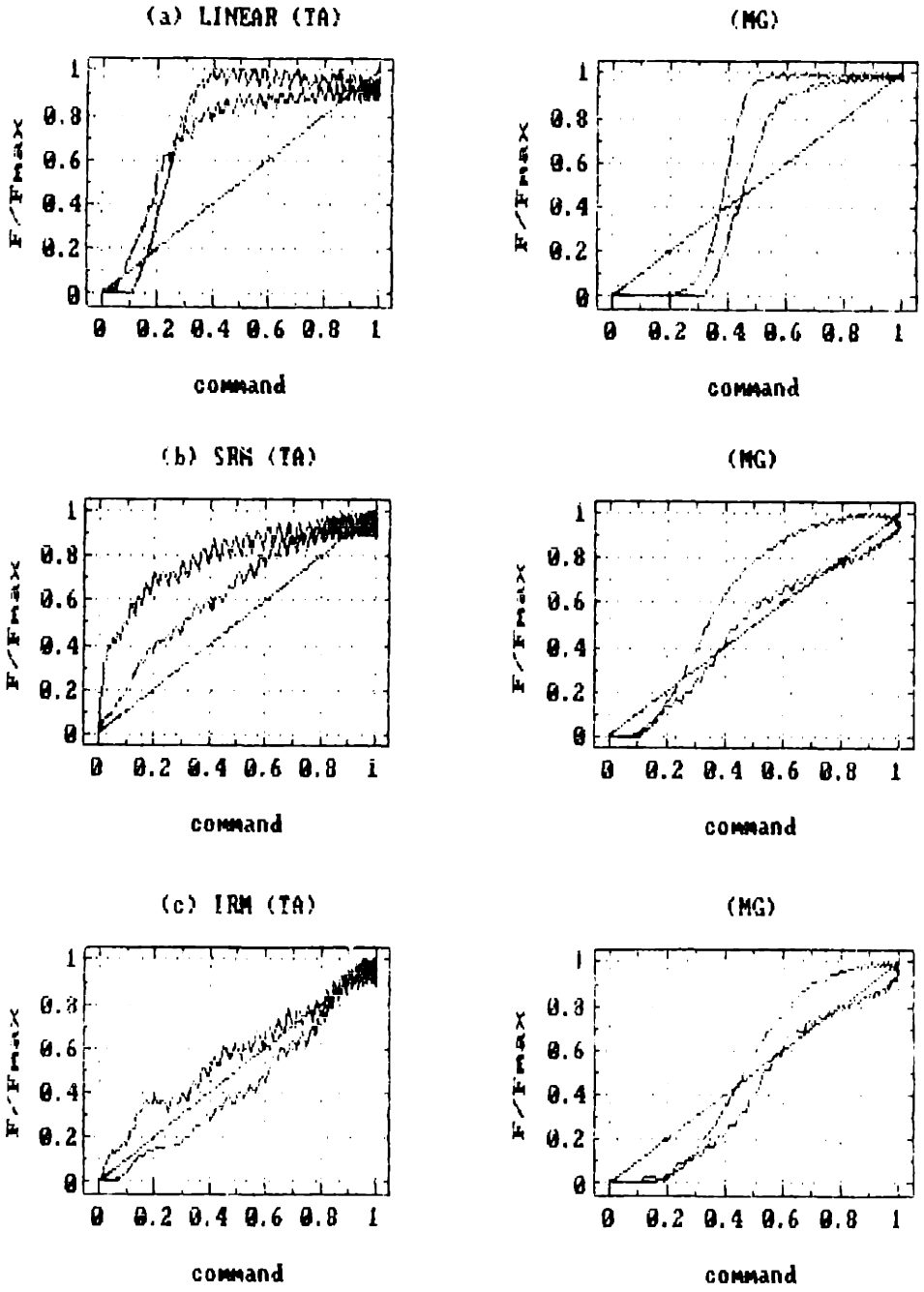
(a) LINEAR (TA)
(MG)
(b) SRH (TA)
(MG)
(c) IRH (TA)
(MG)
F/Fmax
command
0
0.2
0.4
0.6
0.8
1

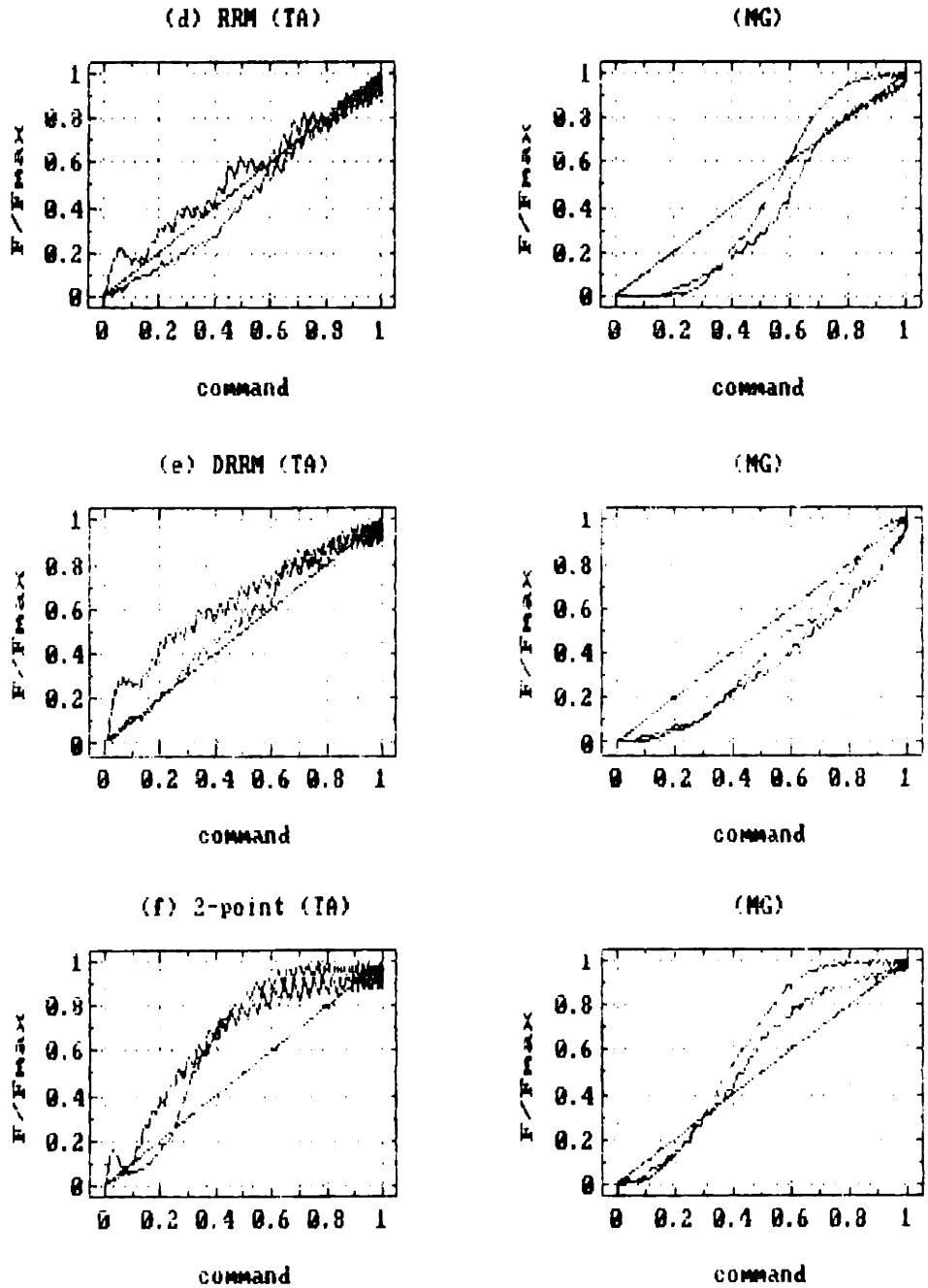

Figure 6.16: Effect of $\widehat{\text{DLS}}$+$\widehat{\text{SNLS}}$ cancellation. Command passed through an inverted $\widehat{\text{DLS}}$ and an IRC estimated by each method. C11.

to turnon, which is not visible in the MG records. The glitch becomes more obvious in the order that the maps were estimated and tested, the SRM sequence being smooth and the ramp and two-point records most corrupted. The glitch is an initial transient due to an abrupt input. The lower zoom limit had been chosen close to theshold for the first method tested in the block, and was not changed for later methods so that the resolution of each IRC in the block would be the same. A plummeting threshold made this a bad idea, because later methods were forced to overestimate threshold. The glitch appears in Figure 6.15 and 6.16 crossplots as well.

Each of the foregoing command/response sequences were condensed into a single number, ε(DOLC) (Eq. 5.11), summing the difference between desired and actual force response for each test. It is displayed for the TA and the MG for a single C11 OLCB and averaged with $n = 2$ in Figure 6.17 and Table 6.8 (static subsystem cancellation only), and in Figure 6.18 and Table 6.9 (SNLS + DLS cancellation).

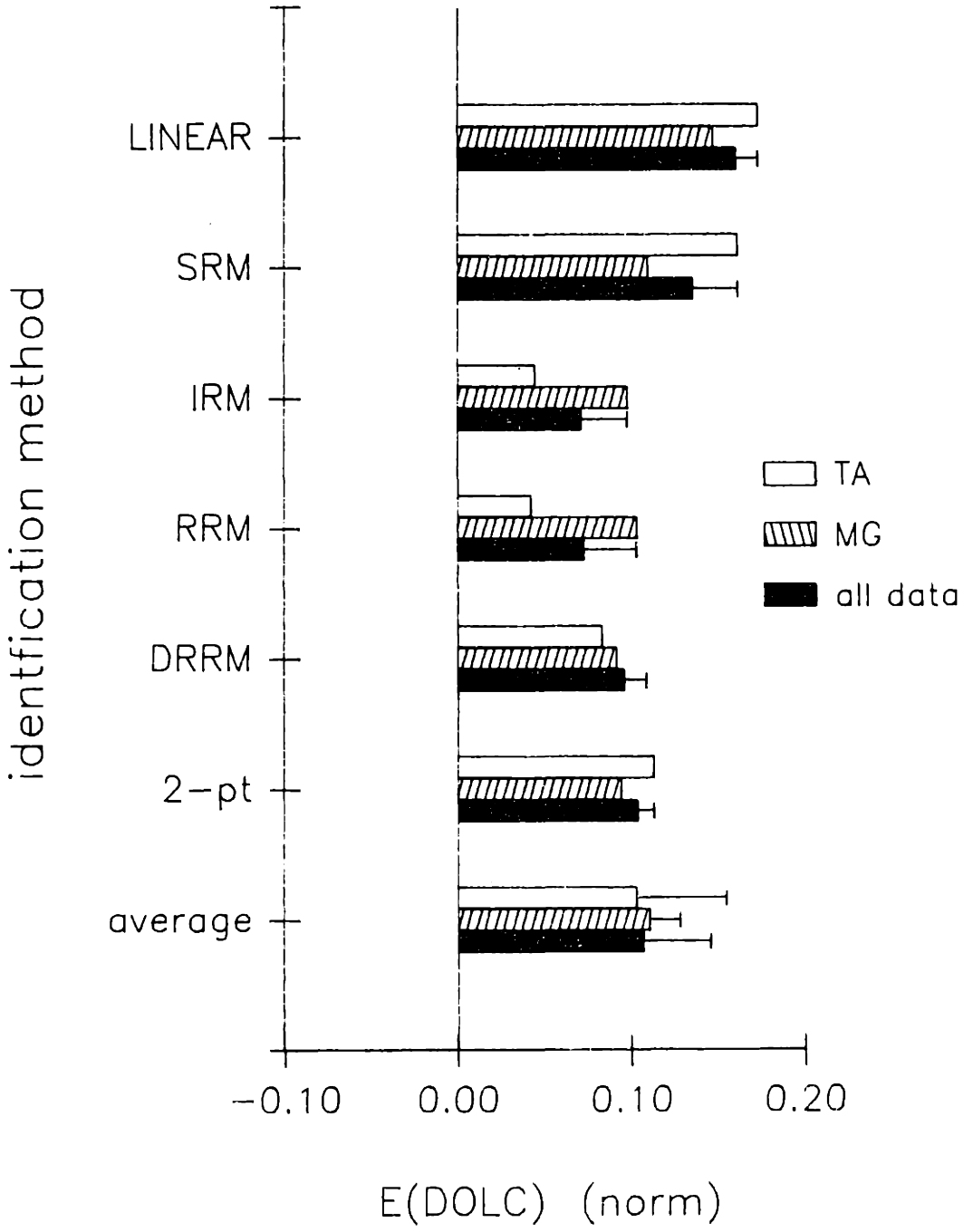

Figure 6.17: Averaged ϵ(DOLC) as a function of IRC ID method, with SNLS cancellation alone. All data: TA/MG, C11 ($n = 2$).

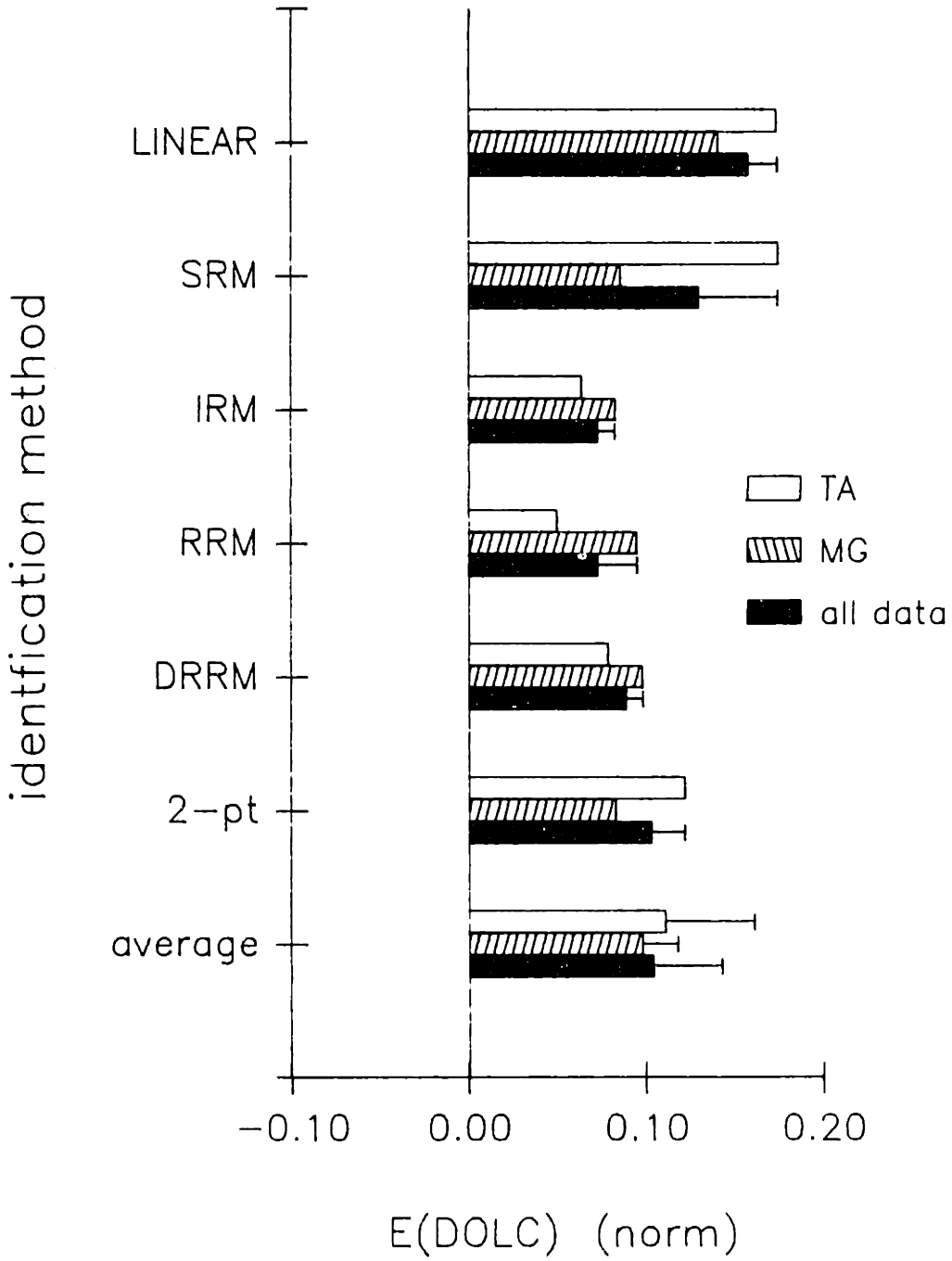

Figure 6.18: Averaged ε(DOLC) as a function of IRC ID method, with SNLS+DLS cancellation. All data: average of TA/MG, C11 ($n = 2$).

ε(DOLC)
Static Inverse Plant

ID Method	muscles	subject	n	range	mean	med	std. dev.
linear	TA	C11	1	.000	.174	.174	.000
	MG	C11	1	.000	.148	.148	.000
	TA, MG	C11	2	.033	.161	.161	.013
SRM	TA	C11	1	.000	.162	.162	.000
	MG	C11	1	.000	.110	.110	.000
	TA, MG	C11	2	.089	.136	.136	.026
IRM	TA	C11	1	.000	.045	.045	.000
	MG	C11	1	.000	.098	.098	.000
	TA, MG	C11	2	.020	.072	.072	.027
RRM	TA	C11	1	.000	.043	.043	.000
	MG	C11	1	.000	.104	.104	.000
	TA, MG	C11	2	.044	.073	.073	.031
DRRM	TA	C11	1	.000	.084	.084	.000
	MG	C11	1	.000	.109	.109	.000
	TA, MG	C11	2	.019	.096	.096	.013
Two-Point	TA	C11	1	.000	.113	.113	.000
	MG	C11	1	.000	.094	.094	.000
	TA, MG	C11	2	.038	.104	.104	.009
all methods (excluding linear)	TA	C11	6	.125	.103	.098	.000
	MG	C11	6	.058	.111	.106	.000
	TA, MG	C11	12	.125	.107	.106	.039

Table 6.8: Statistics for dynamic OLC tests, with a static inverse plant. TA and MG, taken from one C11 OLCB. All values in normalized A/D units.

ε(DOLC)
Static + Dynamic Inverse Plant

ID Method	muscles	subject	n	range	mean	med	std. dev.
linear	TA	C11	1	.000	.174	.174	.000
	MG	C11	1	.000	.141	.141	.000
	TA, MG	C11	2	.033	.158	.158	.017
SRM	TA	C11	1	.000	.175	.175	.000
	MG	C11	1	.000	.086	.086	.000
	TA, MG	C11	2	.089	.130	.130	.045
IRM	TA	C11	1	.000	.064	.064	.000
	MG	C11	1	.000	.083	.083	.000
	TA, MG	C11	2	.020	.073	.073	.010
RRM	TA	C11	1	.000	.050	.050	.000
	MG	C11	1	.000	.095	.095	.000
	TA, MG	C11	2	.044	.073	.073	.022
DRRM	TA	C11	1	.000	.079	.079	.000
	MG	C11	1	.000	.098	.098	.000
	TA, MG	C11	2	.019	.089	.089	.009
Two-Point	TA	C11	1	.000	.122	.122	.000
	MG	C11	1	.000	.083	.083	.000
	TA, MG	C11	2	.038	.103	.103	.019
all methods (excluding linear)	TA	C11	6	.125	.111	.100	.050
	MG	C11	6	.058	.098	.090	.020
	TA, MG	C11	12	.125	.104	.090	.039

Table 6.9: Statistics for dynamic OLC tests, with a static+dynamic inverse plant. TA and MG, taken from one C11 OLCB. All values in normalized A/D units.

Chapter 7

Discussion: IRC Estimate Comparisons and OLC Testing

This chapter interprets and comments on the experimental data of Chapter 6. Evolution and refinement of the identification methods has been described separately (Chapter 4). For the present the ID methods and their implementations are considered complete, though not necessarily perfected. The purpose here is to evaluate the various estimates of the "true" IRC on the basis of both morphological differences in the curves themselves and of intrinsic functional properties manifested in their performances when placed in the feedforward block of an open loop controller.

The chapter's first section comments on the nature and magnitude of system time variation observed while testing the ID methods and their estimated IRCs. While such observations do not reflect directly on ID method efficacy, they will be useful as a guide to the general employment of IRC and dynamic system estimation techniques in any kind of control situation.

7.1 System Time Variation

Characterization of real system time variation is a side issue for this thesis, but one critical in determining the usefulness of any muscle identification and calibration method. It would be convenient to be able to predict system time variation, specifically drift of threshold stimulus, using either elapsed time or muscle activity. Failing that, consistent control requires a quick, reliable way of knowing when the muscle state has changed significantly.

The exact cause of threshold drift is uncertain. It cannot be due directly to fatigue, because long-term fatigue would make the muscle require a greater stimulus to produce a given force, not the smaller one that is consistenly seen here. It is more likely an effect of changing electrode impedance (possibly due to dehydration and concentration of the saline environment surrounding the nerve and implanted electrode) or to slow metabolic changes. No attempt was made here to quantitatively link drift with muscle activity.

The physiological threshold-tracking excercise of Section 6.3 demonstrates the time

variation seen in one subject. Figure 6.1 shows that threshold drops at a fairly uniform, though not constant rate. The slope is different for each muscle, and it also varied from animal to animal. Crude predictions of threshold drift over many hours might be made after measuring rate of drift over the first hour or two. Other investigators (unpublished) have found that threshold drift eventually leveled out after the passage of hours or days. This is not surprising, since the threshold cannot drop forever.

The catastrophic effect of threshold drift on OLC in the absence of IRC recalibration was exemplifed by Figure 6.2. The muscle responsed with a reasonable facsimile of the command using a feedforward block estimated half an hour beforehand, but after 2.57 hours had elapsed control had degenerated severely. Regular identification is clearly crucial.

It is unlikely that an accurate means of predicting system time variation will be developed soon. The frequent-check approach seems more trustworthy for now, and could be effectively implemented in an algorithm such as that used to find THR_{TB}, described in Chapter 5.

7.2 IRC Estimate Morphology

The parameters used to define the physical features of the IRC estimate were threshold estimation error ($\varepsilon(\mathrm{THR}_{meth})$), percent difference in active zone width (ΔAZW) and biaxially normalized difference in active zone shape (ΔSHAPE). These variables were evaluated and presented for the individual ID methods in Section 6.3.

Assessment both of the consistency of individual ID methods and of the variation among them is complicated by the presence of system time variation. It is not always statistically clear whether differences in the three parameters reflect real system changes or ID method estimation error, and the quantitative observations to follow would be more substantial with additional data points. However, some relations are still deducible by comparing cross-method IRC estimate variation with single-method temporal variation. Clear dominance of one type of variation over the other for all

or most of the ID methods makes a statement about the significance of true system time variation relative to ID method estimation error. Clear divergence of any aspect of one method's IRC estimates from those of other methods implies something about that method's consistency or accuracy.

7.2.1 Variation in IRC Estimation among ID Methods

Judgements about cross-method variation may be formed with more confidence than with respect to single-method consistency, by comparing IRC estimates from different methods taken close together in time during RCB data sets. This strategy reduced the uncontrolled variable of long-term temporal system variations, but was unable to completely account for short-term fatigue and other effects of recent activation history.

Before analyzing the IRC estimates quantitatively, some qualitative features of the curves pictured in Figure 6.3 should be noted.

Shifted SRM: The largest divergence in IRC estimate profile in Figure 6.3 is seen for SRM in the TA; this curve has an active zone similar in shape to the others but shifted to the right. Note that the SRM IRC was estimated at the beginning of the block, so its position is consistent with the general downward direction of temporal threshold drift. However, the elapsed time between the SRM's IRC estimation and that of the next method is less than the time separating later estimates, which do not exhibit such a marked variance in threshold from one another. This is an example either of irregular system time variation, or of a substantial method-to-method variation. The observation that the SRM's IRC estimate for the MG (6.3(b)) closely overlays the other curves even though the data was taken from both muscles at the same time, is a clue but still inconclusive. The TA's threshold might be varying more rapidly than the MG's, or the muscle might be more susceptible to the SRM's fatiguing character. Note that short-term fatigue will cause the threshold stimulus and possibly the saturation stimulus to temporarily increase, as a higher stimulus is required to produce the same force; and recall that the SRM's points are obtained in order of decreasing stimulus

strength, which might have the effect of compressing the active zone towards saturation for a fatigue-sensitive muscle. The two factors, method-related fatigue and downward threshold drift, may be related (more about this later) but without more evidence, it is difficult to say which is the more influential.

Two-Point Method Breakpoint Selection Strategies: The two-point curve's two breakpoints were chosen manually. In Figure 6.3 (a) (TA), the two-point curve has breakpoints corresponding to the current threshold and saturation; in (b) (MG), it is aligned with the SRM curve's active zone region. Because of the different strategies used to create the two-point map, it should not be compared to the other IRC ID methods.

Stimulus Artifact: Evident in the TA RRM estimate is the 40 Hz stimulus artifact which characterized all continuous force records taken from this animal model. In general the TA appeared to be affected more than was the MG. Some of this may have been due to the fact that TA produced lower force amplitudes so that the stimulus artifact comprised a larger fraction of the peak amplitude. Subtle differences in electrode placement and physiological conduction pathways may also have contributed. Since the RRM is simply an unfiltered, synchronized, averaged crossplot of output versus ramp input, the stimulus artifact remains.

The DRRM curve is similar in shape to the RRM's, but the noise has been filtered out during deconvolution. Other effects of eliminating the muscle dynamics from the static map are not clear from observation of these two curves alone.

StoRM: It is clear that the Stochastic Response Method could benefit by additional development. Although the StoRM consistently predicts an active zone in about the same SS range as do the other ID methds, the roughness and nonmonotonicity of its IRC estimate and its tendency to predict a nonzero force response in the stimulus deadzone region make one suspect that is not a very accurate picture of what is actually going on inside the muscle. Judgement of the method's value should be withheld pending its

improvement.

...

Statistically, the means of the three descriptive criterion can be used to determine cross-method variation as well as temporal, single-method variation. Since the cross-method parameter evaluations are with respect to a single method, the SRM, relative values of the parameter means are more telling than absolute values.

$\epsilon(\mathbf{THR}_{meth})$: Figure 6.5 showed $\epsilon(\mathrm{THR}_{meth})$, averaged by ID method for all IRCs estimated by that method. The IRM seems to do the best at threshold estimating, in spite of its low resolution. This may be related to the fact that the IRM uses the same type of input to construct its map as that used to find THR_{TB}, used as the reference in calculation $\epsilon(\mathrm{THR}_{meth})$. The RRM's and DRRM's tendency to estimate a threshold stimulus higher than that estimated when an impulse input is used could be an error resulting from imperfectly corrected hysteresis due to a dynamic input signal. In DRRM's case, it could also be a filtering artifact; a low cutoff frequency would soften sharp corners and obscure the true threshold. Also note that the greater consistency in threshold estimation observed above for the continuous methods, in conjunction their large mean errors, implies a consistent bias in estimation.

It would seem that the SRM should underestimate stimulus threshold relative to the IRM, since a step command is a more powerful stimulus than an impulse. Recall, however, that the SRM's fatiguing steps were applied in descending order, so that the data point determining threshold were obtained last, when the muscle was most fatigued. This could cause the muscle's actual threshold to temporarily increase, as a higher stimulus is required to produce a measurable force.

The two-point curve's lack of success is due to the fact that in some cases its breakpoints were selected to match active zone slope rather than threshold stimulus, which meant overestimating threshold and underestimating saturation.

$\Delta\mathbf{AZW}_{meth}$: The cross-method average $\Delta\mathrm{AZW}_{meth}$ values of Figure 6.7 suggest that

the SRM is in the middle of the field with respect to estimating the width of the active zone. The high-resolution ramp methods found narrower zones than did the low-resolution methods IRM and SRM, probably because their interpolation increments were smaller in the quickly changing saturation and threshold regions. The fact that the IRM's active zone is wider than the SRM's is consistent of its lower estimated threshold, and of the progressive fatigue during the SRM narrowing the active zone of its estimates.

ΔSHAPE$_{meth}$: Shape dependence on ID method was shown qualitatively in Figure 6.11 with biaxially normalized IRCs estimated by different methods at approximately the same time, and quantitatively as ΔSHAPE$_{meth}$ in Figure 6.10 and Table 6.6. Surprisingly, the discrete IRM's estimates turned out to be shaped no more like the discrete SRM's, on the average, than do the continuous ramp methods'. Variation of no single method stands out from the others in either temporal or cross-method comparisons.

7.2.2 Consistency of IRC Estimation by Each ID Method

To judge the consistency or repeatability of a given ID method, it is useful to consider the range and standard deviation of temporal, single-method comparisons. An ID method may be said to be more or less consistent than other methods if the range and standard deviation of the three descriptive criterion pertaining to its IRC estimates are significantly smaller or larger than those of the other methods.

ϵ(THR$_{meth}$): Reference to Figure 6.5 and Table 6.2 shows that on the average, the continuous ID methods (RRM, DRRM) had slightly smaller ranges and standard deviations in threshold estimation error, ϵ(THR$_{meth}$), than did the discrete methods. The SRM had the largest values. This implies either a lack of resolution in the discrete ID methods or a lack of sensitivity in force response to the imputs that those methods use. Note that if the two-point method's threshold had always been chosen equal to

the current THR_{TB}, its threshold-estimation error would always have been zero along with its range and deviation.

ΔAZW/Δt: The percent rate of change in active zone width for a given ID method must be interpreted with caution, since nonzero values do not necessarily signify inconsistency on the part of the ID method. The active zone width could actually be changing, in either direction and at a variable rate. ID method influence must be inferred by comparison of values for the different methods; the saturation stimulus level is not estimated as easily as is THR_{TB} for a reference AZW.

All of the ID methods show an active zone width (Figure 6.6, Table 6.3) which decreases with time ($\Delta AZW/\Delta t < 0$), suggesting that a narrowing active zone is an actual physical phenomenon. However, there is a variation in both the ranges and standard deviations of $\Delta AZW/\Delta t$ values for each ID method, which implies that some of the methods are less consistent than others in this parameter. The SRM has a range of 6.1 and a standard deviation of 2.4 μsec, compared with ranges of 2.4-2.7 and devations of 0.9-1.0 for the IRM, RRM and DRRM. A close look at Table 6.3 pinpoints the bulk of this SRM variation in the C11 TA records, *i.e.* to a single sample point. A larger sample size is needed before any statement should be made regarding the SRM's relative consistency.

ΔSHAPE/Δt: Table 6.5 and Figure 6.8 show an enormous variation with respect to ID method in normalized shape rates of change. It is interesting to note that both ranges and standard deviations are much larger for the discrete methods, the SRM and IRM, than for the continuous methods RRM and DRRM ($.033 \pm .012$ for the SRM as opposed to $.020 \pm .007$ for the DRRM), while their means do not follow such a pattern. It is possible that the ΔSHAPE parameter itself is distorted by low resolution during the x-axis normalization. However, such an artifact ought to have appeared with similar impact in the $\Delta AZW/\Delta t$ data and did not.

It appears from this data that the continuous methods estimate IRC shapes which

are more alike than are the discrete method estimates. If the IRC actually has a constant shape, this could mean that the continuous methods are more consistent. It could also mean that the continuous methods estimate the same curve shape regardless of the shape of the real one. Once again, the population size is too small to base a conclusion on.

...

The morphological criterion are limited in scope in two respects. (1) There is no absolute reference for any of the parameters; and (2) the populations are statistically too small for definitive trends to emerge as an indirect solution to (1). Solving (2) and perhaps (1) by adding subjects to the study was not warranted since more valuable information was attianed through the functional OLC tests. On the other hand, the morphological studies were worth doing because they would have uncovered strong trends or differences between the ID methods not visible through inspection of raw data, had they existed, and would have helped to correlate them to subsequent differences in OLC performances.

Within the limits of statistical inference, it would seem that while the IRC ID methods do not give identical results, neither are any of them distinguished by either their internal consistency or theircross-method variation. Perhaps the most interesting thing to emerge from this attempt at a quantitative analysis are (a) that the RRM's IRC estimate does not appear physically very different from the DRRM's, and (b) that the IRCs estimated by the two discrete methods do not resemble each other more closely than they do those from the continuous ID methods. Morphological observations alone, however, do not tell us how small is small.

7.3 IRC Performance in Open Loop Control

Having established that the IRCs estimated by the various identification methods vary, it remains to see how these physical differences relate to functionality in open loop control.

Note that since data referred to in the following sections were taken from interspersed RCB/OLCB pairs, changes in muscle state should have been minor and should affect all tests equally.

7.3.1 Static Command Following

The first point to be taken from Figures 6.12 and 6.13 and Table 6.7 is that, based on the error criterion for static open loop control, ε(SOLC), all of the IRC estimates tested improved muscle control. The second point is that on the average, IRM estimates improved control significantly more than did those of other methods.

The DRRM does only slightly better than does the RRM, as might be predicted from the physical similarity of their recruitment maps. This raises the question of whether any consistent improvement, however small, merits the additional effort of data proccesing to construct the DRRM curve.

The relatively poor performance of the two-point curve should be considered with reservation, since the curve's breakpoints were subject to operator discretion. For this study they were not always chosen in a manner that would be rewarded by a test that weighted the active zone points equally with those in the threshold and saturation regions.

As usual, fatigue is the most likely explanation for SRM's estimate being less effective than some of the others. The SRM estimate was constructed from eleven step inputs applied in descending order. The static command following task consisted of only four inverted step commands, also applied in descending order, and was consequently less fatiguing than the estimation procedure. Consistent with this hypothesis, Figure 6.12 showed that the SRM curve tended to underestimate the force that would be elicited by a given input. This emphasizes that any memoryless recruitment map will be limited in its ability to deal with such sensitivity to recent activation history.

7.3.2 Dynamic Command Following

With the introduction of dynamics to the command following task, the significance of inverting the static nonlinearity and that of cancelling the roots of the dyanamic system in the feedforward block must be considered separately.

Effect of $\widehat{\text{SNLS}}$ Inversion

When compared with Figures 6.15 (a) (linear IRC estimates), Figures 6.15 (b)-(f) exhibit the improvement in dynamic command following that was attained by inverting IRC estimates for each ID method. These results were summarized by the variable ε(DOLC), representing error in dynamic command following (Figure 6.17).

If ε(DOLC) is accepted as a meaningful measure of control quality, the most effective ID method appears to be the IRM and the least is the SRM. Although at $n = 2$ the population size is not imposing for all the claims about to be made concerning dynamic command following, ε(DOLC) values imply a considerable range in control performances between the two muscles tested, both in individual methods and for the muscle as a whole. Most of the methods had similar success in controlling the MG, but not in TA tests. Averaged ε(DOLC) values for all the ID methods were similar for the two muscles, as were values for the tests using a linear IRC estimate.

To justify and assess the validity of these findings and to understand the performances of all of the ID methods, it is necessary to return to the original, unaveraged data.

Sensitivity of Dynamic Control to Pole Locations: Differences in the dynamic responses of the two muscles examined explains some of the OLC results. The variation in root location suggested by the impulse response τ_{peak} values is manifested in greater hysteresis in the MG ramp response crossplot in Figure 6.4[1]. The odd and non-second-order shape of the MG impulse response for this subject animal sheds doubt on the

[1]Because of the varying slope of the dynamic OLC test input, the OLC response/cosine bell input records display hysteresis in a confusing way.

validity of the second-order, critically damped muscle dynamics assumption on which the DRRM bases its deconvolution step.

The implications of root location for dynamic control are twofold. Obviously, muscle dynamics become negligible if the roots are fast enough relative to the command's frequency response. This is virtually the case for the TA.

A more subtle effect of muscle dynamics slow compared to the type of OLC input signal being used here is heightened sensitivity of the force response to error in the estimated threshold. The inverted cosine bell was chosen because of its smoothness. Since the muscle has inertia it is unable to produce force instantaneously, and cannot be expected to perfectly follow a command with nonzero initial slope. If the IRC estimate has correctly identified the threshold stimulus strength, the part of the inverted command that the muscle perceives also has zero initial slope. If the controller underestimates the stimulus threshold, however, the inverted command will have a nonzero slope by the time it excites the muscle. Force must lag command initially by an amount that increases as the muscle's roots slow, and because of the muscle's physical limitations, no dynamic feedforward element will be able to fully compensate for the poorly chosen input range. This situation is illustrated by the DRRM MG test, Figure 6.15 (e), compared with the two-point's (f).

Artifacts of Input Signal: A second phenomenon apparent in the force/cosine bell input crossplots deserves comment. The MG OLC test using a linear IRC, Figure 6.15 (a), shows force "liftoff" occurring at a higher command than force "touchdown", with the ascending and descending sides of the response almost — but not quite — parallel. Response/$\widehat{\text{SNLS}}$-inverted commands records (b)–(f), on the other hand, show force beginning and ending at the *same* command level, as if the $\widehat{\text{SNLS}}$ inversion had reduced the hysteresis at low commands. Obviously, a static, causal feedforward block cannot do anything of the kind. The real explanation is that by moving threshold from a command of 0.3-0.4 to one of 0.2 or less, the inverted $\widehat{\text{SNLS}}$ block moves muscle turn-on from a high-slope region of the command input to the flat initial region. This

is why it is difficult to assess hysteresis magnitude from a crossplot of response to a variable-slope input; the visible hysteresis is small where the input changes slowly and response can keep up with it, and large when the input is steep. If threshold is estimated perfectly by the IRC, force liftoff and touchdown will converge at a command just over 0.0.

SRM Performance: The most striking feature of the open loop control tests is how poorly the SRM estimate performs relative to the others; the average ϵ(DOLC) gap is greater than it was for the variable ϵ(SOLC), representing static command following error. Since the SRM is the most commonly used ID method for FES control, evidence of its inadequacy is portentuous.

Although ϵ(DOLC) and ϵ(SOLC) are both mean error indices, their magnitudes should not be compared directly because they refer to command inputs of a different nature. Therefore, it cannot be said that the SRM estimate performed more poorly in dynamic command following than it did in static command following. It *can* be said that it effected a smaller improvement over a linear IRC estimate than the other maps did, while in static OLC it offered improvement comparable to that of the others.

One explanation for the SRM's lack of effectiveness might be that is a discrete method relying on static input, but being tested with dynamic input. If there is dynamic nonlinearity in the system, the SRM will not find it. This is fine for static control, and it is proper for dynamic control because the IRC estimate is treated as if it represents static phenomenon alone and any dynamic contribution is theoretically a flaw. But if the task command is dynamically similar to the identification method's input, the dynamic information in the IRC estimate would be in the right place for that particular case and might deterministically improve response. Although the ramp methods and the dynamic OLC tests used differently shaped input (ramps and cosine bells), both inputs had the same half-periods and this conceivably could have been an advantage to them.

Two arguments make such an hypothesis unlikely. First, the impulse response

shape/stimulus strength relation explored in Section 4.2.3 suggested that dynamic nonlinearity was small compared to static nonlinearity in the stimulated muscle. The continuous methods' advantage would not have been large. Second, the IRM is also a discrete method and it does better (according to the ϵ(DOLC) criterion) than do the continuous methods. It does rely on the muscle's dynamic response for its IRC estimate, but dynamic nonlinearity in a system refers to an output *frequency* response that depends nonlinearly on the input's amplitude [27]. The impulse response's shape, reflecting its frequency response, thus might vary with SS in a dynamically nonlinear system for the first reason, but since the input's frequency response is identical except for a gain factor at each SS, the amplitude of the response must be a static gain relation. Thus, the IRM can neither benefit from nor be harmed by dynamic contributions to the "static" nonlinearity.

A more compelling argument concerning the SRM's deficiency is the same one that was used to explain why this method took second place to the IRM in static command following. The difference between the SRM and all the other methods is that the SRM is much more fatiguing. By tiring the muscle with high-strength stimuli before applying the low-strength ones, it produces a curve which overestimates the stimulus needed to produce small forces. Fatigue may be responsible for the rounded SRM response/inverted command relation of Figure 6.15 (b), whether the stimulus strength for peak force was underestimated, those for smaller forces overestimated, or both. It is not clear from the data that this effect is more pronounced in the muscle's dynamic response than in its steady state response. However, since the static command following task is more fatiguing than the dynamic one, the fatigue-contaminated SRM IRC estimate might accomplish the former more effectively. Fatigue sensitivity would also explain why the SRM ϵ(DOLC) was closer to the average of all the methods for the MG than for the TA (Figure 6.18). The TA of this subject (C11) evidently had a dynamic response with faster roots than did the MG (Figure 6.4), with a time-to-peak (τ_{peak}) half that of MG's. The quicker response implies a greater proportion of

fast-twitch, highly fatiguable muscle fibers in the TA than in the MG, making it more susceptible to the SRM's defect.

IRM Performance: The IRM's relatively strong showing should not be discounted, but it could be a case of success by default. Its performance was far from perfect, at least for the MG, and the technique is limited. The only direction open for improvement is in increasing resolution by applying more impulses, making it both more time-consuming and more fatiguing.

DRRM and RRM Performances: The ε(DOLC) criterion indicates a mediocre performance for this labor-intensive identification method relative to the others. The extra effort involved must be justified when perhaps simple ramp-response averaging would be just as or even more effective.

This is in fact not a difficult assignment. Holding a straight edge to the DRRM MG force/command crossplot (Figure 6.15 (e)) and comparing the straightness of the ascending and descending responses with those of the IRM, RRM, and two-point records should convince most readers that the DRRM is doing the best job of unkinking the force response. This does not show up in the mean error criterion ε(DOLC) because a low threshold estimate caused an initial and final lag, which skewed the slope of the linear part of the crossplot.

To control a muscle with slow dynamics, the DRRM — and the other ID methods as well — need to estimate threshold better. With its high resolution, this is a place where the DRRM ought to shine. The fact that it doesn't may be attributed to two details of its algorithm implementation. First, notice in Figure 6.3 (b) that the IRC estimate used in the DRRM OLC test record discussed just above is smoothly rounded in the threshold area, when perfect control demanded a higher threshold followed by a steeper initial slope. The filtering used to reduce deconvolved noise may also be blurring the map's sharp details. Better dynamic system estimation, deconvolution and more selective filtering techniques are needed to remedy this.

Second, a lesson may be taken from the earlier observations of the input's shape influence on OLC test results: the cosine bell may be a more appropriate input for the DRRM also. The flat region around threshold would increase map resolution in that critical area, and the hysteresis suppression due to the more slowly changing input there would minimize the burden on the apparently inadequate deconvolution process. The cosine bell's smooth nature might also improve deconvolution[2].

Two-Point Method Performance: Little can be said about this method, potentially a simple way to calibrate a muscle for crude control, except that it needs to be standardized and automated in order to be consistent. Decisions must be made about how to select breakpoints — THR/SAT versus best-fit of active zone, or some combination — in a manner appropriate to the contol task.

Validity/Completeness of the ε(DOLC) Criterion: The ε(DOLC) is a good criterion of ID method performance because it measures how well a method has succeeded in its job of identifying the muscle's static nonlinearity. It is not the only criterion and, as the DRRM example suggests, it cannot assess potential for success. Other informative criterion might reward correct threshold or saturation estimation, and perhaps, how closely a straight line fits the force/input crossplot. Which to use depends on what is most important for the control task at hand.

...

On the basis of the ε(DOLC) criterion, the IRM is the most effective ID method in OLC, the SRM is the least effective and judgement must be withheld on the two-point method of IRC estimation. However, by other criterion the DRRM is competitive and with a little more development, it could probably dominate the ε(DOLC) arena as well.

[2]The cosine bell input was tried with the DRRM early in the study (Section 4.2.3), but the significance of its potential benefits were not recognized until after conduction of the OLC tests.

Effect of $\widehat{\text{DLS}}$ Inversion

$\widehat{\text{DLS}}$ Feedforward Block: The improvement in dynamic command following due solely to the presence of an inverted linear dynamic subsystem estimate in the controller's feedforward block was demonstrated in Figures 6.15 (a) and 6.16 (a), response/command crossplots without and with cancellation of estimated dynamic system poles. Hysteresis was substantially reduced for the MG, and it was overcompensated for the faster TA which had very little to begin with. The ϵ(DOLC) values for the two cases reflect this improvement incompletely, since it measures the area between the normalized response and command curves rather than the area between the ascending and descending sides of the response. For sharply nonlinear systems such as these, even complete elimination of hysteresis would not substantially decrease ϵ(DOLC). Indices to specifically target dynamic system contributions would measure reduction of enclosed area[3], or reduction of the horizontal width of the hysteresis at a 50 percent command.

$\widehat{\text{DLS}}$ + $\widehat{\text{SNLS}}$ Feedforward Block: The result of including both SNLS and DLS estimates in the open loop controller was illustrated by Figure 6.16 (b)-(f). By inspection, incremental improvement in response appears to be similar for all the ID methods to what it was using a linear IRC estimate. Again, the ϵ(DOLC) error parameter is unreliable here, so the assessment will be qualitative. The TA results are uninformative since dynamics are a small part of command-following problem. With a sample size of one, it is difficult to say if the $\widehat{\text{DLS}}$ inversion is more effective for one method than another.

It could be conjectured that inversion of this particular estimate of the dynamic system ought to best aid the DRRM, because it was obtained based on the same muscle model assumptions and was used in the DRRM deconvolution. However, this complementarity would be an advantage in forming a deterministic description of the

[3]Beware artifacts of input dynamics: enclosed area means different things at different commands if the command has a variable slope.

complete system only to the extent that the muscle model was correct. If the OLC test input were identical to that used by the DRRM, lack of determinism would be less important and the DRRM's picture of the system might work better than those of the other ID methods.

A purist would probably consider the exploitation of this observation offensive, but in practice it might not be a bad idea. For some repetitive or simple control tasks, employing a non-deterministic description of the muscle in the open loop controller, relevant only for a specific input signal, could be more efficient than attempting to model the muscle more precisely.

Assessment of the Muscle Model: DLS estimate inversion was less effective than it might be because the procedure used to estimate the dynamic system was imperfect. It assumed that muscle dynamics were second-order and critically damped, which was not quite correct. The MG impulse response had a longer tail than does the closed-form solution for a critically damped response with the same time-to-peak, suggesting separated and underdamped poles that are possibly the result of unmodelled tendon elasticity. Therefore the $\widehat{DLS}$ underestimated the duration of force response, and incompletely compensated for hysteresis. The non-second-order shape of the experimental impulse response — for *any* ς — further jeopardized a second-order model's ability to translate desired force into the correct stimulus input.

Clearly, further improvement of control demands better modelling of the muscle dynamics. One approach would be to continue to fit a synthetic closed-form response to the actual one, but relaxing the $\varsigma = 1$ constriction. Recourse to a $\varsigma \leq 1$ model would probably be adequate at a reasonable cost; since the impulse response shape for a given muscle does not change significantly, the dynamic system need be estimated only once for each subject-muscle. The next step would be to use a higher order model, or better yet, find a way to use an experimental measurement of the dynamic system (such as the impulse response) directly.

There remains the question of how to address dynamic nonlinearity in the stimulated

muscle. Although data from this study (Section 4.2.3) show the magnitude of one form of dynamic nonlinearity, the variation of impulse response shape (*i.e.* pole location) with stimulus strength, it is not clear from the tests conducted here how significant this and other forms of dynamic nonlinearity are with respect to open loop control. Before a controller can attempt to compensate for it, the dynamic nonlinearity must be better characterized and sensitivity studies, perhaps simulated, performed. As usual, justification of this effort depends on the requirements of the control task and on characteristics of the particular system being controlled.

Chapter 8

Conclusions and Recomendations

8.1 Appraisal of the Muscle Model

Drawing on the foregoing results, observations and arguments, what may be said about how well the muscle model used here fits the real system? On what grounds can this assessment be based?

In its most general form, the muscle model described in Chapter 2 is an ideal Hammerstein system. For some purposes, it was necessary or convenient to further restrict it, particularly its dynamic part. The appropriateness of the general model and of the various constraints put on it are considered separately.

8.1.1 The Hammerstein Model

The Hammerstein model makes some assumptions about a system's structure and characteristics which, in the case of the stimulated muscle studied in this thesis, required justification.

Time Invariance

The claim of time invariance is the model's most critical shortcoming. Muscle response is clearly a function of activation history, one which will be difficult if not impossible to accurately define. Further, this experimental model demonstrated another source of time variation, also irregular and unpredictable, which has been attributed to changing electrode impedance. Since the artificially stimulated muscle's state changes rapidly (in seconds and minutes) as well as over hours of activation, modeling or otherwise dealing with its time variation is essential to the success of feedforward control, and an important element of a robust closed loop control strategy.

Ordering and Number of Subsystem Blocks

The Hammerstein model defines a system with tandem static nonlinear and dynamic nonlinear subsystems. This arrangement appears to satisfactorily describe the experimental model used here, in that the description would not be improved by adding

elements, *e.g.* a second static nonlinear block following the dynamic block or another dynamic block before the Hammerstein model's static one.

Linearity of Dynamic Block

Muscle dynamics are not linear, exhibiting an impulse response shape that varies with stimulus strength. From the tests performed here, however, the significance of the nonlinear dynamics with respect to muscle controllability is still unknown. Neither has it been proved beyond a shadow of a doubt that nonlinear dynamics do not affect the output of the continuous IRC estimation methods. These uncertainties need to be resolved before the identification methods can be used with confidence, and before their estimated IRCs can be effectively employed in control algorithms.

Isometric Contraction

The isometric constraint was adequately met in this study. However, this experimental model will be used in the future to explore the additional capabilities of nonisometric contraction. The variation of muscle dynamic response with muscle length and velocity of contraction will have the effect of adding nonlinearity of a highly complex nature to the dynamic subsystem, and appropriate revisions to the muscle model must be made to anticipate this.

8.1.2 Constraints Applied to the Hammerstein Model

Both the continuous Deconvolved Ramp Response Method and the open loop control algorithm used to test all of the identification methods relied on some important restrictions to the Hammerstein model. In some cases, determined by characteristics of muscle dynamics and task, these more precise definitions proved tenable but in others they did not.

Second Order Dynamics

The dynamic responses of most of the muscles studied were modelled with reasonable accuracy by a second order system; *i.e.*, the error due to this constraint was probably small compared to error from other sources, such as system time variation and unmodelled system noise. For the purposes of this study, the second-order assumption is justified, and it is a useful constraint.

Damping Ratio

The experimental dynamic response was best fit by a critically damped or slightly underdamped model. The $\hat{\sigma} = 1/\tau_{peak}$ shortcut to estimating critically damped roots was hampered by non-second order system characteristics which an optimization approach is better able to handle. This generalization is inexpensive because the fitting only needs to be performed once for each system.

In order to avoid constraining the damping ratio at all, and to model non-second-order dynamics when they do appear, it will be necessary to employ either a higher order model or a direct measure of the system, such as its impulse response, in deconvolution and inversion. In practice, the latter procedure was found to be complicated by the presence of measurement noise, but if simpler approaches fail it merits further development.

8.2 Identification Method Evaluation

Physical comparisons of IRC estimates from all the identification methods showed that the methods produced different results. The differences proved to be significant in tests of estimated IRC effectiveness in open loop control, although all improved control over that attained with a linear IRC estimate. It cannot be concluded from the limited number and type of tests performed that the ID methods should be rated differently in their effectiveness in static vs. dynamic control.

Following is a synopsis of each ID method's strengths and weaknesses.

Step Response Method

Fatigue contamination cripples the SRM for both static and dynamic control; its slowness makes it even less attractive. If it must be used because only static force measurements are available, consideration should be given to ordering input stimuli by their increasing, rather than decreasing, strengths, when a correct threshold estimate is critical to control.

Impulse Response Method

In some respects the IRM seems to have been the most successful of the identification methods examined. However, it did not provide perfect control and since the algorithm itself leaves little room for further development, the method is limited. Until the DRRM is improved, it is the fastest means of identifying a system's static nonlinearity with reasonable accuracy and without fatiguing it.

Deconvolved Ramp Response Method

The DRRM is hampered by dependence on an inadequate dynamic system approximation in its deconvolution step, by its filtering technique and possibly by an inappropriate input. With attention to these details, it is predicted to be not only an improvement over the simple ramp averaging of the RRM but also the most accurate and effective of the ID methods, and to provide the best answer to the need for calibration technique that is rapid and nonfatiguing as well as correct.

Stochastic Response Method

Because of the generality of its assumptions, the StoRM is a potentially valuable tool for characterizing unknown systems. Its implementation requires, and merits, further development, particularly in its strategy of dealing with noise.

Two-Point Method

The effectiveness of the two-point technique of SNLS-approximation depends on the shape of the actual IRC, on how the estimated IRC's breakpoints are chosen, and on the demands of the controller. In this study, it was not refined into an "identification method" with a standardized protocol for estimating an IRC from experimental data. It holds promise as a quick-and-dirty approach to muscle control, and more extensively OLC testing will ascertain exactly how dirty its control actually will be.

8.3 Identification Method Usage

Knowledge gained about real IRC variation provides some clues about how and when the methods are best used.

8.3.1 Task Appropriateness

- Never use the SRM unless only static measurements of muscle response are available, because it is slow, fatiguing and ineffectual.
- Use the low-resolution IRM or the two-point method when fine control is not required, and to avoid the development and customization cost of more complex methods.
- The DRRM should be used for high-resolution, accurate and rapid SNLS and DLS identification, after the improvements enumerated above.
- With refinement, the StoRM can be used to characterize a Hammerstein system or variant thereof when it is not known how the dynamic system is best modelled.

8.3.2 Frequency of Muscle Calibration

How often does a muscle need to be calibrated? The answer is simple: often enough. This will depend on the quality of control required and on the magnitude and nature

of time variation characteristic of a particular muscle and/or experimental model. If the time variation consists primarily of drift in threshold stimulus with smaller or less critical changes in active zone width and shape, it may prove efficient to estimate the IRC infrequently, but to update it at short intervals to reflect easily measured changes in threshold.

For the experimental model of this study, a map typically lost its effectiveness within an hour of its estimation. After two hours it was of no more use than a linear map.

8.3.3 Importance of DLS Cancellation to Dynamic Control

As for any controlled system, pole cancellation is imperative when muscle dynamics are significant compared to the input's frequency response; IRC inversion alone is not enough for good command following.

Further, the poles must be approximated using an accurate muscle model. For the muscles studied here, a second order model is appropriate and an optimized, critically damped one does not appear to be too restrictive.

8.4 Where From Here

Anyone who labors under the delusion that all the interesting FES problems have been figured out, that by next week or next year, paraplegics will be rising from their wheelchairs and dancing their ways to office, supermarket and football field, and that he or she could make a bigger contribution to the field by devising innovative ways of swelling the demand for FES techniques, may hereby stand corrected. There are plenty of interesting problems left — most of them, in fact — and none lack in challenge.

The first step is to finish the job begun in this thesis, that of characterizing the electrically stimulated muscle. The identification methods described here need to be improved as has been recommended. The muscle dynamics must be modelled more accurately, dynamic nonlinearity identified and its importance evaluated, and the issue of nonisometric contraction attacked. Physiological stimulation must be better mimicked

in order to free artificial stimulation from the tyranny of fatigue.

After satisfactory open loop control has been attained for tidy, well-measured models such as the one used here, closed loop strategies can be explored along with the development of clinically realizable feedback channels and the design of interactive and user-friendly command interfaces.

There is a long way to go, but someday human FES subjects may again control their own limbs.

Bibliography

[1] *National Institute of Handicapped Research: Long Range Plan.* Washington D.C., 1981. US Department of Education.

[2] Allin, J. and Inbar, G. Fns control schemes for the upper limb. *IEEE Trans. Biomed. Eng.*, BME-33(9):818-828, 1986.

[3] Allin, J. and Inbar, G. Fns parameter selection and upper limb characterization. *IEEE Trans. Biomed. Eng.*, BME-33(9):809-817, 1986.

[4] Bawa, P., Mannard, A., and Stein, R. Effects of elastic loads on the contractions of cat muscles. *Phys. Ther.*, 22:129-137, 1976.

[5] Bawa, P., Mannard, A., and Stein, R. Predictions and experimental tests of a visco-eleastic muscle model using elastic and inertial loads. *Biol. Cybern.*, 22:139-145, 1976.

[6] Bendat, Julius S. and Piersol, Allan G. *Engineering Applications of Correlation and Spectral Analysis.* John Wiley & Sons, Inc., New York, NY, 1980.

[7] Bendat, Julius S. and Piersol, Allan G. *Random Data : Analysis and Measurement Procedures.* John Wiley & Sons, Inc., New York, NY, 1971.

[8] Benton, L.A., Baker, L.L, Bowman, B.R., and Waters, R.L. *Functional Electrical Stimulation — A Practical Clinical Guide.* Rancho Los Amigos Rehabilitation Engineering Center, Downey, California, second edition, 1987.

[9] Bernotas, L., Crago, P., and Chizeck, H. A discrete-time model of electrically stimulated muscle. *IEEE Trans. Biomed. Eng.*, BME-34(2):140-147, 1987.

[10] Biscoe, T. and Taylor, A. The effect of admixture of fast and slow muscle in determining the form of the muscle twitch. *Med. Biol. Eng. Comput.*, 5:473-479, 1967.

[11] Brown, G. and von Euler, U. The after effects of a tetanus on mammalian muscle. *J. Physiology*, 93:39-60, 1938.

[12] Brummer, S. and Turner, M. Electrochemical considerations for safe electrical stimulation of the nervous system with platinum electrodes. *IEEE Trans. Biomed. Eng.*, BME-24:59-63, 1977.

[13] Burke, R. Catch property in single mammalian skeletal muscle. *Science*, 168:122-124, 1970.

[14] Burke, R. Physiological types and histochemical profiles in motor units of the cat gastrocnemius. *J. Physiol.*, 234:723-748, 1973.

[15] DeLuca, C. et al. Behaviour of human motor units in different muscles during linearly varying contractions. *J. of Physiology*, 329:113-128, 1982.

[16] Dongarra, J.J., Moler, C.B., Burich, J.R., and Stewart, G.W. *Linpack User's Guide*. Society for Industrial & Applied Mathematics (SIAM), Philadelphia, PA, 1986.

[17] Dum, L. and Kennedy, T. Physiological and histochemical characteristics of motor units in cat tibialis anterior and extensor digitorum longus muscles. *J. of Neurophys.*, 43(6):1615-1630, 1980.

[18] Durfee, William K. *Task control with an electrically stimulated antagonist muscle pair*. PhD thesis, Massachusetts Institute of Technology, June 1985.

[19] Guyton, M.D., Arthur C. *Textbook of Medical Physiology*. W.B. Saunders Co., Philadelphia, PA, 1986.

[20] Hatze, H. A general myocybernetic control model of skeletal muscle. *Biol. Cybernetics*, 28:143-157, 1978.

[21] Hausdorff, Jeffrey M. *Gait orthosis combining controllable damping and muscle stimulation*. Master's thesis, Massachusetts Institute of Technology, August 1988.

[22] Hunter, I.W. and Kearney, R.E. Two-sided linear filter identification. *Medical & Biological Engineering & Computing*, 21:203-209, 1983. McGill University, Montreal, Canada.

[23] Hunter, I.W. and Korenberg, M.J. The identification of nonlinear biological systems : Wiener and Hammerstein cascade models. *Biological Cybernetics*, 55:135-144, 1986. McGill University, Montreal, Canada.

[24] Mannard, A. and Stein, R. Determination of the frequency response of isometric soleus muscle in the cat using random nerve stimulation. *J. of Physiology*, 229:276-296, 1973.

[25] McDonagh, J. et al. A commentary on muscle unit properties in cat hindlimb muscles. *J. Morph.*, 166:217-230, 1980.

[26] Milner-Brown, H.S. and Stein, R.B. The relation between the surface electromyogram and electrical force. *J. of Physiology*, 246:549–569, 1975.

[27] Ogata, Katsuhiko. *Modern Control Engineering.* Prentice-Hall, Inc., Englewood Cliffs, NJ, 1970.

[28] Petrofsky, J. Control of the recruitment and firing frequencies of motor units in electrically stimulated muscles in the cat. *Med. Biol. Eng. Comput.*, 16:302–308, 1978.

[29] Petrofsky, J. and Phillips, C. Determination of the contractile characteristics of the motor units in skeletal muscle through twitch characteristics. *Med. Biol. Eng. Comput.*, 17:525–533, 1979.

[30] Press, William H., Flannery, Brian P., Teukolsky, Saul A., and Vetterling, William T. *Numerical Recipes : The Art of Scientific Computing.* Cambridge University Press, New York, NY, 1986.